Physics – Uspekhi **65** (12) 1248 – 1289 (2022)

REVIEWS OF TOPICAL PROBLEMS PACS numbers: **74.20. – z**, **74.78. – w**, **85.25. – j**

Superconducting spintronics: state of the art and prospects

A S Mel'nikov, S V Mironov, A V Samokhvalov, A I Buzdin

DOI: https://doi.org/10.3367/UFNe.2021.07.039020

Contents

Abstract. Significant progress has been achieved recently in a new field of low-temperature electronics, the physics of superconducting hybrid systems based on superconductors (Ss) and ferromagnets (Fs), which is known as superconducting spintronics. We present theoretical and experimental results on studies of the proximity effect with a ferromagnet, which forms an unusual superconducting state in the vicinity of the S/F interface and allows controlling dissipationless charge and spin transport in hybrid structures by changing the texture and properties of the magnetic subsystem. Particular attention is devoted to the properties of the generation of spin-triplet Cooper pairs at the S/F interface that ensure the most efficient interplay between superconductivity and ferromagnetism, including in systems with full spin-polarization of bands (semimetals) and considerable spin–orbit coupling. Problems with the electrodynamics of S/F structures, which have not been covered by previous reviews on superconducting spintronics, are discussed in detail, including the features of the formation of inhomogeneous superconducting and magnetic states due to spin–orbit coupling, long-range triplet correlations in ferromagnets, the electrodynamic proximity effect, and Larkin–Ovchinnikov–Fulde–Ferrell-type instability with a modulation vector in the plane of S/F structure layers. We also discuss the current state of experimental work and promising theoretical concepts and problems relevant to the further development of superconducting spintronics.

Keywords: proximity effect, electromagnetic response, singlet and triplet superconducting correlations, hybrid superconductor–ferromagnet structures, spin-orbit coupling

A S Mel'nikov [1, 2, a], **S V Mironov** [1], **A V Samokhvalov** [1, 2, b], **A I Buzdin** [3]

[1] Institute for Physics of Microstructures, Russian Academy of Sciences, 603950 Nizhny Novgorod, GSP-105, Russian Federation

[2] National Research Lobachevsky State University of Nizhni Novgorod, prosp. Gagarina 23, 603950 Nizhny Novgorod, Russian Federation

[3] Université de Bordeaux, LOMA UMR-CNRS 5798, F-33405 Talence Cedex, France

E-mail: [a] melnikov@ipmras.ru, [b] samokh@ipmras.ru

Received 4 June 2021, revised 7 July 2021
Uspekhi Fizicheskikh Nauk **192** (12) 1339 – 1384 (2022)
Translated by S Alekseev

1. Introduction

The competition between two antagonistic phenomena — superconductivity (S) and ferromagnetism (F) — has attracted the attention of researchers for more than half a century. The importance of this problem was discussed as early as the 1950s in the pioneering work of Ginzburg [1]. The mutual antagonism of superconductivity and ferromagnetism obviously follows from the fundamental property of the

superconducting state of metals, the Meissner effect. The persistent currents of superconducting electrons, which are responsible for screening external magnetic fields, have a destructive effect on superconductivity itself, which disappears when the applied magnetic field exceeds a certain threshold. Any magnetic material is a natural source of magnetic fields, which should therefore destroy the superfluid state of electrons in the material. This argument illustrates the so-called electromagnetic (or orbital) mechanism of competition between superconductivity and magnetism. This interaction should significantly hinder the simultaneous coexistence of these phenomena in natural materials or artificial structures.

In [1], Ginzburg analyzed the London electrodynamics of a ferromagnetic superconductor in detail, calculated the distribution of superconducting currents compensating the magnetization currents, and constructed phase diagrams of ferromagnetic superconductors in external fields. The back reaction of superconductivity on ferromagnetism in the framework of the orbital mechanism was first discussed in [2–4].

The advent of a microscopic theory of a superconducting state (the Bardeen–Cooper–Schrieffer theory) allowed establishing an even stronger mechanism [5] that hinders the emergence of superconductivity on the background of a developed ferromagnetic state due to the exchange interaction between the spins of conduction electrons and the ordered spins of ferromagnet electrons. The exchange field of the ferromagnet tends to orient the electron spins in one direction, which obviously conflicts with the formation mechanism of singlet Cooper pairs from electrons with opposite spins in a standard s-pairing superconductor [6]. It is the exchange interaction that is responsible for the strong suppression of superconductivity by magnetic impurities. It was shown experimentally in [5] that even a very small (of the order of a few percent) relative concentration of magnetic atoms is sufficient for the complete destruction of the superconducting order.

The influence of the exchange field and magnetic scattering on superconducting pairing was first analyzed in [7, 8]. The effect exerted by magnetic impurities on superconducting properties is described within the now classical Abrikosov–Gor'kov theory [9]. As in the case of the orbital mechanism, the interaction of ferromagnetism and superconductivity in the framework of the exchange mechanism is also mutual, which suppresses magnetism in the superconducting state [10]. As a result, ferromagnetic superconductors can exist as natural materials either at a sufficiently low Curie temperature [11, 12] or in very exotic situations where the interaction of electrons gives rise to triplet Cooper pairs (formed by electrons with codirectional spins) [13, 14]. In contrast to the electron–phonon (Cooper) pairing mechanism, which is decisive in standard s-wave superconductors, the most probable pairing mechanism in triplet superconductors is related to the interaction between electrons and magnons [15]. We note that the possibility of electron pairing due to magnetic excitations has been actively discussed as a superconductivity mechanism in strongly correlated systems, including high-temperature superconductors (HTSCs) (see, e.g., [16–21]).

The mentioned effects of competition between superconductivity and magnetism are very difficult to observe in natural materials (see, e.g., reviews [22, 23]), which not only complicates experimental work in this field but also creates an apparently obvious obstruction to the use of these effects in any applications. Nevertheless, we can currently assert that progress in technology and the success of experiments in the early 21st century demonstrated that the competition between superconducting and magnetic states of a substance not only is an intriguing and beautiful physical problem but also offers prospects for practical use in a new class of cryoelectronic devices — solid-state devices operating at cryogenic temperatures. Such unique opportunities become available due to the use of hybrid structures made of interacting ferromagnetic and superconducting subsystems (for example, multilayer thin-film SF structures). Using an external magnetic field to change the magnetic moment distribution opens up the way to directly control the electron spins in a superconductor. The quantum mechanical nature of their motion gives rise to a range of rather nontrivial phenomena, which can be unified under the name of 'superconducting spintronics' (from SPIN TRansport electrONICS) [24, 25].

The idea of using hybrid structures made of combinations of magnetic and superconducting materials separated by insulating or conductive layers as the hardware component of cryoelectronics is underlain by the possibility of controlling superconducting currents by changing the magnetic state of the ferromagnetic subsystem. Of course, such a control method implies the use of rather weak control magnetic fields applied to the system. Advances in modern technology (deposition and lithography techniques) have allowed experimenters and technologists to fabricate and study a very wide class of structures of that sort. Moreover, in the last decade, the flow of work in this direction has been steadily increasing, offering quite realistic prospects for creating prototypes of elements of so-called superconducting spintronics. The use of such devices, despite the need for very low temperatures for their operation, can be quite expedient, because it allows significantly reducing the dissipative losses inherent in devices of conventional (nonsuperconducting) spintronics [26–28].

The electrodynamic and transport properties of hybrid SF structures are essentially determined by the characteristics of the interface between the superconducting and magnetic subsystems. In SF systems with low-transparent insulating barriers at the SF interfaces, which suppress the electron transport between the superconducting and ferromagnetic subsystems, or in systems with ferromagnetic insulators, we should expect the exchange interaction mechanism to be suppressed. The properties of such magnetically coupled superconductor–insulator–ferromagnet structures are described in detail in reviews [29, 30].

The ferromagnetic subsystem is typically characterized by an inhomogeneous spatial distribution of magnetization, i.e., a domain structure. As a consequence, ferromagnet stray fields can also be highly inhomogeneous and ultimately lead to modulation of the density of Cooper pairs. Under certain conditions, the concentration of superconducting carriers can increase near the boundaries of magnetic domains, a phenomenon referred to as domain-wall superconductivity [31, 32]. The formation of localized superconductivity over an extended domain wall can lead to the appearance of a superconducting channel in the sample; the channel position and width can be controlled by changing the temperature T and the external field H perpendicular to the structure surface. The existence of superconducting channels along the domain walls was confirmed experimentally using low-temperature scanning laser microscopy [33] and tunneling spectroscopy [34].

An increase in the transparency of SF interfaces and a corresponding decrease in the resistance of these interfaces lead to the exchange of electrons between the S and F subsystems, which creates conditions for the so-called proximity effect. Penetrating into a ferromagnet, Cooper pairs are acted upon by the exchange field, which tends to destroy the bound state of two electrons. The characteristic decay scale of singlet superconducting correlations in an F metal usually does not exceed 10 nm, even for weak CuNi-type ferromagnets [35]. But in a certain layer near the SF interface, superconducting correlations persist, forming an unusual superconducting state: due to specific quantum mechanical interference, the damping of the wave function of Cooper pairs in a ferromagnet is accompanied by sign-alternating oscillations on a scale of the order of several nanometers. These oscillations arise essentially due to the well-known Larkin–Ovchinnikov–Fulde–Ferrell (LOFF) mechanism [36, 37], which leads to instability of the homogeneous superconducting state in the presence of spin splitting due to the Zeeman or exchange field.

The basic idea underlying the mechanism of the formation of an inhomogeneous superconducting state can be illustrated as follows. The energy shift of the spin subbands, determined by the exchange field h in the ferromagnetic layer, leads to a shift in the momenta of electrons with opposite spins that form a singlet Cooper pair: $k_{\uparrow\downarrow} = k_{\mathrm{F}} \pm h/(\hbar v_{\mathrm{F}})$, where k_{F} is the Fermi wave number and v_{F} is the Fermi velocity. Because a Cooper pair combines electrons of different spin subbands, its total momentum in a ferromagnet is nonzero: $Q = 2h/(\hbar v_{\mathrm{F}})$. The appearance of this momentum actually implies the occurrence of spatial oscillations of the Cooper pair wave function on the scale $\xi_h = \hbar v_{\mathrm{F}}/(2h)$.

We note that the obtained estimate for the oscillation scale is valid only in the clean limit, when the scale ξ_h is small compared to the mean free path ℓ. In the usual LOFF phase (for example, in superconducting films in a parallel magnetic field), scattering by impurities suppresses the LOFF instability [38]. In hybrid structures, wave function oscillations of Cooper pairs in the direction perpendicular to the SF interface are also possible in the dirty limit, i.e., for $\ell \ll \xi_h$. In this case, the oscillation scale can be estimated within the diffusion approach as the characteristic diffusion length $\xi_{\mathrm{f}} \sim \sqrt{Dt}$ for some time t, where D is the electron diffusion coefficient. Taking ξ_h/v_{F} as the characteristic time t, we obtain $\xi_{\mathrm{f}} \sim \sqrt{\hbar D/h}$.

Oscillations of the wave function in a ferromagnet lead to interesting effects arising when the oscillation period and the F-layer thickness are commensurable (see review [39] and references therein). For example, the critical temperature T_{c} of the superconducting transition of an SF bilayer depends on the ferromagnet thickness nonmonotonically [40, 41]. Such a nonmonotonic dependence of T_{c} and reentrant superconductivity [42, 43] have been observed in numerous experiments with layered SF hybrids [44–49].

Oscillations of the wave function in an SFS layered structure (Fig. 1) can also give rise to an unusual π-state [50], in which the equilibrium phase difference equal to π between the order parameters of two superconductors is established and the Josephson current is inverted [51, 52] (see also review [39]). The interference phenomena described by the quantum mechanics of Cooper pairs underlie the principles of operation of the currently best known spintronic devices: Josephson junctions with an inverted relation

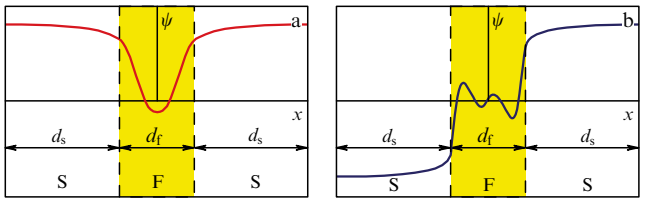

Figure 1. Qualitative behavior of the wave function of Cooper pairs in an SFS Josephson junction in the absence of a potential barrier at the SF interface: (a) 0-type junction, (b) π-type junction.

between the superconducting current and the phase difference of superconducting electrodes (π-contacts) [51–53] and spin valves, in which the critical transition temperature is controlled by the mutual orientation of the magnetic moments in the magnetic subsystem [54–59].

The possibility of forming a weak Josephson coupling of superconducting electrodes through a ferromagnetic layer (SFS junction) and the π phase inversion was predicted in the works of Buzdin and Kupriyanov [51, 52], which had a significant impact on the entire subsequent development in this field. Experimental evidence of the possibility of a superconducting current flowing through a ferromagnet and the formation of a π-state was first obtained by Ryazanov's group (Institute of Solid State Physics, Russian Academy of Sciences) [53]. Later, these results were abundantly confirmed by other groups [60–64].

Figure 1 qualitatively shows the distribution of the wave function of Cooper pairs in an ordinary (0-type) Josephson SFS junction and in a π-junction. The transition between the 0- and π-states of an SFS junction is usually accompanied by a nonmonotonic dependence of the critical current of the SFS transition: the maximum current flowing without dissipation through the Josephson junction depends on the temperature and thickness of the F layer (which was in fact first confirmed experimentally in [53]). Similar Josephson phase inverters and more general engineering of the current–phase relation [65] can be used to design qubits (basic elements for storing information in a quantum computer) [66, 67] and create low-noise SQUID (Superconducting Quantum Interference Device) magnetometers — high-precision devices for magnetic flux measurements [68].

The quantum interference phenomena of Cooper pairs become even more nontrivial in the presence of inhomogeneous exchange fields, e.g., in systems containing several ferromagnetic layers with different orientations of the magnetization vector. If the magnetization in one of the layers is fixed, e.g., with the help of an additional antiferromagnetic layer, then the mutual orientation of the magnetization vectors in the ferromagnetic film can be controlled by applying a relatively weak external magnetic field [54–56, 69].

Variations in the exchange field profile near the superconductor surface have a strong effect on the penetration of Cooper pairs into the ferromagnetic subsystem and hence shift the critical superconducting transition temperature in the entire system. As a result, the temperature dependence of the resistance shifts, and we obtain the potential to effectively control the sample resistance by a weak magnetic field. Such a structure is called a spin valve; it can be classified as a promising element of future cryoelectronic circuits. For most ferromagnetic metals, unfortunately, the critical temperature shift is extremely small (of the order of a fraction of a degree). We note, however, that the shift increases signifi-

cantly (see [70–73]) when using ferromagnets whose exchange energy exceeds the Fermi energy.

We note that the overall manifestations of the proximity effect in SF systems change significantly if materials with an extremely strong spin polarization of conduction electrons are used as a ferromagnet. Such materials are often called half-metal ferromagnets or half-metals (HMs) [74–78]. Such materials have nonzero conductivity for electrons with one of the possible spin projections on the exchange field direction and are simultaneously insulators or semiconductors for electrons with the opposite spin projection. As a result, singlet Cooper pairs formed by electrons with opposite spins cannot directly penetrate from the superconductor into the HM, and the proximity effect between these materials is suppressed.

At the same time, a number of experiments suggest the penetration of Cooper pairs into HMs to distances comparable to the scale of penetration of pairs into normal metals. The traditional explanation for this effect is based on the assumption that local inhomogeneities in the direction of the exchange field arise at the HM boundary, making the boundary spin-active (when crossing it, the spin state of the electron changes) and thereby leading to the generation of long-range triplet correlations with the spin projection $s_z = \pm\hbar$. Moreover, if both electron spins are directed along the HM quantization axis ($s_z = \hbar$), then the corresponding superconducting correlations penetrate into the HM, and if both spins are directed against the quantization axis ($s_z = -\hbar$), then the penetration of correlations is impossible. To date, the study of the superconducting proximity effect with HMs has become one of the most actively developing fields in superconducting spintronics.

We note that the problem of discrepancy between the experimentally detected penetration depth of superconducting correlations in ferromagnetic materials and theoretical estimates is typical not solely for HMs (see review [79]). Indeed, based on the simplest estimate of the depth of penetration of superconducting correlations into a dirty ferromagnet $\xi_f \sim \sqrt{\hbar D_f/h}$, where D_f is the diffusion coefficient in a ferromagnet and h is the exchange field, we cannot explain the experimental evidence [80–89] on the observation of an anomalously long (up to 0.5 μm) decay length of superconducting correlations in an F metal. Various mechanisms of generation of spin-triplet pairs from electrons with the same spin projection on the quantization axis are usually considered in order to explain such an anomalous proximity effect and long-range interaction [90–92] (see also reviews [93, 94]).

The presence of induced triplet correlations in a ferromagnet and the related features of the proximity effect between a superconductor and a ferromagnet manifest themselves, in particular, in the screening properties of hybrid SF structures. At a temperature T close to the critical temperature T_c, the effective penetration depth Λ of the magnetic field is determined by the average density of singlet, $\langle n_s\rangle$, and triplet, $\langle n_t\rangle$, pairs [79]: $\Lambda^{-1} \propto \langle n_s\rangle - \langle n_t\rangle$. Here, n_s and n_t are the local densities of singlet and triplet correlations. Because the singlet and triplet superconducting correlations behave in a significantly different manner in a ferromagnet, the local supercurrent density $\mathbf{j}_s = -e^2(n_s - n_t)\mathbf{A}/(mc)$ can become locally paramagnetic in domains where triplet correlations dominate ($n_t > n_s$).

Generally, we note that the study of the electrodynamic response of SF structures provides unique opportunities both for elucidating the fundamental physics of the proximity effect and for developing effective methods to test the properties of prototypes of superconducting spintronic devices. An important problem here is the inverse proximity effect, which amounts to taking the inverse effect of a ferromagnet on Cooper pairs into account in the superconducting subsystem. The inverse effect arises due to both the spin mechanism [10] and the orbital (electromagnetic) effect [2–4]. The observed manifestations of the inverse effect of a magnet on a superconductor are associated with both the spontaneous currents generated in the superconductor and a possible instability with respect to the appearance of a spatially modulated density of Cooper pairs in the plane of the superconducting layers. This instability, which is similar to the LOFF instability [36, 37], can significantly change the characteristics of SF hybrid structures.

Let us take special note of a number of important manifestations of the proximity effect associated with the influence of the spin–orbit (SO) coupling on superconducting correlations in SF structures, in particular, the Rashba-type interaction [95] arising at the interfaces of SF structures. Spin–orbit effects can lead to both new mechanisms of excitation of spontaneous currents and the formation of an anisotropic structure of superconducting correlations in momentum space, more specifically, p-type correlations. The combined effect of a strong exchange field and SO coupling leads to a topological transition and the formation of so-called Majorana states, which are widely discussed in the literature in the context of the implementation of topologically protected quantum computing [96, 97]. We note that SO coupling can also provide conditions for the appearance of so-called phi-contacts with a spontaneous phase difference between superconducting electrodes in the ground state.

Even a fairly brief description of some of the most interesting, in our opinion, areas of modern research in the field of superconducting spintronics should convince the reader that this area has indeed become a hot topic in condensed matter physics. Writing this review therefore looks well justified and timely. The purpose of the review is to acquaint *Physics–Uspekhi* readers in more detail with some of the most important results in the field of superconducting spintronics, paying special attention to the effects that are of interest to a general physical audience. The structure of the review is as follows. In Section 2, we discuss the best known types of superconducting spintronic devices in somewhat greater detail than in the Introduction. Being more specific about the subjects of study allows us to relate the further presentation of physical effects to possible applications. Section 3 is devoted to the rather intriguing problem of long-range effects in the propagation of superconducting correlations in a ferromagnet. The electrodynamics of SF structures is discussed in Section 4. Section 5 contains a description of the modern experimental and theoretical situation as regards the use of ferromagnetic metals with extremely strong spin polarization of conducting electrons in superconducting spintronics. In Section 6, we recapitulate and briefly discuss possible prospects for the development of the physics of SF systems. In Appendix A, for the convenience of the reader, we provide a brief summary of the main theoretical approaches that are used in the theory of the proximity effect in SF systems, which allows us to refer to the equations of the basic theory when presenting theoretical results in the main body of the paper.

2. Devices of superconducting spintronics

Although research of hybrid systems is still mainly focused on studying the fundamental problems of the interplay between superconductivity and ferromagnetism, applied superconducting electronics and spintronics are currently undergoing rapid development, motivated by the urgent need for cryogenic memory for quantum logic devices and by designing new applications that involve superconducting qubits. Superconducting spintronics allows producing circuits in which logical operations controlled by spin currents can be performed faster and with higher energy efficiency [28, 98] than analogous operations based on charge transfer in semiconducting devices [99]. The potential possibilities and properties of hybrid SF systems, which are not shared by superconductors and ferromagnets taken separately, motivate applied interest in such structures, in particular, due to the prospects of their use as elements of superconducting computational schemes [66, 67] or other devices with tunable transport and magnetic properties based on spin-polarized supercurrent [26, 79].

In Sections 2.1–2.3, we consider possible solutions and examples of devices that can be useful for developments in the field of superconducting spintronics.

2.1 Spin valves

The foundations of the theory of superconducting spin valves were laid in the works of the groups of Tagirov, Buzdin, and Beasley [54–56], where it was shown that the relative orientation of the magnetizations $\mathbf{M}_{1,2}$ in neighboring ferromagnetic layers in three-layer structures F_1F_2S [56] (Fig. 2a) or F_1SF_2 [54, 55] (Fig. 2b) can have a significant effect on the critical temperature T_c of the superconducting transition. With suitably chosen structure parameters, the difference between critical temperatures of the superconducting transition in the cases of codirectional, $T_c^{\uparrow\uparrow}$, and oppositely directed, $T_c^{\uparrow\downarrow}$, magnetizations in F-layers can easily be observed. Because the structure-averaged exchange field for a configuration with oppositely directed magnetizations is obviously smaller than for a configuration with codirectional magnetizations, it is natural to expect that $T_c^{\uparrow\downarrow} > T_c^{\uparrow\uparrow}$.

Such hybrid SF structures are analogous to a conventional spin valve [99] with the normal (N) metal layer replaced with a superconducting one; they have a colossal magnetoresistance when the system switches from the normal (resistive) state to the superconducting state and are therefore promising devices for controlling electron transport by relatively weak external magnetic fields.

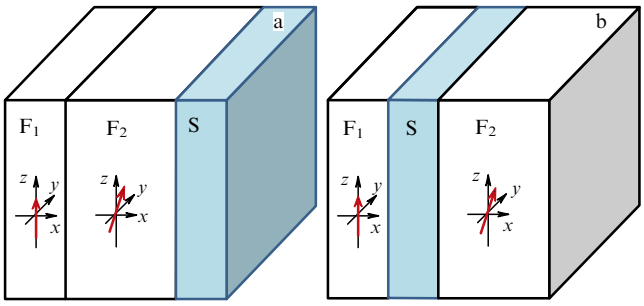

Figure 2. Variants of superconducting valves: (a) F_1F_2S structures; (b) F_1SF_2 structures.

The effect of the mutual orientation of the F-layer magnetizations on T_c has been convincingly confirmed experimentally for F_1SF_2 structures with a weak solution of CuNi as a ferromagnet [57, 58]. But the measured values of $\Delta T_c = T_c^{\uparrow\downarrow} - T_c^{\uparrow\uparrow}$ turned out to be much less than predicted and did not exceed the superconducting transition width δT_c, thus failing to ensure complete switching between the normal and superconducting states. The use of strong ferromagnetic metals (Fe and Ni) in such structures made it possible to somewhat increase ΔT_c [100, 101] and even to realize the case $\Delta T_c \gtrsim \delta T_c$ [102] corresponding to infinite magnetoresistance. In some cases, an unusual decrease in the critical temperature was observed when the codirectional magnetization orientation in the F-layers was replaced with an oppositely directed one ($T_c^{\uparrow\downarrow} < T_c^{\uparrow\uparrow}$), which was called the inverse spin-valve effect [103–108]. This behavior, which contradicts the original ideas [54, 55], can be caused by, among other things, the effect of stray fields of magnetic domains in ferromagnetic layers, which depend on the mutual orientation of their magnetizations [109, 110].

More encouraging results were obtained with F_1F_2S systems, in which, using the thin-film heterostructure CoO_x/Fe/Cu/Fe/In as an example, the complete switching between the normal and superconducting states was observed, ensuring the relation $\Delta T_c > \delta T_c$ [111, 112]. Further studies showed that both usual ($T_c^{\uparrow\downarrow} > T_c^{\uparrow\uparrow}$) and inverse ($T_c^{\uparrow\downarrow} < T_c^{\uparrow\uparrow}$) spin-valve effects are possible in such hybrid structures, depending on the thickness of the ferromagnetic layer F_2 [113, 114]. The change of sign of the spin-valve effect and ΔT_c oscillations with a change in the F_2 layer thickness is explained by the interference of the wave function of Cooper pairs in the ferromagnetic layer in the vicinity of the SF interface [115]. The physics of hybrid SF structures with several F layers becomes even more nontrivial and diverse if the magnetizations in the layers are noncollinear. In this case, superconducting correlations contain odd in the Matsubara frequency spin-triplet components with the spin projection $s_z = \pm\hbar$ on the quantization axis, which are not destroyed by the exchange field, and decay weakly in a ferromagnetic metal on the scale of the correlation length ξ_n [90, 92] (see also reviews [93, 94]).

The appearance of long-range spin-triplet correlations creates an additional mechanism for superconductivity suppression, such that the minimum of the dependence $T_c(\theta)$ can correspond to a noncollinear configuration with $\theta \neq 0, \pi$ (the triplet spin-valve effect). The possibility of the triplet spin-valve effect for diffusive F_1F_2S systems (dirty limit) was shown theoretically in [115] and confirmed experimentally using CoO/Fe/Cu/Fe/Pl [59] and Nb/CuNi/Nb/Co/CoO_x [116] structures. Numerical calculations based on a self-consistent solution of the Bogoliubov–de Gennes (BdG) equations (see Appendix A.1) for F_1F_2S ballistic conduction systems (clean limit) also confirmed the possibility of a nonmonotonic $T_c(\theta)$ dependence for $0 \leqslant \theta \leqslant \pi$ [117]. Issues related to the physics of the long-range triplet proximity effect are discussed in more detail in Section 3.

For F_1SF_2 spin valves, calculations performed for symmetric FSF structures (with identical ferromagnetic layers) predict only the usual spin-valve effect, with $T_c^{\uparrow\downarrow} > T_c^{\uparrow\uparrow}$ in both dirty [54, 55, 118–120] and clean [121–123] limits. Numerical calculations of the critical temperature of asymmetric F_1SF_2 structures in the dirty limit [124, 125] showed that $T_c(\theta)$ increases monotonically as the misorienta-

tion angle θ increases ($0 \leqslant \theta \leqslant \pi$), which means that the usual spin-valve effect is also preserved in this case. For hybrid FSF structures with atomic layers, the configuration with oppositely directed magnetic moments in F layers turns out to be preferable for the appearance of superconductivity and has a higher T_c [126, 127], except in the case of band inversion in strong ferromagnets due to spin splitting [128].

At the same time, the results of experimental studies of F_1SF_2 spin valves look less conclusive. Although most experiments with F_1SF_2 structures, in agreement with the theory, demonstrated only the usual spin-valve effect [57, 58, 100, 101, 129–132] and a monotonically increasing $T_c(\theta)$ for θ increasing from 0 to π [133], some instances of the structure parameter selection led to the inverse spin-valve effect, with $T_c^{\uparrow\downarrow} < T_c^{\uparrow\uparrow}$ [104–108, 134]. A change of sign of the spin-valve effect can be achieved, for example, by adding spin-active layers between the superconductor and the ferromagnet [135]. To reliably control the relative directions of magnetization in the layer plane, an additional antiferromagnet layer and/or magnetic anisotropy are typically used. The maximum suppression of the critical temperature ΔT_c achieved in such structures varies from 20 mK for diffuse systems [59, 136, 137] to 120 mK when using thin ballistic layers of strong ferromagnets [138]. Explanations of the inverse spin-valve effect in three-layer F_1SF_2 diffusive structures usually invoke additional assumptions that lie outside the standard theory of the proximity effect at the SF interface. In the case of strong ferromagnets, a configuration with mutually opposite directions of magnetic moments in the F layers should lead to the accumulation of spin-polarized quasiparticles in the S layer due to the relatively low probability of quasiparticle transition between the F layers [104]. The inverse spin-valve effect can also be caused by a parasitic field from the domain walls in ferromagnets [105, 110] or by dissipative motion of vortices induced by the domain walls [109]. In the case of asymmetric three-layer F_1SF_2 structures with ballistic transport, in addition to the usual effect, the inverse and triplet spin-valve effects are possible for suitably selected thicknesses of the ferromagnetic layers [139].

Relatively recent advances in the physics of SF structures demonstrating spin valve properties include the implementation of a complete switching from the superconducting state to the normal state and back by a weak external magnetic field [111], the triplet and inverse spin-valve effects, demonstrated in the works of Garifullin's and Tagirov's groups [59, 112, 116, 138, 140] (see review [141] for details), and the magnetic memory effect [28, 142].

Summarizing, we can conclude that the spin-valve effect in SFF and FSF systems has been studied quite well both experimentally and theoretically. The dependence of the critical temperature of the superconducting layer on the misorientation angle of magnetic moments in ferromagnetic layers is determined by three main factors. First, the suppression of the critical temperature T_c occurs due to the exchange field in ferromagnets, which destroys the spin structure of Cooper pairs. Second, an increase in the angle θ between the magnetic moments in the F layers leads to a decrease in the average exchange field in the structure, which would suggest a monotonically increasing dependence $T_c(\theta)$. But if the thickness of the ferromagnetic layers exceeds the correlation length ξ_f, then the dependence $T_c(\theta)$ is significantly affected by the interference effects due to the oscillatory behavior of the wave function of Cooper pairs in a ferromagnet. As a result, depending on the ratio between the thickness of the F layers and ξ_f, the maximum of $T_c(\theta)$ can correspond to both codirectional and oppositely directed orientations of the magnetic moments. Finally, the noncollinearity of the magnetic moments leads to the appearance of long-range triplet correlations, which form an additional channel for the escape of Cooper pairs from the superconductor and hence contribute to the suppression of T_c. As a result, the $T_c(\theta)$ dependence can have a minimum at angle $\theta \neq 0, \pi$.

Further progress in improving the characteristics of spin valves is associated with the use of strong ferromagnets with full spin polarization of the bands. For example, a recent experiment in [70] demonstrated a huge increase in the absolute value of the critical temperature shift with a change in the mutual orientation of magnetic moments. We defer a detailed discussion of this subject until Section 5.

2.2 Josephson π-junction

Similar effects also underlie the physics of Josephson SFS junctions containing a ferromagnetic layer sandwiched between two ordinary superconductors in the spin-singlet state. Owing to the proximity effect, the pair wave functions partially penetrate from the superconductors into the ferromagnet, resulting in weak coupling in the overlap region. Sign-alternating damped oscillations of the superconducting wave function in a ferromagnet near the SF interface can lead to the appearance of a spontaneous phase difference π at the electrodes, i.e., to the transition of a Josephson SFS junction to the π state [50] with the current–phase relation $I(\varphi) = |I_c| \sin(\varphi + \pi) = -|I_c| \sin\varphi$ involving an anomalous shift by π.

The transition from the ordinary state (0) to the π-state is implemented by selecting the thickness d_f and/or the exchange energy E_{ex} of the F layer [41, 51, 52, 143]. Experimentally, the formation of the π phase is most often determined by the behavior of the critical temperature T_c of the transition of the hybrid system to the normal state [41, 44, 45] or by measuring the critical current I_c of a Josephson SFS structure [53, 61, 144]. Formally, the change in the ground state of the SFS junction ($0 \leftrightarrows \pi$) is described by the sign change of I_c [51, 52], which should mean a noticeable suppression of the critical current when the junction passes from the 0-phase to the π-phase. The nonmonotonic dependence of the critical current of an SFS junction in the vicinity of the 0–π transition was first observed in [53, 145] and was later measured in more detail in [61, 63]. A noticeable suppression of the critical current under the transition of the junction from the 0-phase to the π-phase can be unobservable due to the strong anharmonicity of the SFS junction, whose current–phase relation

$$I(\varphi) = I_{c1} \sin\varphi + I_{c2} \sin(2\varphi) + \ldots \quad (1)$$

involves significant contributions of the higher harmonics I_{cn} with $n \geqslant 2$ [146–152].

The first successful experimental studies of the Josephson characteristics of SFS junctions were performed with structures where ferromagnetic alloys (CuNi [53, 63] and PdNi [61]) with a relatively weak exchange field $h/k_B \sim 100-500$ K (where k_B is the Boltzmann constant) were used as the ferromagnetic material, which allowed significantly increasing the decay length of singlet pair correlations in the ferromagnet layer and ensured the diffusive leak of the supercurrent through the F layer up to ~ 30 nm in thickness. The presence of a π shift in the

phase difference of the Josephson junction was confirmed by phase-sensitive measurements of the dependence of the critical current of a superconducting interferometer on the magnetic field [153, 154] and direct measurements of the current–phase relation of the SFS junction [155]. The advantage of using weak ferromagnets is that the low Curie temperature T_{Curie} and the presence of magnetic inhomogeneities in the alloys [156, 157], leading to spin-flip scattering, allow observing several 0–π transitions at a fixed temperature and a temperature transition between 0 and π states in the same device [144].

A signature of the formation of a π-state is the generation of a spontaneous direct current in a superconducting ring with an odd number of π-junctions [50], which is accompanied by the appearance of a state with a 'trapped' half-quantum $\Phi_0/2$ magnetic flux [158, 159]. Because the ground state of such a ring is doubly degenerate with respect to the direction of the spontaneous current and the magnetic flux, π-junctions were proposed as one of the main elements of a superconducting qubit [68, 160, 161].

The use of ferromagnets (Fe, Co, and Py) with a higher T_{Curie} and a strong exchange field as an F metal requires very thin F layers ($\sim$ 2–10 nm) for observing the Josephson junction transition to the π-state [64, 162–164]. A detailed study of the transport properties of the Nb/Co/Nb junction under the $0-\pi$ transition showed that current–phase relation (1) involves a significant contribution of the second harmonic $I_{c2}\sin(2\varphi)$ [64]; the sign of its amplitude I_{c2} determines the order of the phase transition between the 0- and π-states of the SFS Josephson junction (for $I_{c2} > 0$, the transition between the 0 and π states is first-order) [146, 147, 149].

An effective decrease in the exchange energy, which leads to an increase in the characteristic decay scale and in the period of oscillations of the pair wave function, can be achieved by using two-layer (three-layer) structures made of normal and ferromagnetic metals to ensure a weak coupling between superconducting electrodes such that the supercurrent is directed along the FN interface [165–168] (Fig. 3). Experimental realization of such structures in planar geometry showed that the Josephson effect persists in them when the weak-link length is much longer than the coherence length determined by the exchange field of the ferromagnet [169].

The effect of additional normal and/or insulating (I) layers between a superconductor and a ferromagnet was studied in detail theoretically in [170]. It was found that even a thin additional normal conducting layer can shift the position of the $0-\pi$ transition toward higher or lower ferromagnet thicknesses, depending on the conducting properties, while the presence of an insulating layer can greatly reduce the F-layer thickness ensuring the $0-\pi$ transition [170–172]. In S/F/I/S tunneling Josephson structures, evidence of π-state formation is the inversion of the spectrum of the density of states (DOS) and of tunneling conductivity [173] observed in experiments [60, 62, 174, 175]. The possibility of forming the π-state in SFS tunnel junctions by replacing the composite F/I layer with a ferromagnetic insulator (FI) was theoretically shown in [176] and discussed further in [177, 178]. The creation of S/FI/S type Josephson devices is typically hindered by the large effective spin polarization of the barrier [179], which prevents the tunneling of singlet pairs. It may be promising to use the magnetically soft GdN insulator as an F barrier [180]. It has been shown that NbN/GdN/NbN structures with such a barrier have a significant critical current and a high spin polarization, which allows using them as a Josephson spin valve [181, 182].

In recent years, special interest has been attracted to Josephson devices based on SFS structures with an inhomogeneous exchange field, allowing long-range spin-triplet correlations. To create conditions for such correlations, the interlayer between superconducting electrodes was realized, for example, by multilayer F_1FF_2 structures with noncollinear magnetic moments in the different ferromagnetic layers [88, 183–188] (Fig. 4) or by rare-earth ferromagnets (Ho and Gd), which have their intrinsic magnetic texture [88, 189–193]. Long-range spin-triplet correlations can also arise in the presence of magnetization rotation in a domain wall [90, 92, 194–196] or in a magnetic vortex [197, 198]. Significant conversion into triplet pairs is also possible on a spin-active FS interface [199–201]. In the case of an SF_1FF_2S junction, the triplet component of the pair function is formed by a thin ($\sim \xi_f$) ferromagnet layer between the superconducting electrode and a thick ($\gg \xi_f$) central domain with noncollinear magnetization. Experiments in [88, 186, 188, 202] showed that the triplet Josephson current noticeably increases upon increasing the magnetization misorientation angle between the outer and central layers (F_1F and FF_2). We emphasize that the long-range effect is ensured here by the propagation of the triplet correlations of electrons with parallel spins, and the use of the F_1F bilayer as a ferromagnetic barrier in the SFS junction is insufficient for the formation of a long-range triplet Josephson current [203–205]. The strong dependence of the supercurrent amplitude and phase on the misorienta-

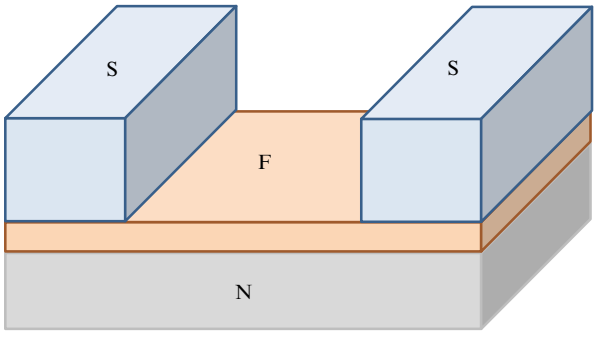

Figure 3. Weakly coupled planar S/FN/S Josephson junction made of a two-layer structure of normal (N) and ferromagnetic (F) metals.

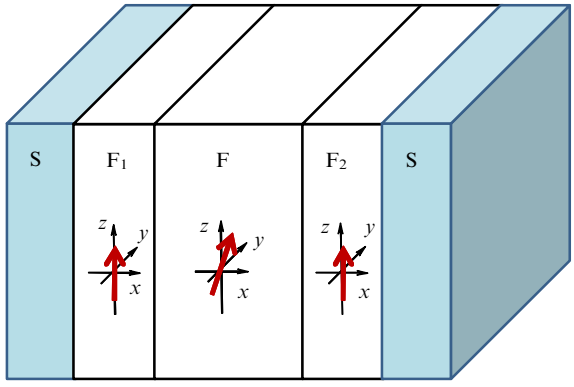

Figure 4. Josephson junction based on a multilayer F_1FF_2 ferromagnetic structure.

tion angle of the magnetization of the outer layers allows controlling the transition between the 0- and π-states of such a junction [199, 206, 207].

An inhomogeneous exchange field **h** can also contribute to the long-range effect in Josephson SFS structures in the clean limit, when the characteristic mean free path of electrons in a ferromagnet noticeably exceeds its dimensions [195, 203, 204]. The method proposed and studied in [208] allows controlling the critical current and the $0-\pi$ transition of a weak SFS link between singlet superconductors by creating a small-scale noncollinear exchange field texture in a ferromagnet, which changes the spin structure of propagating Cooper pairs.

We note that, when using ferromagnets as a barrier, the effect of the magnetic flux created by the F layer in the transition region must be taken into account (except when the magnetization is orthogonal to the barrier); it leads to an additional shift in the Fraunhofer pattern — the dependence of the contact critical current I_c on the external magnetic field H. The dependence $I_c(H)$ becomes hysteretic if the field H exceeds the coercivity field of the ferromagnet [209, 210], thereby allowing such SFS junctions to be used as Josephson magnetic switches or memory elements [211–218]. Compensation of the magnetic flux, whenever necessary, can be achieved by using a composite three-layer F/N/F ferromagnet with antiferromagnetically ordered F layers as a barrier [219]. Switching between the ferromagnetic and antiferromagnetic configurations of the F layers allows significantly affecting the critical current of S/F/N/F/S ballistic junctions [89, 90, 220].

2.3 Josephson φ_0-junction. Phase batteries and Josephson diodes

In recent years, attention has been attracted to the possibility of implementing Josephson junctions with an arbitrary phase difference in the ground state [221–223], described by the current–phase relation $I(\varphi) = I_c \sin(\varphi + \varphi_0)$, with the Josephson energy minimum $E_J = [\hbar I_c/(2e)][1 - \cos(\varphi + \varphi_0)]$ corresponding to an arbitrary phase difference $\varphi = -\varphi_0$ $(0 < \varphi_0 < \pi)$.

A Josephson junction with such unusual properties can be implemented on the basis of (a) junctions in which the $0-\pi$ modulation of the phase difference is formed artificially and the ground state is realized with an arbitrary value of the averaged Josephson phase difference φ [221, 224]; (b) junctions with a sufficiently large second harmonic in the current–phase relation $I(\varphi) = I_{c1}\sin\varphi + I_{c2}\sin(2\varphi)$ if $I_{c2} < 0$ and the first harmonic is considerably suppressed ($|I_{c2}| \sim |I_{c1}|$) [222]; (c) junctions in which charge transport between superconducting electrodes occurs through a magnetic system with SO coupling [223]; (d) junctions with an inhomogeneous distribution of the exchange field in the F layer [225] or spin-active interfaces [226, 227]; (e) junctions in which the superconducting electrodes are separated by an antiferromagnet with uncompensated magnetic moments in the sublattices [228]; and (f) junctions with HM layers, i.e., ferromagnets with the full spin polarization of electrons [199, 229–235].

Such φ_0 junctions with an anomalous Josephson effect have good prospects for use in superconducting electronics [68, 161, 236–240]. The creation of φ_0 junctions allows implementing various designs of so-called phase batteries [26, 241, 242], which provide phase shifts in superconducting circuits. An example of such device consisting of a superconducting ring partially covered with a ferromagnet has been recently proposed in Ref. [243]. A tunable phase battery based on a combination of SO coupling and exchange interaction in an InAs nanowire was recently implemented in [244].

We note that to have a nontrivial current–phase relation in the form $I(\varphi) = I_c \sin(\varphi + \varphi_0)$ (i.e., to be a φ_0-junction) the system should satisfy certain symmetry conditions formulated in [245]. Time reversal symmetry imposes a general constraint on the form of the current–phase dependence of Josephson junctions: it must satisfy the condition $I(\varphi, \mathbf{M}) = -I(-\varphi, -\mathbf{M})$. The necessary conditions for the realization of a nontrivial ground state for $\varphi = -\varphi_0 \neq 0, \pi$ are a noncoplanar distribution of the magnetization and symmetry breaking with respect to the magnetization inversion in the expression for the superconducting current, $I(\varphi, \mathbf{M}) \neq I(\varphi, -\mathbf{M})$. The authors showed that this symmetry can be absent in the general case, even if it is preserved in the semiclassical approximation. The conditions under which the $I(\varphi, \mathbf{M}) = I(\varphi, -\mathbf{M})$ symmetry is violated in diffusive structures and the associated appearance of an anomalous phase φ_0 were discussed in detail in recent review [246].

The φ_0 ground state of the Josephson junction was studied experimentally, for example, in an asymmetric $0-\pi$ SFS transition with a variable thickness of the ferromagnetic layer [247, 248]. The anomalous Josephson effect with a tunable phase shift was also implemented in [249] based on InAs/Al junctions. New options for creating Josephson φ_0 junctions have emerged due to progress in the synthesis of hybrid superconducting structures with strong SO coupling [250] and junctions based on topological insulators [251] with broken spatial inversion symmetry [252, 253].

Obviously, the violation of spatial inversion symmetry can lead to the appearance of a peculiar diode effect in the transport characteristics of Josephson junctions: the superconducting critical current of the junction depends on the direction of the current. Such a diode effect has been predicted theoretically for a variety of Josephson structures, including topological junctions on helicoidal edge states [254], SF systems with spin-active interfaces [226, 227], and junctions based on multichannel semiconducting wires with a strong SO coupling and Zeeman splitting in an external magnetic field [255]. Changes in the geometry of single-channel semiconducting wires with induced superconductivity can be attended by a spontaneous phase difference [256–258] and a diode effect [259] (also see review [260]). A superconducting diode was recently implemented experimentally on the basis of Nb/Va/Ta superlattices [261].

3. Long-range superconducting correlations in ferromagnets

The brief review of the options for superconducting spintronics devices and their operating principles presented in Section 2 shows that all of them are highly sensitive to quantum mechanical interference effects of the wave functions of Cooper pairs, which in turn strongly depend on the characteristic scales of penetration of correlations into a ferromagnet. The simplest estimates of these scales in the dirty limit given in the Introduction firmly suggest that they are small at realistic values of the exchange fields, which should apparently impose significant constraints on the admissible thicknesses of ferromagnetic layers and create additional technological difficulties. At the same time, a number of experiments are known [80–89] to have observed

the so-called long-range proximity effect in a ferromagnet: the propagation of superconducting correlations over anomalously large distances in ferromagnetic metals, contrary to traditional ideas about the strong suppression of singlet superconductivity by the exchange field.

Experimental data testify that superconducting correlations are preserved at distances comparable to the coherence length ξ_n in a normal (nonmagnetic) metal. For example, in Co/Al [80] and Ni/Al [81] hybrid structures, the effect of superconducting correlations on the ferromagnet conductivity was preserved at distances from the SF interface much longer than the typical scale of the proximity effect for the singlet component. In the experiments in [84], a considerable supercurrent was observed to flow through a thin cobalt wire about 0.5 μm in length, which is several orders of magnitude greater than the characteristic decay length of the singlet superconducting correlations in cobalt. A strong Josephson effect was revealed in SFS structures with an inhomogeneous ferromagnetic layer and with a total thickness much larger than the characteristic scale ξ_f [83, 88, 188]. Such a mysterious discrepancy between theoretical estimates and experimental results, as well as the need for an appropriate description and explanation for long-range effects, gave rise to a large number of theoretical papers [90, 92, 187, 194, 195, 197, 198, 208, 262–267] proposing various mechanisms underlying the long-range proximity effect.

Before proceeding to elucidate the physics behind the possible increase in the penetration length of superconducting correlations in a ferromagnet, we must consider the standard mechanisms for suppressing these correlations by an exchange field in more detail. As in the case of superconductor–normal-metal structures, the proximity effect at the SF interface can be understood by considering the quantum mechanics of quasiparticle excitations. The occurrence of the proximity effect is associated with the Andreev reflection of quasiparticles [268], which ensures the correlated motion of electrons and holes in the metal and hence a nonzero amplitude of superconducting correlations, even in the absence of a pairing potential [269, 270]. In ferromagnetic metals, quasiparticles acquire an additional exchange energy, depending on the direction of the spin, which strongly affects the process of Andreev reflection [271].

Spin splitting leads to a mismatch by $|\delta q| = |q_{u\uparrow(\downarrow)} - q_{v\downarrow(\uparrow)}| \simeq 2h/(\hbar v_F)$ between the wave vectors of quasiparticles with the energy $\varepsilon \ll h \ll \varepsilon_F$ and opposite directions of the spin projection. The sign of δq is determined by the spin structure of the wave function components u and v relative to the exchange field direction (Fig. 5b) and is reversed in two cases: when the exchange field direction changes, $\mathbf{h} \to -\mathbf{h}$, and when an electron–hole pair is scattered with spin flip.

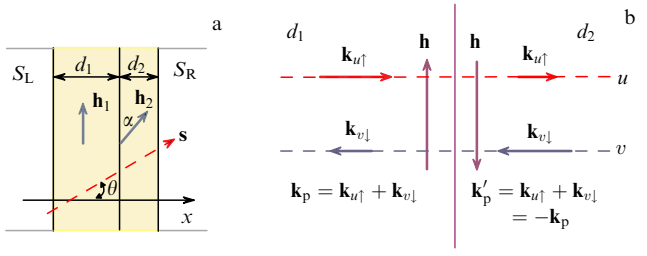

Figure 5. (a) Josephson SFS junction with a ferromagnetic bilayer. Quasiparticle trajectory is shown by a dashed line. (b) Spin structure $\mathbf{q} = \mathbf{k}_{u\uparrow} - \mathbf{k}_{v\downarrow}$ of pair wave function ψ in a ferromagnetic bilayer with opposite directions of exchange fields in the layers. (From [263, 265].)

The action of the exchange field h along a trajectory of length L gives rise to the phase difference $\gamma \sim \delta q\, L = \pm L/\xi_h$ between the u and v components of the wave function ψ, where $\xi_h = \hbar v_F/(2h)$ is the characteristic length determined by the magnitude of the exchange field h [195, 203].

Because the calculation of any measurable values (current density, conductance, etc.) involves averaging over different trajectories, i.e., calculating a superposition of rapidly oscillating contributions $uv^* \sim \exp(i\gamma(L))$ from trajectories of different lengths L, the phase difference between the u and v components of the wave function ψ causes destructive interference of the electron and hole states in the F metal over the characteristic length $\sim 1/\delta q \sim \xi_h$. In clean systems with ballistic transport, this leads to a power-law decrease, with a characteristic scale ξ_h, in the amplitude of superconducting correlations along the direction into the bulk of the F layer. In diffuse (dirty) systems, the calculation of disorder averages leads to expressions of the form $\langle uv^* \rangle \sim \langle \exp(i\gamma(L)) \rangle$, which decay exponentially with the distance from the SF interface [143, 272], with the characteristic length $\xi_f = \sqrt{\hbar D_f/h}$. Inside the F metal, superconducting correlations then decay on the scale ξ_f in accordance with an exponential law.

The destructive phase difference γ created by the exchange field can be significantly reduced or even made equal to zero if the exchange field changes direction along the semiclassical trajectory [195]. In some cases, it is thus possible to achieve complete compensation of the destructive phase difference γ and qualitatively change the behavior of superconducting correlations in a ferromagnet under conditions of the proximity effect. In essence, this compensation is one of the possible ways to ensure the long-range character of superconducting correlations.

An alternative way to eliminate the interference of trajectory contributions to superconducting correlations is to generate triplet correlations with Cooper pair spin projections $\pm\hbar$. The point is that, in the foregoing argument, the products uv^* were assumed to involve the components u and v corresponding to a singlet Cooper pair (the singlet anomalous average). For a triplet Cooper pair with spin projections $\pm\hbar$, the wave function is proportional to the product of the electron and hole components, which no longer contain the above phase factor that causes dephasing between the contributions of individual trajectories to physical quantities. Obviously, such superconducting correlations no longer experience a strong exponential suppression due to the influence of the exchange field.

The generation of spin-triplet pairs with spin projections $\hbar$ and $-\hbar$ on the quantization axis allows resolving the contradiction between superconductivity and ferromagnetism: because such pairs are not destroyed by the exchange field, the depth of penetration of the triplet component into the ferromagnet is much larger than the penetration depth of the singlet component. An important point in implementing such a long-range mechanism is the method of converting singlet Cooper pairs $(\uparrow\downarrow - \downarrow\uparrow)$ formed in the superconductor into triplet pairs $(\uparrow\uparrow)$ and $(\downarrow\downarrow)$ in the ferromagnet. The problem is that correlations of this type are not directly excited by superconducting pairing in a superconductor, but can be generated due to the inhomogeneity of the exchange field [273] or spin-dependent scattering at the SF interfaces. A triplet mechanism for the formation of long-range super-

conducting correlations in SF systems was proposed in [90, 92] (also see review [93]).

It is useful to start our analysis from the discussion of the technical side of describing singlet and triplet correlations within the microscopic approach presented in Appendix A. The wave function of triplet Cooper pairs (or, more precisely, the anomalous Green's function) has three different components corresponding to different values of the spin projection of the Cooper pair on the quantization axis: $s_z = \pm\hbar, 0$. The Cooper pairs with $s_z = \pm\hbar$ have a slowly decaying wave function in a dirty ferromagnet, in contrast to pairs with $s_z = 0$, whose wave function rapidly decays on the ξ_f scale. Physically, this is due to the absence of spin splitting and hence of the decoupling effect of the exchange field on triplet Cooper pairs with $\pm\hbar$ spin projections.

We consider the behavior of the anomalous Green's function

$$\hat{f} = \begin{pmatrix} f_{\uparrow\downarrow} & -f_{\uparrow\uparrow} \\ f_{\downarrow\downarrow} & -f_{\downarrow\uparrow} \end{pmatrix} = f_s + \mathbf{f}_t\boldsymbol{\sigma} = \begin{pmatrix} f_s + f_{tz} & f_{tx} - \mathrm{i}f_{ty} \\ f_{tx} + \mathrm{i}f_{ty} & f_s - f_{tz} \end{pmatrix}, \quad (2)$$

which is a 2×2 matrix in spin space [93, 274, 275], taking a system with the diffusive conductivity type as an example. For simplicity, we restrict ourselves to the case of weak superconducting correlations in a ferromagnet, which are realized either in the vicinity of the critical temperature of the superconducting transition or at a sufficiently low transparency of the SF interfaces. Under these conditions, the singlet (f_s) and triplet ($\mathbf{f}_t$) components of the Matsubara Green's function satisfy the linearized Usadel equations (see Appendix A.4):

$$\hbar D\nabla^2 f_s = 2\omega_n f_s + 2\mathrm{i}\mathbf{h}\mathbf{f}_t\,, \quad (3)$$

$$\hbar D\nabla^2 \mathbf{f}_t = 2\omega_n \mathbf{f}_t + 2\mathrm{i}\mathbf{h} f_s\,. \quad (4)$$

We note that, according to the Pauli principle, the triplet s-wave component induced in a ferromagnet must change sign under time reversal and therefore has an odd frequency dependence (as a function of the Matsubara frequency). Obviously, even a homogeneous exchange field leads to the appearance of a triplet anomalous function such that the vector function $\mathbf{f}_t$ is directed along the exchange field vector $\mathbf{h}$ [274, 275]. But, in accordance with the above equations, the $\mathbf{f}_t$ component experiences an exponential decrease in the direction away from the interface. The decay scale of the $\mathbf{f}_t$ component parallel to $\mathbf{h}$ coincides with the decay scale of the singlet component f_s and is equal to ξ_f.

A totally different spatial dependence arises for the vector function component $\mathbf{f}_t$ orthogonal to $\mathbf{h}$ because it satisfies the Usadel equation that does not contain an exchange field and coincides from this standpoint with the equation for superconducting correlations in normal metal. The decay scale of such correlations therefore coincides with the coherence length $\xi_n = \sqrt{\hbar D/(2\pi T)}$, which is typically much longer than ξ_f for not too small exchange fields h and, moreover, diverges at low temperatures T.

To date, a large amount of experimental evidence has been obtained for the manifestation of a long-range triplet component in hybrid SF systems. Particularly noteworthy are experiments with SFS junctions containing a composite F layer [85–89] where long-range phase coherence and an anomalously strong Josephson current were observed for an F layer thickness significantly exceeding the penetration depth of the singlet component. The possibility of an unusual 'triplet' spin-valve effect in SF_1F_2-type structures was demonstrated in [59, 70, 112, 116, 138, 140, 276] by measuring the dependence of the superconducting transition temperature T_c on the angle between the magnetizations of the ferromagnetic layers. The minimum critical temperature T_c in such structures is attained for a noncollinear orientation of the magnetizations, when the long-range triplet component is generated in the system. Experimental evidence of the transformation of singlet Cooper pairs into triplet pairs was also extracted from DOS measurements in SF systems with different magnetic textures [174, 175, 277].

3.1 Long-range singlet superconducting correlations in a ferromagnet. Clean limit

As we have noted, the destructive phase difference between the electron and hole components of the wave function of singlet states created by the exchange field can be significantly reduced by forming a suitable magnetic texture. The presence of inhomogeneous magnetization can strongly change the proximity effect in SF structures, which can be manifested, for example, in a noticeable increase in the Andreev conductivity of the SF interface [278] and in the DOS in the F layer [279] whenever domain walls are present in a ferromagnet. The effect of compensating the destructive γ phase difference can be seen most clearly in the example of Josephson SFS systems, whose current–phase dependence

$$I(\varphi) = \sum_n I_n(\varphi) = \sum_n I_{cn} \sin(n\varphi) \quad (5)$$

is highly sensitive to inhomogeneities in the F-layer magnetization. In the case of a short junction, the leading contribution to the supercurrent is made by subgap states with an energy depending both on the Josephson phase difference φ and on the additional spin-dependent phase shift γ along a semiclassical trajectory.

Singlet Josephson transport in ballistic SFS structures with domains. Complete compensation of the destructive γ phase difference and the long-range Josephson effect are realized in a clean SFS junction if weak link is implemented in an F bilayer (Fig. 5a) consisting of two ferromagnetic layers (domains) with the same thicknesses $d_1 = d_2 \ll \xi_s$ and with the opposite exchange field directions [195, 203, 280, 281]. The phase gains of the wave functions of quasiparticles during the ballistic passage of each of the layers $\gamma_{1,2}$ then differ only in sign, $\gamma_{1,2} = \pm d_{1,2}/\xi_h$. As a result, the total phase shift in a ferromagnet, $\gamma = \gamma_1 + \gamma_2$, vanishes, as does the destructive effect of the exchange field, and the amplitude of singlet superconducting correlations (the singlet component of the anomalous Green's function) decays toward the bulk of the ferromagnetic bilayer over the same length ξ_n as in a normal metal. This process is qualitatively illustrated in Fig. 5b.

The long-range effect is also preserved in the more general case of a short junction, $d_1, d_2 \ll \xi_s$, when the exchange fields $\mathbf{h}_1$ and $\mathbf{h}_2$ in the layers are equal in magnitude ($|\mathbf{h}_1| = |\mathbf{h}_2| = h$) but are rotated by an arbitrary angle α relative to each other (Fig. 5a). Finding the phase shift γ reduces to solving the linearized Eilenberger equations at the zero Matsubara frequency (see Eqn (B.4) in Appendix B). The first harmonic of the current–phase dependence for a two-dimensional (2D) SFS junction with a bilayer serving as a weak link is given by [263]

$$I_1 = \left[\cos^2\frac{\alpha}{2} I_{c1}\left(\frac{d_1 + d_2}{\xi_h}\right) + \sin^2\frac{\alpha}{2} I_{c1}\left(\frac{d_1 - d_2}{\xi_h}\right)\right] \sin\varphi\,, \quad (6)$$

where I_{c1} is the critical current of the first harmonic of the SFS junction with the F-layer thickness $d = \xi_h \delta$ and a homogeneous exchange field h,

$$I_{c1}(\delta) = \frac{eT_c}{8\hbar} N \left(\frac{\Delta}{T_c}\right)^2 \int_0^{\pi/2} d\theta \cos\theta \cos\left(\frac{\delta}{\cos\theta}\right), \qquad (7)$$

and N is the number of transverse modes in the junction (see Appendix B). The asymptotic form of dependence (7) for $d \gg \xi_h$ ($\delta \gg 1$), calculated in [282], is

$$I_{c1}(\delta) \sim \frac{\sqrt{\pi}}{2} \frac{\cos\delta - \sin\delta}{\sqrt{\delta}}. \qquad (8)$$

Thus, the destructive interference of contributions from different trajectories leads to a power-law decrease in the critical current I_{c1} with an increase in the F-layer thickness d, $I_{c1} \propto d^{-1/2}$ for 2D transitions [282]. Such a slow power-law decrease in the critical current I_{c1} with increasing ferromagnetic layer thickness is specific to Josephson systems in the clean limit. A similar dependence for three-dimensional (3D) transitions was obtained in [51]: $I_{c1} \propto d^{-1}$. In the symmetric case ($d_1 = d_2$), we immediately see from (6) that the amplitude of the long-range component of the Josephson current is

$$I_1^{LR} = \sin^2\frac{\alpha}{2} I_{c1}(0) \sin\varphi, \qquad (9)$$

which is independent of the ferromagnetic bilayer thickness d and is preserved at any nonzero angle α between magnetic moments in the adjacent F layers.

The long-range effect is also observed for the second harmonic $I_2(\varphi)$ in current–phase relation (5) for a ballistic SFS junction with a ferromagnetic bilayer. The amplitude of the long-range component of the supercurrent second harmonic I_{c2}^{LR} oscillates with a change in the F-layer thickness d_2 at a fixed total bilayer thickness $d = d_1 + d_2 \gg \xi_h$ with a period $\sim \xi_h$ and, slowly decreasing, for $d_2 \gg \xi_h$, tends to the value

$$I_{c2}^{LR} = -\frac{a_2 \sin^2\alpha}{2}, \qquad a_2 = -\frac{eT_c}{384\hbar} N \left(\frac{\Delta(T)}{T_c}\right)^4.$$

We note that with the contribution of the second harmonic of current–phase dependence (5) taken into account, the long-range Josephson current in an SFS junction with a ferromagnetic bilayer is also preserved for $d_1 \neq d_2$, $d_{1,2} \gg \xi_h$ [263].

Such a behavior of the supercurrent is typical for even harmonics of the current–phase dependence (5) of a ballistic SFS junction and for a homogeneous F layer with one spin-active interface [266] on which Andreev reflection couples electrons and holes with both identical and opposite spins. Then, compensation of the additional phase shift γ on a semiclassical trajectory can occur due to a change in the spin structure of the wave function $\hat{\psi}$ in the course of spin-flip scattering. It can be expected that, for the compensation effect to appear, an even number of spin-flip reflections of quasiparticles must be taken into account. Each of these reflections, in addition, imparts an additional phase shift to the wave functions of the quasiparticles, as determined by the difference between the superconducting phases in the junction. We thus conclude that the long-range effect should only be expected for even harmonics of current–phase dependence (5).

Using the proposed approach, it can be shown that, in the case of ballistic Josephson transport, even a single domain wall of atomic thickness (Fig. 6a) can provide an effective channel for the supercurrent [195]. For collinear magnetic domains, the contribution to the Josephson current due to the presence of a domain wall in a 2D junction with a thick F layer ($\xi_h \ll d \ll \xi$) is described by the expression

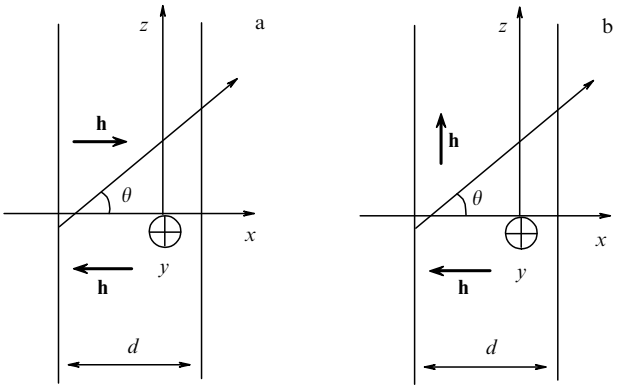

Figure 6. Josephson SFS junction with a domain wall in the $z = 0$ plane. (a) Oppositely directed domain magnetization. (b) Orthogonal magnetization of domains. (From [195].)

$$\delta I \simeq \frac{e\Delta_0^2 k_F \xi_h}{2\pi\hbar T} \sin\frac{d}{\xi_h} \sin\varphi. \qquad (10)$$

The current oscillates with a period $\sim \xi_h$ and decreases with increasing F-layer thickness d (we recall that, in a clean 2D SFS junction without domains, the Josephson current decreases as $\sqrt{\xi_h/d}$ [282]). These results, which are valid in the clean limit, can also be obtained using the approach based on the Eilenberger equations (see formula (A.11) in Appendix A.3) by taking the elastic scattering of quasiparticles on nonmagnetic impurities into account.

In the approach based on the Eilenberger equations, for a moderate impurity concentration $h\tau \gg 1$ (where τ is the time corresponding to the mean free path of electrons), the critical current of the SFS junction simply acquires an additional factor $\exp(-d/\ell)$ [93, 282, 283] (where ℓ is the mean free path of an electron, $\ell = v_F\tau \ll \xi$). The same is true for the domain-wall contribution δI in (10), including in the case of a moderately disordered F layer.

Singlet Josephson transport in ballistic SFS structures with spin-flip scattering. Another way to suppress destructive interference caused by the exchange field of a ferromagnet is associated with a change in the spin structure of propagating Cooper pairs due to scattering [208]. The difference between the phases γ of the electron and hole components of the wave function on a semiclassical trajectory can be significantly reduced if an inhomogeneity of the exchange field **h** is formed that scatters the Cooper pair so as to change its spin structure.

Such a localized inhomogeneity can be created, e.g., by a magnetic probe of an exchange-force microscope or by another source of a strongly inhomogeneous magnetic field that can cause magnetization reversal of part of the ferromagnetic channel with a characteristic size $\sim \xi_h$ (Fig. 7). The region created by the 'magnetic gate' with the direction of the exchange field **h** different from the initial direction gives rise to the long-range singlet component of the Josephson current.

Depending on the parameters of the central domain d_2, the total momentum of the singlet pair $\hbar\mathbf{q} = \hbar\mathbf{k}_\uparrow - \hbar\mathbf{k}_\downarrow$ can

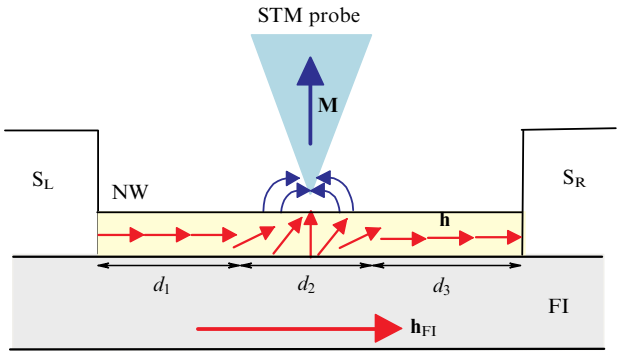

Figure 7. Schematic of the SFS structure under study: thin layer of a normal nonmagnetic metal (nanowire — NW) on the surface of a ferromagnetic insulator (FI), which induces effective exchange field **h** in the metal. Magnetic probe **M** of a scanning tunneling microscope (STM) remagnetizes the domain in the central part of the structure, creating an exchange field inhomogeneity. (From [208].)

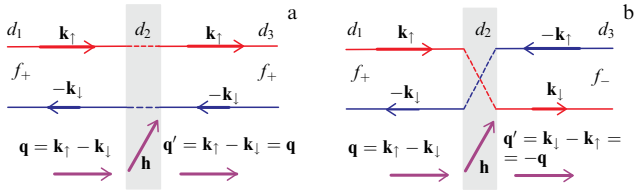

Figure 8. (a) Scattering of a Cooper pair by inhomogeneities of exchange field **h** without electron spin flip. Spin structure of the pair $\mathbf{q} = \mathbf{k}_\uparrow - \mathbf{k}_\downarrow$ remains unchanged with respect to field **h**: $\mathbf{q}' = \mathbf{q}$. (b) Scattering of a Cooper pair by inhomogeneities of the exchange field **h** with electron spin flip. Spin structure of the pair is reversed: $\mathbf{q}' = \mathbf{k}_\downarrow - \mathbf{k}_\uparrow = -\mathbf{q}$. Scattering domain with inhomogeneities of exchange field **h** is highlighted in gray. (From [208].)

either remain unchanged, $\hbar\mathbf{q}' = \hbar\mathbf{q}$ (Fig. 8a), or reverse its direction, $\hbar\mathbf{q}' = -\hbar\mathbf{q}$ (Fig. 8b). In the first case, the spin structure of the pair with respect to the exchange field **h** does not change, and the total phase difference between the electron and hole parts of the wave function $\gamma \approx (d_1 + d_3)/\xi_h$ is large, which leads to strong destructive interference of electron and hole states in the characteristic length $\sim \xi_h$. In the second case (spin-flip scattering), the spin structure of the singlet pair changes to the opposite compared with the exchange field, the phase differences in the d_1 and d_3 regions have opposite signs, and the total phase difference $\gamma \approx (d_1 - d_3)/\xi_h$ depends on the relative position of the scattering domain d_2. With a symmetric arrangement of the scatterer ($d_1 \approx d_3$), the total phase shift γ in the ferromagnet is close to zero, and the destructive effect of the exchange field on the singlet component of the f_s wave function is small or absent altogether.

Thus, the singlet component f_s of the anomalous Green's function in a ferromagnet with a localized inhomogeneity of the exchange field in the middle of the structure decays over the same distance $\xi_n = \sqrt{D_f/(2\pi T_c)} \gg \xi_h$ as in a nonmagnetic metal. This indicates the appearance of long-range Josephson transport in the considered hybrid SFS system. We emphasize once again that in this case we are talking not about the triplet mechanism of long-range effect [90, 92] but about stimulating the supercurrent of singlet pairs.

In Fig. 9, we show examples of calculations of the critical current I_{c1}^{LR} dependence on the displacement x_0 of the central domain relative to the weak-link center

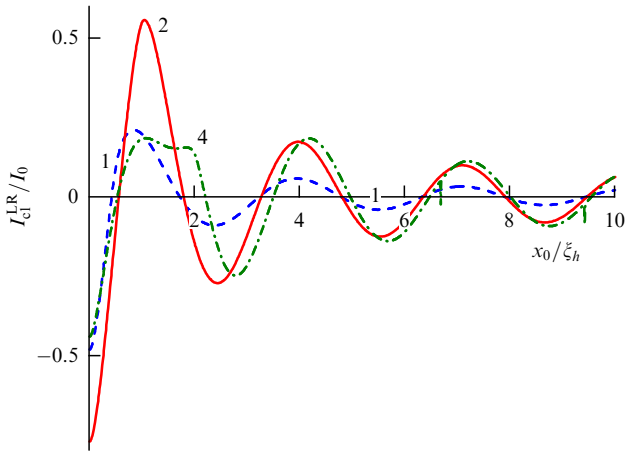

Figure 9. Dependence of the critical current I_{c1}^{LR} on the offset x_0 of the central 90-degree domain d_2 for: $d_2 = \xi_h$ — blue dashed curve; $d_2 = 2\xi_h$ — red solid curve; $d_2 = 4\xi_h$ — green dotted curve. Numbers next to the curve indicate values of d_2/ξ_h. $T = 0.9T_c$, $d = 50\xi_h$, $I_0 = [eT_cN/(8\hbar)](\Delta/T_c)^2$. (From [265].)

for several thicknesses of the 90-degree domain d_2 with a stepped-profile exchange field $\mathbf{h}(x) = h\mathbf{x}_0[0 \leqslant x \leqslant d_1, d - d_3 \leqslant x \leqslant d]; h\mathbf{y}_0[d_1 \leqslant x \leqslant d_1 + d_2]$. The critical current is highly sensitive to the position of the d_2 domain and changes considerably in both magnitude and sign when the domain position changes. When the domain d_2 is displaced away from the center of the structure ($x_0 \neq 0$), a sequence of transitions of the junction from the 0-state to the π-state and vice versa is observed; for a symmetric d_2 domain position ($d_1 = d_3$), $I_1^{LR} < 0$, showing that the SFS structure is a π-junction for the long-range component of the Josephson current.

Thus, by changing the position x_0 of the magnetic probe (and thus the position and properties of the induced inhomogeneity of the exchange field), we can induce a significant change in both the magnitude and sign of the critical current I_{c1} of such a Josephson coupling, i.e., modify the junction current–phase relation $I(\varphi)$ as a whole. An interesting consequence of the strong dependence of the critical current I_c of the SFS structure on the magnetic probe position x_0 is the possibility of effectively manipulating the Josephson transport in SFS systems by acting on the spin structure of the Cooper pair. Under the 0−π transition, as noted above, the first harmonic vanishes ($I_{c1}^{LR} = 0$) and the second harmonic of the current–phase relation becomes dominant.

The simple examples presented above demonstrate the fundamental possibility of significantly changing the characteristic decay scale of the superconducting order parameter in a ferromagnet and hence altering the transport properties of ballistic SFS systems by changing the structure of the exchange field in the ferromagnetic layer along the trajectory of Andreev quasiparticles. A similar effect arises, as noted above, in spin-flip scattering of Cooper pairs in a homogeneous exchange field.

3.2 Long-range triplet superconducting correlations in a ferromagnet. Dirty limit

As we have noted, inhomogeneous magnetization can cause triplet superconducting correlations $\mathbf{f}_t$ that are long range [93] and penetrate into the ferromagnet to the same characteristic depth ξ_n as in the case of normal metal. These long-range triplet superconducting correlations induced by the proximity

effect are odd under time reversal (i.e., odd in the Matsubara frequency) and should lead to a noticeable Josephson effect in SFS structures at a large thickness ($\sim \xi_n$) of the ferromagnetic layer.

We note that pairwise triplet correlations with an odd frequency enhance the DOS [284, 285], which can be observed with tunneling spectroscopy. It has been shown that the proximity effect in FNS or NFS diffusion structures (where N is a normal nonmagnetic metal) with a magnetically active interface or precessing magnetization also leads to the generation of frequency-odd superconducting correlations [286, 287].

The dominant effect of long-range triplet correlations on the Josephson current can be realized in SFS junctions with magnetically active interfaces [199, 206] with narrow domain walls between the superconductor and a thick F layer with noncollinear magnetizations [184, 187, 229, 288, 289] or superconductors with SO coupling [290]. Another type of Josephson SFS system in which long-range interaction is possible is a ferromagnet placed between two superconductors, with a Néel-type domain structure, such that the magnetization vector rotates in the plane parallel to the interface [194, 291, 292].

For the interference of long-range triplet correlations to ensure the supercurrent flow, the weak link must have a complex three-layer F_1FF_2 structure [187] with the magnetic moments in the F_1 and F_2 layers being noncollinear to the magnetic moment of the central F layer. In this case, the F_1 and F_2 layers play the role of a converter that transforms singlet pairs into triplet pairs (and vice versa), and the central layer with a strong ferromagnet acts as a filter that prevents the supercurrent of singlet Cooper pairs.

Convincing experimental evidence of the long-range triplet Josephson effect through a weak link containing a layer of a strong ferromagnet was obtained in [293, 294] using SF_1FF_2S structures. The triplet Josephson effect is also possible in an F_1SFSF_2 structure with thin S layers and a noncollinear texture of magnetic moments in the layers [295]. Because the Josephson current arises only upon interference of the corresponding superconducting correlations induced by the S-electrodes forming the junction, the long-range triplet Josephson effect at the fundamental harmonic ($I(\varphi) \sim \sin\varphi$) is impossible in SF_1F_2S-type junctions with only two ferromagnetic layers [187, 205, 296–298]. But a long-range interaction similar to that in the case of junctions with ballistic transport is still present for even harmonics of the current–phase relation of a strongly asymmetric bilayer consisting of thin (weak) F_1 and thick (strong) F_2 layers with noncollinear magnetizations. The Josephson current–phase relation (5) of such a junctions is dominated at low temperatures by the second harmonic $I_2(\varphi)$, while the first harmonic $I_1(\varphi)$ is suppressed ($I_{c2} \gg I_{c1}$). The junction with the current–phase dependence $I(\varphi) = I_{c2}\sin(2\varphi)$ then turns out to be bistable: it has two degenerate ground states with a Josephson phase difference of 0 or π.

Interestingly, homogeneous helical modulation of the magnetization in the F-layer plane [289] and a planar domain wall of atomic thickness [299] do not give rise to a long-range triplet component in the diffusive limit. More generally, when magnetic domains are separated by Néel walls, long-range triplet components are manifested on the domain walls but disappear inside the domains [194, 291].

It can therefore be concluded from [194, 299] that very narrow or very thick Néel domain walls cannot serve as effective sources of long-range triplet correlations in the dirty limit, and the optimal domain wall thickness is of the order of ξ_f. Interestingly, long-range triplet components induced by the proximity effect are generated by a ferromagnetic vortex in a mesoscopic ferromagnetic disk in contact with superconducting electrodes, forming a 0- or π-junction, depending on the junction geometry [197, 198].

Studies of the effect of a domain wall on the Josephson current are typically limited to a very special case of collinear oppositely directed magnetizations in the domains (Fig. 6a), which fails to incorporate the diversity of domain structures whose shape depends on the nature of magnetic anisotropy [300]. It was shown in [195] that an F layer containing noncollinear planar domains (see the geometry in Fig. 6b) serves as an efficient source of long-range triplet correlations, even in the case of an atomic-thickness domain wall. In the case of an F layer with the diffusion conductivity type ($h\tau \ll 1$ being the dirty limit), the Josephson current can be calculated using the semiclassical Usadel equations (see Eqn (A.13) in Appendix A and reviews [39, 65, 93]) for the anomalous wave function $\hat{f}$ in Eqn (2). In the presence of high potential barriers at the SF interfaces (or at temperatures T close to the critical temperature T_c), we can restrict ourself to simpler linearized equations (3) and (4), which should then be supplemented by conditions [39, 65, 93] on the SF interfaces $x = \pm d/2$:

$$\left.\frac{\partial f_s}{\partial x}\right|_{\pm d/2} = \pm\frac{\pi\Delta}{\gamma_b\sqrt{\Delta^2+\omega_n^2}}\exp\left(\pm\frac{i\varphi}{2}\right), \tag{11}$$

$$\frac{\partial \mathbf{f}_t}{\partial x} = 0, \tag{12}$$

where Δ is the superconducting order parameter in the contact electrodes and φ is the difference between their phases. The parameter $\gamma_b = R_b\sigma_f$ characterizes the transparency of the SF interface and is determined by its conductance per unit area $1/R_b$ and the specific conductivity of the ferromagnetic metal σ_f. The expression for the supercurrent flowing through the junction has the standard form

$$I = \frac{2eDN_F T}{\pi}\int_S d^2s\sum_n \mathrm{Im}\left(f_s^*\frac{\partial}{\partial x}f_s - \mathbf{f}_t^*\frac{\partial}{\partial x}\mathbf{f}_t\right), \tag{13}$$

where the summation is carried out over all Matsubara frequencies ω_n and N_F is the DOS at the Fermi level of the ferromagnet. In the case of domains with noncollinear magnetic moments (Fig. 6b), the triplet component $\mathbf{f}_t = (f_{tx}, f_{tz})$ of the Matsubara Green's function (2), in addition to the usual component f_{tz} decaying on the scale ξ_f, contains the component f_{tx} describing long-range superconducting correlations in ferromagnets. The additional contribution δI to the Josephson current due to the presence of a single domain wall with orthogonal magnetizations of adjacent domains is given by

$$\delta I = \frac{eN_F DL_y}{2}\frac{\xi_f^4}{\gamma_b^2 d^2}\Delta\tanh\left(\frac{\Delta}{2T}\right)\sin\varphi \tag{14}$$

and exceeds the critical current of the homogeneous SFS junction [39]

$$I_c \sim eN_F DL_y L_x\xi_f\frac{\Delta}{\gamma_b^2}\tanh\left(\frac{\Delta}{2T}\right)\exp\left(-\frac{d}{\xi_f}\right)\cos\left(\frac{\pi}{4}+\frac{d}{\xi_f}\right),$$

if the characteristic domain size $d_{\rm dom}$ satisfies the condition $d_{\rm dom} < \xi_{\rm f}^3 \exp(d/\xi_{\rm f})/d^2$. The power law for the decrease in the current δI with an increase in the F-layer thickness indicates the generation of long-range superconducting correlations in a ferromagnet decaying on the scales $\xi_{\rm N} \gg \xi_{\rm f}$.

3.3 Spin–orbit effects and long-range superconducting correlations

In Sections 3.1 and 3.2, we discussed the mechanisms for transforming singlet Cooper pairs in a superconductor into triplet pairs that can propagate over long distances in a ferromagnet. It is generally accepted that the long-range effect in hybrid SF systems occurs only in the presence of magnetic inhomogeneities, such as magnetic domain walls [90, 194, 195, 296] or composite ferromagnetic layers with different magnetization orientations [187, 295].

Controlling the superconducting properties of hybrid SF systems by changing the magnetic state of the F subsystem is one of the possible avenues to be pursued in superconducting spintronics; however, controlling changes in the magnetization distribution in such structures is by no means a simple task. An alternative mechanism for the formation of long-range superconducting correlations in proximity-effect SF structures is SO coupling, which can either be an intrinsic property of the material without an inversion center [301, 302] or result from geometric constraints such as low dimensionality of structures or interfaces between different materials [252, 253, 264, 303, 304].

The study of SO effects in superconducting systems has a long history (see, e.g., reviews [246, 301, 302]). In contrast to scattering by magnetic impurities, SO scattering itself does not exert a destructive effect on the superconducting state. In the presence of SO coupling, the electron momentum $\mathbf{p}$ is coupled to the spin σ, which makes states with different spin projections (and hence momentum) nonequivalent whenever some mechanism of spin splitting of electron states operates in the system. In ballistic systems, the SO coupling and the exchange field, acting together, create various types of superconducting states with a helicoidal structure and a nonzero momentum of Cooper pairs [305–310], which play an important role in the physics of Majorana states [96, 97] and lead to the formation of unusual Josephson junctions with an arbitrary phase difference in the ground state (φ_0-junctions) [223, 244–246, 311–317]. Thus, in a sufficiently strong (even homogeneous) exchange field, the SO coupling provides anisotropic pairing and transformation of singlet Cooper pairs into triplet ones, thereby forming long-range superconducting correlations in ballistic SF structures. In the presence of impurity scattering, the SO coupling also favors the generation of odd-frequency triplet superconducting correlations. Interestingly, this generation can be affected by the total momentum of Cooper pairs, i.e., the supercurrent flowing along the SF interface [318].

In the ballistic case, the SO coupling can compensate the destructive phase difference γ between the electron and hole parts of the wave function, even in the case of a spatially homogeneous magnetization. The necessary change in the effective exchange field $\mathbf{h}$ along an arbitrary semiclassical trajectory occurs due to multiple reflections of quasiparticles from the ferromagnet surface: SO coupling in this case leads to the dependence of the exchange field on the quasiparticle momentum direction $\mathbf{h} = \mathbf{h}(\mathbf{k})$ [319]. If anisotropy is absent in a system described by a polar vector, then the simplest

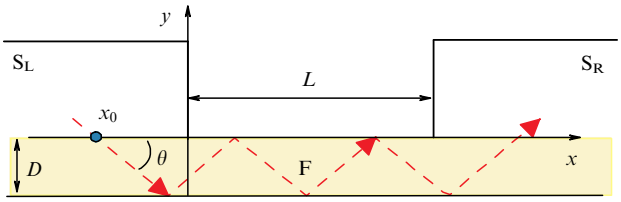

Figure 10. Schematic representation of a quasi-two-dimensional Josephson SFS junction formed by a ferromagnetic wire of thickness D. Trajectory of quasiparticles s repeatedly reflected from the free surface of the wire is shown with a dashed line. (From [263].)

dependence of the effective exchange field $\mathbf{h}$ has the form

$$\mathbf{h}(\mathbf{k}) = \mathbf{h}_0 + \beta_{\rm SO}(\mathbf{h}_0, \mathbf{k})\,\frac{\mathbf{k}}{k_{\rm F}^2}\,, \tag{15}$$

where $\mathbf{h}_0 = h_0\mathbf{x}_0$ is a pseudovector directed along the wire, determined by the ferromagnet magnetic moment $\mathbf{M}$, $\beta_{\rm SO}$ is a constant determined by the SO coupling, and $k_{\rm F}$ is the wave number corresponding to the Fermi momentum $p_{\rm F} = \hbar k_{\rm F}$.

A model of the long-range singlet proximity effect, taking the direction-dependent momentum $\mathbf{h}(\mathbf{k})$ of quasiparticles into account, was proposed in [281] for describing ballistic transport through a thin single-domain single-crystal nanowire with a spatially homogeneous magnetization. In such a system, the effective exchange field $\mathbf{h}(\mathbf{k})$ in (15) changes with the period $s_\theta = 2D/\sin\theta$ along a broken-line trajectory that describes the specular reflection of quasiparticles from the wire surface (Fig. 10). Such a periodic change in the exchange field along the trajectory ensures the condition $\gamma(\theta_m) = 0$ for the system of resonance angles θ_m satisfying the Bragg condition $\sin\theta_m = 2h_0D/[\pi\hbar v_{\rm F}(2m+1)]$. Assuming that the resonances are rather narrow and overlap weakly with each other, we can express the amplitude $I_{\rm c1}^{\rm LR}$ of the long-range component of the first harmonic of the supercurrent $I^{\rm LR}(\varphi) = I_{\rm c1}^{\rm LR}\sin\varphi$ as a sum over the system of resonance angles θ_m,

$$I_{\rm c1}^{\rm LR} \simeq a_1 \sum_{m \geqslant m^*} \frac{\sqrt{2}\pi\hbar v_{\rm F}\beta_{\rm SO}}{h_0 D}\,\sin^3\theta_m\cos\theta_m\,, \tag{16}$$

where m^* is the smallest integer (including zero) satisfying the condition $(2m^*+1) \geqslant D/(\pi\xi_h)$ and a_1 is a coefficient of the Fourier expansion of the current–phase relation $I_{\rm SNS}(\varphi)$ for a Josephson junction with the same geometry and with the normal metal assumed to be nonmagnetic (see Appendix B). In the limit $D \gg \hbar v_{\rm F}/(2h_x)$, the resonance angles θ_m are densely packed in the range $0 < \theta_m < \pi/2$ and $I_{\rm c1}^{\rm LR} \simeq a_1\sqrt{2}\beta_{\rm SO}/3$ is independent of the wire length $L \ll \xi_{\rm n}$.

In Fig. 11, we show the dependence of the amplitude of the long-range component of the first supercurrent harmonic $I_{\rm c1}^{\rm LR}$ on the F-wire thickness D. Oscillations of the critical current $I_{\rm c1}^{\rm LR}(D)$ corresponding to wire thickness changes with a period $\Delta D = 2\pi\xi_h$ are caused by a change in the number of resonance (Bragg) semiclassical trajectories with zero phase shift γ between the electron and hole parts of the wave function. It is clear, however, that the existence of such a long-range supercurrent component is very sensitive to both the SFS structure configuration and possible disorder, which can arise, e.g., due to violation of specular reflection of trajectories from the wire surface. Nevertheless, as in the

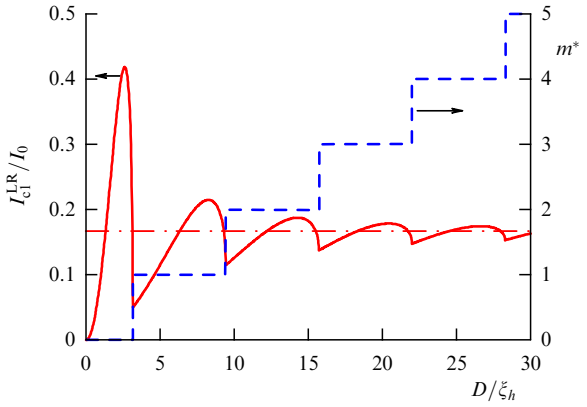

Figure 11. Dependence of the amplitude of the long-range component of the first harmonic of supercurrent I_{c1}^{LR}, Eqn (16) (solid curve), and the number m^* (dashed line) on thickness D of the F-wire. For comparison, the horizontal dashed–dotted line shows the asymptotic value of the amplitude I_{c1}^{LR} for $D \gg \xi_h$, defined as $I_{c1}^{LR} \simeq a_1\sqrt{2}\beta_{SO}/3$ ($I_0 = a_1 2\sqrt{2}\beta_{SO}$). (From [265].)

case of a ferromagnetic bilayer, the long-range supercurrent at higher (even) harmonics is resistant to disorder and insensitive to the geometry of the SFS structure.

The semiclassical approach to describing ballistic hybrid structures in the presence of an arbitrary effective field that depends on both the coordinates and the momentum of quasiparticles and describes the joint effect of the SO coupling and the exchange or Zeeman spin splitting was developed further in [314]. The formalism was then used in [315] to study the proximity effect and the Josephson effect in such structures with different types of magnetic ordering. Studies [262, 320] can also be classified as part of this theoretical research: they discussed how the long-range spin-singlet Josephson transport is affected by the difference between the effective masses of conduction electrons and by the Fermi surface anisotropy in the spin subbands of a ferromagnet.

The proximity effect and the generation of long-range superconducting correlations in ferromagnetic elements of diffusive SF structures in the presence of SO coupling were studied in detail in [264, 321]. The authors obtained semiclassical equations for the Green's functions that generalize the linearized Usadel equations to the case involving SO coupling, the exchange field, and superconducting correlations. The SO coupling was shown to be an additional source of the long-range triplet component. In the special case where the SO coupling is linear in momentum, an analogy was established between the spin diffusion process in normal metals and the generation of all triplet components of the condensate in a hybrid SF structure with diffusive conductivity in the presence of SO coupling.

We illustrate this with the example of the simplest structure, a bilayer whose SF interface is perpendicular to the x-axis and the exchange field in the F layer is homogeneous and directed along z: $\mathbf{h} = h\mathbf{z}_0$. As previously, to simplify the presentation, we restrict ourself to the case of weak superconducting correlations in the ferromagnet where the singlet (f_s) and triplet ($\mathbf{f}_t$) components of the Matsubara Green's function (2) satisfy the linearized Usadel equations and the Kupriyanov–Lukichev boundary conditions (see Eqn (A.14) in Appendix A) with a due modification that takes the SO coupling into account. In the particular case of the SO coupling linear in the momentum $\mathbf{p}$,

$$H_{SO} = \frac{\hbar}{2m}\,\mathcal{A}_k^a\, p_k \sigma^a\,,$$

the modified linear Usadel equations for the anomalous Green's function $\hat{f}$ in (2) have the standard form (3), (4) with the derivatives $\partial_k\psi$ replaced with the covariant operator $\tilde{\nabla}_k\psi = \partial_k\psi - \mathrm{i}[\mathcal{A}_k^a\,\sigma^a,\,\psi]/2$ [264]. (Here, σ^a are the Pauli matrices and the indices k and a take the values x, y, z.) A similar change of operators $\nabla_k \to \tilde{\nabla}_k$ must also be made in the Kupriyanov–Lukichev boundary conditions (see Eqn (A.14) in Appendix A). Assuming that the structure is homogeneous in the yz plane and the SO coupling is isotropic, $\mathcal{A}_k^a = \alpha\,\delta_k^a$, we obtain the following equations for the singlet, f_s, and triplet, $\mathbf{f}_t = f_{tz}\mathbf{e}_z + f_{ty}\mathbf{e}_y$, components of the anomalous Green's function (2):

$$\hbar D_f\,\partial_x^2 f_s - 2|\omega_n| f_s - 2\mathrm{i}\,\mathrm{sgn}\,(\omega_n) h f_{tz} = 0\,, \tag{17}$$

$$\hbar D_f\,\partial_x^2 f_{tz} - 2\bigl(\hbar D_f\alpha^2 + |\omega_n|\bigr) f_{tz} + 2\hbar D_f\alpha\,\partial_x f_{ty} - 2\mathrm{i}\,\mathrm{sgn}\,(\omega_n) h f_s = 0\,, \tag{18}$$

$$\hbar D_f\,\partial_x^2 f_{ty} - 2\bigl(\hbar D_f\alpha^2 + |\omega_n|\bigr) f_{ty} - 2\hbar D_f\alpha\,\partial_x f_{tz} = 0\,, \tag{19}$$

where the terms depending on the SO coupling constant α describe two spin rotation mechanisms: spin density relaxation $\sim \alpha^2$ and spin precession $\sim \alpha$.

Equations (17) and (18) describe the diffusion of strongly coupled condensates: singlet $(\uparrow\downarrow - \downarrow\uparrow)$ and triplet $(\uparrow\downarrow + \downarrow\uparrow)$ with zero spin projection on the z-axis. These equations are dominated by the last term $\sim h$, which describes the singlet–triplet interaction. As a result, the f_s and f_{tz} components decay on the scale ξ_f defined by the exchange field. Equation (19) determines the spatial distribution of the f_{ty} component orthogonal to the exchange field direction, which describes the diffusion of triplet condensates $(\uparrow\uparrow)$ and $(\downarrow\downarrow)$ with the spin projection $\pm\hbar$. This component is generated near the interface due to spin precession and decays on a scale that is independent of the exchange field h and greatly exceeds the usual length ξ_f. As in the case of an inhomogeneous exchange field (see Section 3.2), these triplet correlations f_{ty} slowly decaying in a ferromagnet are responsible for the long-range effect in hybrid SF structures with SO coupling.

Although the linearized Usadel equations taking the SO coupling into account reflect some qualitative effects such as long-range interaction [264, 321] and the anomalous Josephson effect [316, 322], they do not allow comprehensively describing the low-temperature regime and the local spectral properties of the system. For materials with SO coupling, the nonlinear Usadel equations applicable to both superconducting and normal systems were obtained in [323]. In the normal state, they reduce to the well-known spin–charge diffusion equations [324–326] and are suitable for describing various magnetoelectric effects in diffuse hybrid structures with SO coupling.

Thus, an exchange field that is inhomogeneous in real or momentum space ensures efficient mutual conversion of singlet (damped) superconducting correlations into triplet (undamped) ones, which leads to a slow decay of the pair correlation function in a ferromagnet and a significant Josephson current in SFS structures. The resulting interplay between the superconducting and ferromagnetic subsystems allows controlling superfluid (nondissipative) transport, which is necessary for the operation of superconducting spintronics and nanoplasmonics devices. Notably, recent

studies [223, 311] of SFS systems with SO coupling have shown that the effect of the SO coupling on the joint dynamics of interacting superconducting and magnetic order parameters may be a promising new direction in the physics of hybrid SF systems.

3.4 Mesoscopic fluctuations

We finally discuss yet another possible mechanism for suppressing the destructive effect of the interference of various quasiparticle trajectories on the superconducting current in an SFS junction: mesoscopic fluctuations of the Josephson current. The point is that the exponential decay of the supercurrent through the F layer at the length ξ_f considered above implies averaging over random scatterers when calculating the current. In other words, we define the current $\langle I\rangle$ averaged over an ensemble of different scatterer configurations in different samples. When measuring in practice, however, we are not dealing with such an averaged quantity but with a specific magnitude of the current flowing through a given contact with a given distribution of scatterers. In an individual sample, it can differ significantly from the ensemble average due to random changes in the sign of the critical current (i.e., a change by π in the equilibrium phase difference in the junction) [272, 327–330]. A measure of such mesoscopic fluctuations is given by the standard deviation $\delta I = (\langle I^2\rangle - \langle I\rangle^2)^{1/2}$. The current value is the sum of the contributions I_k from N different transport channels, in each of which the phase difference is shifted by a random γ (see Appendix B). When calculating the mean square $\langle I^2\rangle$, we obtain the double sum of N^2 contributions. For the N terms of the form I_k^2 in this double sum, the random phases γ must cancel, which gives the expression $\delta I \sim \sqrt{N}$. Using the Landauer relation between the normal contact resistance R and the number of transport channels and recalling the characteristic contribution to the supercurrent from one transport mode, we obtain the estimate $\delta I \sim \Delta_0/\sqrt{\hbar R}$, where Δ_0 is the width of the superconducting gap between the superconducting electrodes. For an SFS junction with the F-layer thickness d, the resulting estimate can give a very significant critical current of the contact, greatly exceeding the ensemble average:

$$\langle I\rangle \sim \frac{\Delta_0 \exp(-d/\xi_f)}{eR}\,.$$

We note that the above square-root dependence of the root-mean-square deviation δI on the number of transverse modes N agrees with the results in [272, 328, 329], despite the difference in the approximations and theoretical approaches adopted there. The discrepancy between the results in [272, 328] is presumably related to significantly different bounds on $h\tau$, which was assumed to be small in [272] and sufficiently large ($h\tau \gtrsim 1$) in [328].

4. Electrodynamics of superconductor–ferromagnet structures

One of the key properties of superconductors is their ability to screen the external magnetic field (the Meissner effect). The simplest description of this phenomenon is based on the London relation between the superconducting current density $\mathbf{j}_s$ and the vector potential $\mathbf{A}$,

$$\mathbf{j}_s = -\frac{c}{4\pi\lambda^2}\,\mathbf{A}\,, \tag{20}$$

where λ is the London penetration depth of the magnetic field, which characterizes the scale of the magnetic field decay in the direction into the bulk of the superconductor. Moreover, the sign in (20) fixes the diamagnetic nature of the Meissner response. In hybrid SF systems, relation (20) is substantially modified by taking the exchange effects into account. This modification is in the focus of interest of both theorists and experimenters due to both the nontrivial physics behind it and the importance of electrodynamic properties for designing superconducting spintronic devices.

4.1 Electromagnetic response of superconductor–ferromagnet structures. Diamagnetic and paramagnetic contributions to the response

The reason for significant changes in relation (20) in SF systems is the occurrence of spin-triplet correlations that are odd in the Matsubara frequency. In contrast to singlet Cooper pairs (which are described by the anomalous Green's function that is even in the Matsubara frequency), the induced triplet correlations make a paramagnetic rather than diamagnetic contribution to the Meissner response, and λ^{-2} then becomes strongly inhomogeneous. For example, in the framework of the Usadel theory, the dependence of λ^{-2} on the coordinate $\mathbf{r}$ for an SF system is given by [331, 332]

$$\lambda^{-2}(\mathbf{r}) = \frac{16\pi^3 T}{ec\Phi_0}\,\sigma(\mathbf{r}) \sum_{n=0}^{\infty}\left[\left|f_s(\mathbf{r})\right|^2 - \left|\mathbf{f}_t(\mathbf{r})\right|^2\right], \tag{21}$$

where $\sigma(\mathbf{r})$ is the local Drude conductivity of the SF structure materials in the normal state, T is the temperature of the system, and summation is carried out over positive Matsubara frequencies $\omega_n = \pi T(2n+1)$. We note that, due to spatial oscillations of the anomalous Green's function components $f_s(\mathbf{r})$ and $\mathbf{f}_t(\mathbf{r})$, SF systems contain spatial regions where the local Meissner response is diamagnetic ($\lambda^{-2}(\mathbf{r}) > 0$) and where triplet correlations dominate the singlet ones, providing the paramagnetic ($\lambda^{-2}(\mathbf{r}) < 0$) response type [91, 333, 334].

Experimental measurement of $\lambda^{-2}(\mathbf{r})$ profiles is a difficult task, because it requires reconstructing the spatial distributions of the magnetic field inside the SF structure. Such measurements are carried out using muon spin spectroscopy [335–337] or in neutron scattering experiments [338–341]. At the same time, most of the existing methods are sensitive only to the total electromagnetic response of SF systems. For multilayer structures with a thickness d much smaller than the London depth λ, the total response is determined by the effective penetration depth Λ of the magnetic field, found by averaging $\lambda^{-2}(\mathbf{r})$ over the structure thickness:

$$\Lambda^{-1} = \int \frac{\mathrm{d}x}{\lambda^2(x)}\,, \tag{22}$$

where x is the coordinate across the structure [331]. Despite the local change of sign of the response associated with triplet correlations, Λ^{-1} typically remains positive for SF systems. At the same time, the parameters of the system can be chosen such that Λ^{-1} calculated in accordance with Eqns (21) and (22) formally becomes negative. From a physical standpoint, such a change of sign signals the instability of the homogeneous superconducting state for which the response was calculated with respect to the occurrence of spatial modulation of the superconducting order parameter [332]. In this case, states similar to LOFF states occur with the order

parameter modulated in the plane of structure layers. Moreover, the resulting inhomogeneous superconducting states have a diamagnetic response. The mechanism of formation of longitudinal LOFF states and their properties are considered in more detail in Section 4.5.

A detailed experimental analysis of the screening properties of SF and SFS structures was carried out in [342, 343] based on measurements of the mutual inductance of two coils with a sample placed between them [344]. The mutual inductance then depends on the conductivity of the sample, which is in turn determined by the density of the superfluid component averaged over the thickness of the structure, i.e., the effective screening length Λ in Eqn (22). A similar technique had been used previously to study the screening properties of thin S-films [345–347]. Due to the peculiarities of the proximity effect on the SF interface, the screening properties of layered hybrid structures exhibit anomalous behavior, which manifests itself in a nonmonotonic dependence $\Lambda^{-1}(d_f)$ at low temperatures $T \ll T_c$, first observed in Nb/Ni bilayers [342]. The behavior of $\Lambda^{-1}(d_f)$ correlates with the nonmonotonic dependence of the critical temperature $T_c(d_f)$ of the SF bilayer.

Analytic calculations in the framework of the nonlinear Usadel theory for a thin SF bilayer ($d_s + d_f \ll \Lambda$) with a diffusive conductivity type showed that the oscillations of $\Lambda^{-1}(d_f)$ can be associated with spatial oscillations of the anomalous Green's function in a ferromagnet and the resulting interference effects for $d_f \sim \xi_f$ [331]. Similar oscillations of $\Lambda^{-1}(d_f)$ are also observed for SFS systems. Subsequent temperature measurements of the effective screening length $\Lambda^{-1}(T)$ in three-layer Nb/Ni/Nb SFS structures allowed tracing the evolution of superconductivity as the coupling between the S layers changed from weak to strong, which was followed by the transition of the structure into a π-state [343].

4.2 Electromagnetic response of Josephson superconductor/ferromagnet/superconductor systems

Proximity-effect hybrid SF structures are a convenient subject for studying various phase transitions caused by the interplay of two competing order parameters, superconducting and ferromagnetic [39, 348]. The dependence of the temperature of the transition to the normal state on the SF structure parameters has been studied both theoretically [118, 349–351] and experimentally [44, 45, 47, 164] (also see reviews [39, 46]).

Most of the effects in Josephson SFS systems are associated with the π-superconductivity phenomenon [50], under which a nontrivial difference π between the phases of neighboring superconducting layers is established in the ground state. Of particular interest from the standpoint of experiment is the possibility of realizing the transition between the 0- and π-states as the hybrid system temperature T changes. Experimental evidence of a temperature stimulated $0-\pi$ transition in the Josephson SFS structure $Nb/Cu_xNi_{1-x}/Nb$ was obtained by critical current measurements in [144, 155, 352]. An analysis in [146] showed that the nature of the transition between the 0- and π-states of the Josephson SFS junction with a homogeneous diffuse F layer is determined by the sign of the amplitude of the second harmonic I_2 in the current–phase relation (1), and this is a first-order phase transition if $I_2 > 0$.

Self-consistent calculations of ballistic SFS structures using BdG equations revealed a jump in the amplitude of the wave function of Cooper pairs and in the system entropy $S(T)$ at the $0-\pi$ phase transition temperature [353, 354]. The existence of first-order phase transitions to the superconducting state is also characteristic of diffuse FSF structures with thin F layers [351]. A second-order $0-\pi$ phase transition occurs in Josephson systems with $I_2 < 0$ and is possible, e.g., in SFS junctions with an inhomogeneous diffuse F layer [146, 149].

Along with resistive measurements used in most experiments with hybrid FS systems, a convenient tool for studying phase transitions is the study of the screening properties of such systems, which allows extracting information on both the value and the temperature dependence of the effective density of the superfluid component. Such measurements allow gaining insight into the properties of the superconducting state in hybrid systems and are a natural development of earlier studies of the behavior of SN hybrids in external magnetic fields [355–357].

The influence of the proximity effect on the screening properties of Josephson SFS structures becomes pronounced in the case of thin S layers (of the order of the superconducting coherence length ξ_s in thickness) when the suppression of the superconducting order parameter Δ becomes sufficiently strong. Microwave measurements of the temperature dependence of the effective penetration depth (22) of Nb/PdNi/Nb three-layer structures were performed in [358, 359] using dielectric microcavities (see, e.g., reviews [360, 361]). The reentrant behavior of $\Lambda(T)$ was revealed, with the effective penetration depth sharply increasing with decreasing temperature T in the vicinity of $T_0 \sim 0.9T_{c0}$ if the F-layer thickness was $d_f \simeq d_f^* = 2$ nm. For a different F-layer thickness, $d_f \neq d_f^*$, such a jump of $\Lambda(T)$ was not observed, and the effective penetration depth monotonically decreased with decreasing temperature (Fig. 12). Such a temperature anomaly indicates a sharp decrease in the average concentration of Cooper pairs $n \sim 1/\Lambda(T)$ in the structure at $T \lesssim T_0$ and the corresponding suppression of the superconducting order parameter $\Delta(T)$. Comparing the experimental data with the results of calculations [358, 362] allowed relating

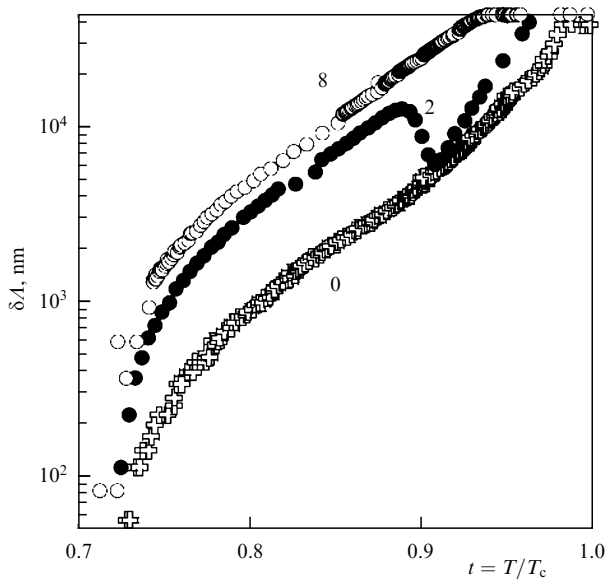

Figure 12. Dependence of the screening properties of the three-layer SFS $Nb/Pd_{0.84}Ni_{0.16}/Nb$ structure with $d_f = 0$, 2, 8 nm on temperature T: $\delta\Lambda = \Lambda(T/T_c) - \Lambda(0.72)$. (From [358].)

this anomaly to switching between the 0- and π-states of the Josephson SFS junction.

The proposed theoretical approach based on the joint solution of the nonlinear Usadel equations (A.13) and self-consistency equation (A.4) (see Appendix A) took into account how the structure of the pair wave function in a ferromagnet affects the equilibrium value of the superconducting order parameter Δ in S layers. The leakage of Cooper pairs from the S layers weakens the superconductivity near the interface with an F metal due to the proximity effect. The degree of the order parameter suppression depends on the parameters characterizing the system, such as the SF interface transparency and the thicknesses of the S and F layers. The influence of these parameters is especially strong in the case of high transparency of the interface and thin S layers, when the conventional 'rigid' boundary conditions [65] for the anomalous Green's function become inapplicable.

We note that it is fundamentally important to take scattering on magnetic impurities into account, because precisely this process provides the main mechanism responsible for the $0-\pi$ transition with a change in the temperature T [144, 172].

A typical dependence of the critical temperature $T_c^{0,\pi}$ of the transition of a diffusive SFS structure from the normal state to the superconducting 0-state ($d_f \leqslant d_f^*$) or the π-state ($d_f \geqslant d_f^*$) on the F-layer thickness is shown in Fig. 13a. The F-layer thickness d_f^* such that $T_c^0(d_f^*) = T_c^\pi(d_f^*)$ determines the position of the tricritical point on the phase diagram in the (T, d_f) plane. If the ferromagnetic layer thickness d_f is only slightly less than d_f^* and $T_c^0 > T_c^\pi$, then, as temperature T decreases to values less than T_c^0, the system first passes from the normal state to the superconducting state corresponding to the 0-phase of the SFS structure, because $E^0(T) < E^\pi(T)$, where $E^0(T)$ and $E^\pi(T)$ are the free energies of the 0- and π-states. When temperature T reaches the value T_0 such that $E^0(T_0) = E^\pi(T_0)$, the SFS structure passes from the 0-state to the π-state. The entropy $S(T)$ experiences a jumps at T_0,

$$\frac{S^\pi(T_0)}{S^0(T_0)} = \frac{T_c^0 - T_0}{T_c^\pi - T_0} > 1\,, \tag{23}$$

which indicates that the system passes from the 0-state to the π-state through a first-order phase transition with the corresponding release of latent heat,

$$Q = T_0\left[S^\pi(T_0) - S^0(T_0)\right] > 0\,. \tag{24}$$

At the same time, at the transition temperature T_0, the superconducting order parameter jumps from the value Δ_0 corresponding to the 0-phase to $\Delta_\pi < \Delta_0$ corresponding to the π-phase. Due to the strong dependence of superconductivity in thin S layers on the structure of the pair wave function in the ferromagnetic layer, the current–phase relation $I(\varphi)$ for such a junction differs significantly from a simple sinusoidal one even at temperatures T close to T_c [362]. The strong anharmonicity of $I(\varphi)$ at $T \approx T_0 \sim T_c$ results in the disappearance of the typical nonmonotonic temperature dependence of the critical current amplitude in the vicinity of the $0-\pi$ transition and in the appearance of metastable 0- and π-states of the junction and in peculiarities in the behavior of radio frequency SQUID with such a transition.

The effect that the thickness of superconducting layers exerts on the ground state and properties of the $0-\pi$ phase transition in Nb/CuNi/Nb hybrid SFS structures with a diffuse conductivity type were studied experimentally and theoretically in [363]. To measure the critical temperature T_c of the transition of an SFS structure with thin ($d_s \lesssim \xi_s$) layers to the superconducting state, a local technique was used based on the detection of a nonlinear microwave response of hybrid structure using a near-field probe [364, 365]. Switching between the 0- and π-states was accompanied by an anomalous increase in the measured temperature T_c with a decrease in the thickness of the superconducting layers in the vicinity of $d_s^* = d_{Nb} \approx 15$ nm. The effect was observed at the F-layer thickness $d_{CuNi} = 5$ nm and was absent in other samples with a thinner F-layer. Such an anomaly arose due to the difference in the effective critical depairing current densities $j_c^{0,\pi}(T)$ for the 0- and π-states of the structure. Calculations performed in the framework of the approach in [362] showed that, for the same deviation $T_c^{0,\pi} - T$ of the temperature T from its critical value $T_c^{0,\pi}$, the condition $j_c^\pi(T) > j_c^0(T)$ holds in a wide range of parameters of the hybrid SFS structure. The quasistatic magnetic field $\mathbf{H}_{ex}$ created by a near-field probe induces a high-frequency current $\mathbf{j}_{ex} = [c/(4\pi)]\,\mathrm{rot}\,\mathbf{H}_{ex}$ in the localization region, which prevents the transition of the SFS structure to the superconducting state. The condition

$$j_{ex} = \begin{cases} j_c^\pi(T_c)\,, & d_s < d_s^*\,, \\ j_c^0(T_c)\,, & d_s \geqslant d_s^* \end{cases} \tag{25}$$

then determines the shift $\delta T_c^{0,\pi}$ of the critical temperature $T_c = T_c^{0,\pi} - \delta T_c^{0,\pi}$ of the transition of the SFS structure to the superconducting state compared with its thermodynamic value $T_c^{0,\pi}$.

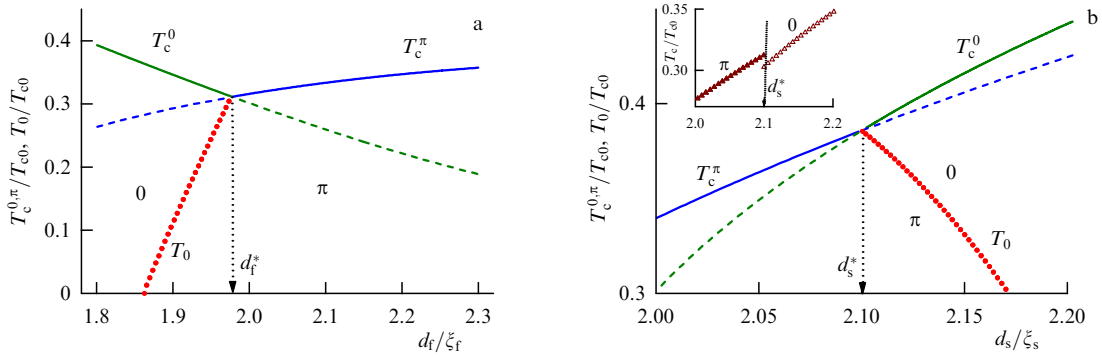

Figure 13. Typical view of the phase diagram of an SFS structure in the vicinity of a tricritical point on the plane of variables (a) (T, d_f) and (b) (T, d_s). Dotted lines show curves $T_0(d_f)$ and $T_0(d_s)$ of the first-order phase transition between the 0- and π-states of the system. Inset to Fig. b shows a typical form of the dependence $T_c(d_s)$ corresponding to a fixed value of external current density j_{ex}.

In Fig. 13b, we show the dependence $T_c(d_s)$ defined by relation (25), exhibiting a jump of the critical temperature $\Delta T_c = \delta T_c^0 - \delta T_c^\pi > 0$ with decreasing superconductor thickness at $d_s = d_s^*$.

It is therefore possible to determine the transverse structure of the pair wave function in Josephson SFS structures with thin S layers in the vicinity of the $0-\pi$ transition based on measurements of the lateral (longitudinal) transport in the layers. Because the depairing current density in the π-state turns out to be somewhat higher than in the 0-state, a change in the external current in the layers allows changing the ground state of the SFS structure ($0 \to \pi$) [366].

4.3 Inverse proximity effect.
Spin and electromagnetic mechanisms

The possibility of electron exchange between a superconductor and a ferromagnet in SF systems leads not only to the appearance of superconducting correlations in a ferromagnet but also to the opposite phenomenon, the penetration of a magnetic moment from the ferromagnet into the superconductor. At first glance, this is unsurprising. Indeed, even in the absence of an electrical contact between the S and F subsystems, inhomogeneities of the magnetic moment in the ferromagnet lead to the formation of stray magnetic fields that can penetrate into the superconductor to a depth of the order of the London length (see, e.g., review [367]). Moreover, it is significant that this effect is sensitive to the structure of the magnetization and the shape of the ferromagnet. For example, an infinite single-domain ferromagnetic film with longitudinal magnetization does not create stray fields and does not therefore induce a magnetic field in a superconductor: the magnetic field is trapped inside the ferromagnet. But the situation changes dramatically if the superconductor–ferromagnet interface is transparent to electrons. In this case, even if the ferromagnet does not create stray fields, a magnetic field induced by the ferromagnet arises in the superconductor, which is a manifestation of the so-called inverse proximity effect.

There are two main mechanisms for the occurrence of magnetism in a superconductor due to the proximity effect. The first is related to the spin polarization of electrons forming a Cooper pair near the SF interface (the so-called spin mechanism of the inverse proximity effect) [368–372]. The second is purely electromagnetic: the direct proximity effect excites a superconducting current inside the ferromagnetic layer and hence the compensating Meissner currents inside the superconductor (the electromagnetic proximity effect) [373, 374] (see also review [375]).

The physical mechanism for the occurrence of the inverse spin proximity effect is associated with Cooper pairs localized near the SF interface. Because of the finite size of a pair, a situation is possible where one electron in the pair is in the superconductor and the other is in the ferromagnet. In this case, it is energetically favorable for the magnetic moment of the electron in the F layer to be directed along the magnetization of the ferromagnet. Moreover, because the Cooper pair has a zero spin projection, the electron remaining in the superconductor must have an oppositely directed spin. Thus, in the surface layer of a superconductor with a thickness of the order of the Cooper pair size (i.e., the correlation length $\xi_0 \sim 1-10$ nm), a magnetic moment is induced that is directed against the magnetization vector in the ferromagnet.

The possibility of the appearance of a magnetic moment in a superconductor near the SF interface due to spin effects was first predicted in [368]. The calculation of the local DOS $N_\uparrow(x)$ and $N_\downarrow(x)$ for electrons with opposite spin projections, based on a numerical solution of the Usadel equation, allowed analyzing the magnetization profile of free electrons $M_e(x) = \mu_B[N_\uparrow(x) - N_\downarrow(x)]$ as a function of the distance x from the SF interface. One of the surprising predictions in [368] was that the direction of the magnetic moment induced in the superconductor can change at some distance from the SF interface inside the superconductor.

However, the analytic theory of the inverse proximity effect constructed in [369] did not reveal the existence of spatial oscillations of the magnetic moment in the S layer. At the same time, inside the superconductor, the magnetic moment itself can well be directed against the magnetization of the ferromagnet. Just this situation is realized in SF structures with a ferromagnet whose magnetization is due to free electrons.

On the other hand, for a ferromagnet with the magnetization due to the antiferromagnetic interaction of electrons with localized moments, the direction of the induced moment in the superconductor is the reverse: parallel to the magnetization of the ferromagnet. The direction of the induced magnetic moment also depends on which of the two spin subbands in the ferromagnet has a higher density of electron states at the Fermi level: the induced magnetic moment in the S layer is directed against the magnetization of the ferromagnet if the lower-energy subband has a higher DOS, and along the F-layer magnetization if the upper-spin subband has a higher DOS [376]. Finally, for SF structures in the clean limit ($h\tau \gg 1$, where h is the exchange energy in the ferromagnet and τ is the characteristic relaxation time of the electron momentum), the interference of quasiparticle trajectories leads to an oscillatory dependence of the magnetic moment induced in the superconductor on the product hd_f, where d_f is the F-layer thickness [370, 377].

In contrast to the spin mechanism of the emergence of magnetism in the superconducting part of SF structures, the electromagnetic proximity effect is purely orbital. The penetration of Cooper pairs from a superconductor into a ferromagnet leads to the appearance of Meissner currents *inside* the ferromagnet. These currents screen the magnetization field in the bulk of the ferromagnet and are a source of the magnetic field in the superconductor, a field that decreases on a scale of the order of the London depth λ. In type-II superconductors, such a scale significantly exceeds ξ_0, which makes the electromagnetic proximity effect long range compared to the inverse proximity effect.

A comparison of the two mechanisms for generating the magnetic moment of a superconductor in SF systems shows that the electromagnetic mechanism is dominant for typical ferromagnetic materials [374]. Indeed, a very general estimate of the superconductor magnetization M_s due to the inverse spin proximity effect can be obtained by calculating the derivative of the superconducting condensation energy $E_s \sim -\Delta^2 N(0)$ with respect to the exchange field h: $M_s = -\mu_B \partial E_s/\partial h$ (here, Δ is the superconducting gap, $N(0)$ is the DOS at the Fermi level, and μ_B is the Bohr magneton). At low temperatures, the correction to the superconducting gap $\delta\Delta$ due to superconductivity suppression by the exchange field is proportional to some depairing factor v dependent on the exchange field: $\delta\Delta \propto v(h)$. Assuming that $\partial v/\partial h \sim T_c/h$ and $\Delta \sim T_c$, we obtain an estimate for the superconductor

magnetization $M_s \sim \mu_B n(T_c/h)(T_c/E_F) \sim \mu_B n \times 10^{-5}$, where n is the electron concentration. The resulting estimate of M_s turns out to be even less than the Pauli magnetization of noninteracting electrons $M_P \sim \mu_B n(h/E_F)$ for most typical ferromagnets, for which $h \gg T_c$. On the other hand, inside the superconductor, the magnetization M_{em} associated with the electromagnetic proximity effect is determined by the ferromagnet magnetization M: $M_{em} \propto M$. Not limiting ourselves to materials in which magnetic ordering arises due to free electrons and taking the significant contribution from localized moments into account, we can easily deduce that the ferromagnet magnetization must be of the order of μ_B per atom. The resulting magnetization M_{em} significantly exceeds the magnetization due to the inverse spin proximity effect.

Thus, for typical ferromagnets in which the magnetic order arises due to the interaction of electrons with localized spins, the contribution from the inverse spin proximity effect to the magnetization inside the superconductor is negligible. At the same time, if the dominant mechanism for the formation of magnetic order in a ferromagnet is indeed related to free electrons, then the contribution of the spin mechanism of the inverse proximity effect to the resulting magnetization of the superconductor is significant [378].

The emergence of a magnetic field in the superconducting part of SF structures has been detected experimentally using a number of techniques, including spectral measurements of nuclear magnetic resonance [379], analysis of the polar Kerr effect [380], spin-polarized neutron reflectometry [339, 341, 381, 382], and muon spin spectroscopy [335–337, 383]. Only the last two methods allow drawing a quantitative conclusion about the characteristic scale of penetration of the magnetic field into the superconducting subsystem, which turns out to be much larger than the coherence length ξ_0 [336, 337, 339, 382, 383]. Such a long-range penetration of the magnetic field into the superconducting layer may be a consequence of the electromagnetic proximity effect.

4.4 Electromagnetic proximity effect in hybrid superconductor–ferromagnet structures

An analytic description of the electromagnetic proximity effect in SF systems can be achieved by solving the Maxwell equations for vector potential $\mathbf{A}$, where the linear relation between the superconducting current $\mathbf{j}_s$ and the vector potential (typical for superconducting systems) is assumed [373]. The total current $\mathbf{j}$ flowing in an SF system can then be conveniently represented as the sum of two components, $\mathbf{j} = \mathbf{j}_s + \mathbf{j}_m$, where $\mathbf{j}_m = c\,\mathrm{rot}\,\mathbf{M}$ is the magnetization current in the ferromagnet. The vector potential satisfies the equation

$$\mathrm{rot\ rot}\,\mathbf{A} = \frac{4\pi}{c}(\mathbf{j}_s + \mathbf{j}_m)\,. \tag{26}$$

As the simplest system in which the electromagnetic proximity effect is realized, we consider an SF bilayer (Fig. 14). For simplicity, we first assume that the magnetization $\mathbf{M} = M_0\mathbf{e}_z$ in the ferromagnet is homogeneous and is directed along the z-axis parallel to the SF interface ($\mathbf{e}_z$ is a unit vector in the direction of the z-axis). The chosen magnetization direction rules out the occurrence of stray magnetic fields outside the ferromagnet when the interface between S and F is not transparent to electrons. As a result, in the absence of the proximity effect, the magnetic field is $\mathbf{B} = 4\pi\mathbf{M}$ inside the ferromagnet, and $\mathbf{B} = 0$ outside the ferromagnet, and there are no superconducting currents in the S layer (we also assume the absence of an external magnetic field applied to the SF system).

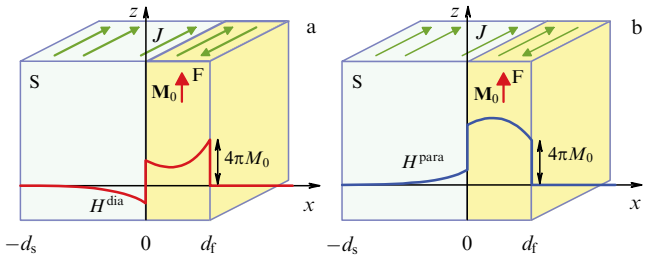

Figure 14. Schematic representation of the spontaneous magnetic field arising in an SF bilayer due to the electromagnetic proximity effect in cases where the integral superconducting current in the ferromagnet is (a) diamagnetic and (b) paramagnetic. (From [375].)

We now consider the situation where the interface between the S and F layers is transparent to electrons. In this case, the superconducting correlations penetrating into the ferromagnet allow the superconducting current to flow *inside* the ferromagnet. The specific type of $\mathbf{j}_s(\mathbf{A})$ coupling is then determined by the relation between the superconducting correlation length and the mean free path. The simplest picture arises for a local $\mathbf{j}_s(\mathbf{A})$ coupling that is characteristic of superconducting systems in the dirty limit,

$$\mathbf{j}_s(x) = -\frac{c}{4\pi}\frac{1}{\lambda^2(x)}\mathbf{A}\,, \tag{27}$$

where the London length λ is determined by the local amplitude of superconducting correlations (21) and hence depends on the coordinate x across the layers (see Fig. 14). Moreover, due to the proximity effect, λ^{-2} is nonzero inside the ferromagnet. For simplicity in what follows, we assume that $d_s \gg \lambda$ for the superconductor thickness and $d_f \ll \lambda$ for the ferromagnet thickness. In addition, we consider the conductivity of a ferromagnet to be much lower than the superconductor conductivity in the normal state, which allows us to neglect the local suppression of the anomalous Green's function on the scale $\sim \xi_0$ near the SF interface due to the proximity effect, assuming the London length λ_0 to be constant inside the superconductor.

These simplifications allow obtaining the simplest form of the solution of Maxwell equation (26): $A_y(x) = A_0 \exp(x/\lambda_0)$ in the superconductor and $A_y(x) = A_0 + 4\pi M_0 x$ in the ferromagnet. The constant A_0 can be found from the condition that the integral superconducting current flowing along the SF system in the ground state vanishes. An alternative (but completely equivalent) way to calculate A_0 is to integrate Eqn (26) with respect to the F-layer thickness. Considering the case where no external magnetic field is applied to the system and $B_z(d_f) = 0$, we obtain

$$B_z(0) = -4\pi M_0 \int_0^{d_f} \frac{x'\,\mathrm{d}x'}{\lambda^2(x')} - A_0 \int_0^{d_f} \frac{\mathrm{d}x'}{\lambda^2(x')}\,. \tag{28}$$

It is easy to see that, in the considered limit $d_f \ll \lambda_0$, the second term on the right-hand side of (28) can be neglected because of its smallness compared to the $B_z(0)$ term on the left-hand side. Indeed, the solution of Eqn (26) for a superconductor implies that $A_0 = B_z(0)\lambda_0$, and hence the term with A_0 on the right-hand side of (28) has the order $(d_f/\lambda_0)B_z(0)$, which is much less than $B_z(0)$. Substituting the found value of $B_z(0)$ into the solution of the Maxwell equation, we obtain the final profile

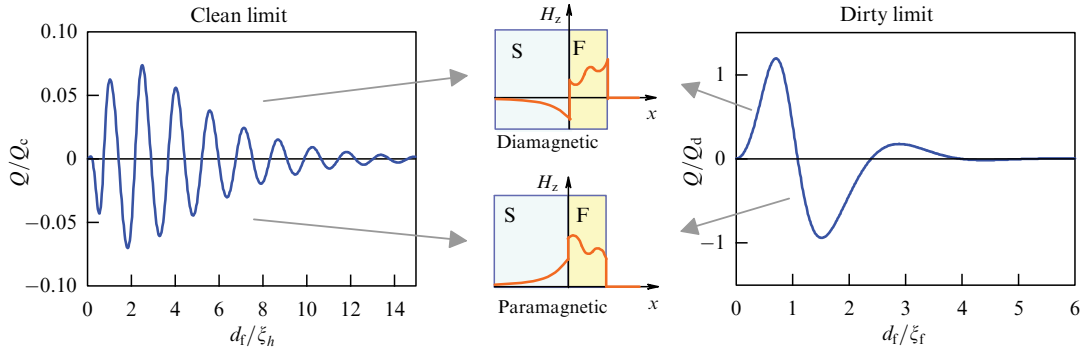

Figure 15. Dependences of kernel Q, which determines the electromagnetic proximity effect, on the ferromagnetic layer thickness d_f in the clean and dirty limits. In the clean limit, system parameters are $h = 10\pi T$ and $\Delta = 2\pi T$; $Q_d = \pi^2\sigma_f\xi_f^2 \tanh[\Delta/(2T)]/(2\hbar c^2)$ and $Q_c = e^2 v_0 \xi_h^2 (v_F/c)^2$, where v_0 is the DOS at the Fermi level per spin projection and per unit volume, $\xi_h = \hbar v_F/h$ is the correlation length in a clean ferromagnet. (From [373].)

of the spontaneous magnetic field inside the S layer,

$$B_z(x) = -4\pi M_0 Q \exp\left(\frac{x}{\lambda_0}\right), \tag{29}$$

where $Q = \int_0^{d_f} \lambda^{-2}(x')x'\,dx'$.

For SF systems in the clean limit, the profile of the magnetic field arising in the superconductor due to the electromagnetic proximity effect is also described by expression (29), but the kernel Q is to be renormalized. To find Q, we must take into account that the coupling $\mathbf{j}_s(\mathbf{A})$ is nonlocal in the clean limit. In the most general form, it can be expressed as

$$\mathbf{j}_s(x) = -\frac{c}{4\pi}\int K(x,x')\mathbf{A}(x')\,dx'. \tag{30}$$

Deep in the bulk of the superconductor (for $|x| \gg \xi_N = \hbar v_F/T$), the kernel $K(x,x')$ in expression (30) takes a local form characterized by the London depth λ_0. Here, ξ_N is the coherence depth in a clean normal metal. Integrating the Maxwell equation, just as in the case of the dirty limit, we then express the kernel Q as

$$Q = \int_{-x_0}^{d_f} dx \int_0^{d_f} dx'\,x'\left[K(x,x') - \lambda_0^{-2}\delta(x-x')\theta(-x)\right], \tag{31}$$

where $\theta(x)$ is the Heaviside step function, and the integration limit x_0 must be chosen such that the inequality $\xi_N \ll x_0 \ll \lambda_0$ holds.

Specifying the expression for Q even further requires microscopic calculations. To illustrate such calculations, we consider an SF bilayer in the dirty limit. The coordinate dependence of the inverse square of the London length λ^{-2} is then determined by expression (21). In the case where the ferromagnet conductivity σ_f is much less than the superconducting layer conductivity σ_s, the Kupriyanov–Lukichev boundary conditions for the Usadel equation reduce to the so-called rigid boundary conditions, which state that, inside the ferromagnetic layer at the SF interface, the singlet part of the anomalous Green's function coincides with the singlet component inside the superconductor, $f_s(0) = f_{s0} = \Delta/(\omega^2+\Delta^2)^{1/2}$ (where Δ is the width of superconducting gap in the superconductor and ω is the Matsubara frequency), and the triplet part of the anomalous Green's function $\mathbf{f}_t$ vanishes.

Choosing the gap Δ to be real, we obtain the solution of the Usadel equation inside the F layer in the form $f_s(x) = \mathrm{Re}\,F(x)$, $f_{tz}(x) = \mathrm{Im}\,F(x)$ with the complex function $F(x) = f_{s0}\cosh[q(x-d_f)]/\cosh(qd_f)$, where $q = 2(\omega+ih)/D_f$ and D_f is the diffusion coefficient in the ferromagnet. Substituting the found solution in (21) and summing over the Matsubara frequencies and integrating over the coordinate, we arrive at the final expression for kernel Q [373]:

$$Q = \frac{\pi^2\sigma_f\xi_f^2\Delta}{2\hbar c^2}\tanh\left(\frac{\Delta}{2T}\right)\mathrm{Im}\left[\frac{q^2d_f^2-1}{\cosh^2(qd_f)}\right]. \tag{32}$$

Figure 15 shows typical dependences of Q on the ferromagnetic layer thickness for the dirty and clean limits. Spatial oscillations of the singlet and triplet components of the anomalous Green's function in a ferromagnet layer give rise to regions with a diamagnetic and paramagnetic response inside the F layer (see Section 4.1). As a result, the sign of the Q kernel is determined by the ratio between the F-layer thickness and the superconducting correlation length ξ_f, and the dependence $Q(d_f)$ is oscillatory. In this case, the vector of the magnetic field induced in the superconductor and the magnetization vector in the F layer can be either codirectional (in the case $Q < 0$) or oppositely directed (in the case $Q > 0$). Moreover, for typical (for example, Nb-based) structures with a ferromagnetic layer thickness $d_f \sim \xi_f$, the kernel has the order $Q \sim (d_f/\lambda)^2 \sim 10^{-2}$.

Until now, we have considered an SF bilayer with homogeneous magnetization, in which only short-range triplet correlations with zero spin projection occur, while long-range triplet correlations are absent. At the same time, in systems with a noncollinear magnetization distribution, the electromagnetic proximity effect is significantly enhanced due to an increase in the integral amplitude of superconducting correlations and the total superconducting current inside the ferromagnet [373, 374].

As an illustration, we consider an SF system in the dirty limit, in which the ferromagnet consists of two layers with noncollinear magnetic moments. We assume that the superconductor is located in the region $x < 0$, the ferromagnetic layer F_1 is in the region $0 < x < d_1$, and the second ferromagnetic layer F_2 occupies the region $d_1 < x < d_1 + d_2$ (Fig. 16). We also assume that the magnetization moduli in both ferromagnetic layers are the same and equal to M_0, but the magnetization is directed along the z-axis in the F_1 layer and along the y-axis in the F_2 layer. The impact of long-range triplet correlations on the electromagnetic proximity effect is most pronounced if the F_2 layer thickness significantly

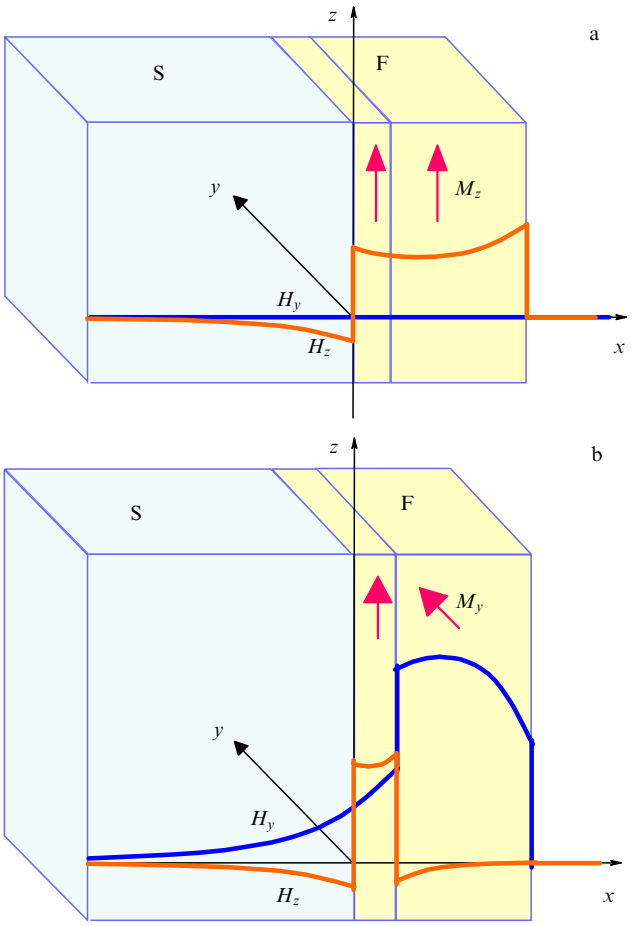

Figure 16. Schematic representation of magnetic field profiles in an SF structure with a composite ferromagnetic layer for two different mutual orientations of the F-layer magnetizations shown in the figure. (From [373].)

exceeds the correlation length $\xi_n = \sqrt{D_f/T}$. Still assuming that $d_2 \ll \lambda$, we can write the solution of the Maxwell equation for the SF_1F_2 system as

$$\mathbf{A} = \mathbf{A}_0 \exp\left(\frac{x}{\lambda_0}\right) \quad \text{at} \quad x < 0\,,$$

$$\mathbf{A} = (A_{0y} + 4\pi M_0 x)\mathbf{e}_y + A_{0z}\mathbf{e}_z \quad \text{at} \quad 0 < x < d_1\,,$$

$$\mathbf{A} = (A_{0y} + 4\pi M_0 d_1)\mathbf{e}_y + [A_{0z} - 4\pi M_0(x - d_1)]\mathbf{e}_z \quad \text{at} \quad d_1 < x < d_1 + d_2\,,$$

where the vector quantity $\mathbf{A}_0$ varies on scales of the order of λ only inside the ferromagnets and can be considered a constant, and $\mathbf{e}_y$ and $\mathbf{e}_z$ are unit vectors in the directions of the y- and z-axes. As in the case of an SF bilayer, integrating Maxwell equation (26) with respect to the thickness of the ferromagnetic layers allows representing the magnetic field profile inside the superconductor in the form

$$\mathbf{B}(x) = -4\pi M_0 \mathbf{Q} \exp\left(\frac{x}{\lambda_0}\right), \tag{33}$$

where the vector $\mathbf{Q}$ has the components

$$Q_z = \int_0^{d_1} \frac{x'\,\mathrm{d}x'}{\lambda^2(x')}\,, \qquad Q_y = \int_{d_1}^{d_1+d_2} \frac{(x' - d_1)\,\mathrm{d}x'}{\lambda^2(x')}\,. \tag{34}$$

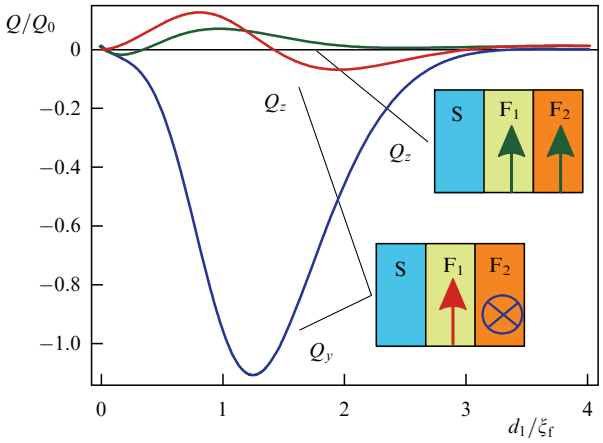

Figure 17. Dependences of the vector kernel components $\mathbf{Q}$ for SF_1F_2 systems in the dirty limit on thickness d_1 of the F_1 ferromagnetic layer. Green curve corresponds to a single Q_z component in the case of codirectional magnetic moments in two F layers, and the red and blue curves correspond to the Q_z and Q_y components for mutually orthogonal magnetic moments. Parameters are $\Delta = 2\pi T$, $h = 50\pi T$, $d_2 = 10\xi_f$, and $Q_0 = 16\pi^2 T\sigma_f\xi_f^2/c^2$. (From [374].)

Figure 16 schematically shows the magnetic field profiles for two mutual orientations of magnetizations in ferromagnetic layers. In the case of mutually orthogonal orientation of the magnetizations, the estimate of Q_y gives $Q_y \sim (\xi_n/\xi_f)^2 Q_z \gg Q_z$. As a result, in experiments that allow changing the orientation of the magnetic moment in one of the ferromagnetic layers, a significant increase in the magnetic field in the superconductor should be observed for the mutually orthogonal orientation of the magnetic moments in ferromagnets. Figure 17 shows the dependences of the components of the vector kernel $\mathbf{Q}$ on the F_1 ferromagnet thickness, obtained by solving the Usadel equation [374]. The calculation results fully confirm the above qualitative arguments about the enhancement of the electromagnetic proximity effect for systems with a noncollinear magnetization distribution.

From the experimental standpoint, the electromagnetic proximity effect leads to a number of features of the magnetic and transport properties of SF structures. An immediate and obvious consequence of the electromagnetic proximity effect is the appearance in a superconductor of a magnetic field that decreases on the scale of the London length λ, which in type-II superconductors significantly exceeds the scale of penetration of superconducting correlations from the ferromagnet into the superconductor (the latter scale is of the order of the superconducting correlation length $\xi_0 = \sqrt{D_s/T}$, where D_s is the diffusion coefficient in the superconductor).

The distribution of the magnetic field inside the SF system can be reconstructed experimentally by analyzing the scattering of spin-polarized neutrons and muons. For example, an anomalous (up to fivefold compared with the correlation length $\xi_s = \sqrt{D_s/T}$) increase in the spatial scale of the magnetic moment penetration into the superconductor was observed in [336–339, 384, 385], which may be related to the manifestation of the electromagnetic proximity effect. The theoretical conclusion about the enhancement of the induced magnetic field in the case of a mutually orthogonal orientation of the magnetic moments in SF_1F_2 structures is in complete agreement with the data in [336]. The magnitudes

of induced magnetic fields for Cu/Nb and Cu/Nb/Co structures were also compared experimentally in [383, 384]. It was shown that the addition of a Co layer to the system enhances the induced field, and the magnetic field profiles inside the structure are different when the collinear magnetic moments in two ferromagnetic layers are codirected and oppositely directed. Thus, to date, a large amount of experimental data has been accumulated indicating the important role of the electromagnetic proximity effect in the electrodynamics of SF systems.

The theory describing the occurrence of magnetic fields in SF systems, as outlined above, allows proposing several alternative methods for detecting the electromagnetic proximity effect and its possible applications. One of the possibilities is the direct detection of Meissner currents flowing through the superconductor. If the superconducting layer thickness is small compared to the London length λ, then the current density near the external boundary of the superconductor is nonzero. Moreover, scanning the surface of the superconductor with a normal (nonsuperconducting) probe of a scanning tunneling microscope can allow a change to be detected in the local DOS associated with a Doppler shift in the spectrum of quasiparticles due to the superconducting current flowing over the surface, while the use of a superconducting probe can allow a shift to be detected in the Fraunhofer dependence of the critical current of the Josephson junction formed by the S-layer and the microscope probe on the external magnetic field [374].

Another curious consequence of the electromagnetic proximity effect is the long-range electromagnetic interaction of the magnetic moments of two ferromagnetic layers separated by a superconducting layer of a thickness $d_s \lesssim \lambda$. To illustrate the possibility of such an interaction, it suffices to consider the free energy of the $F_1/S/F_2$ structure, which in the dirty limit can be written as

$$F = \int \left[\frac{(\mathbf{B} - 4\pi\mathbf{M})^2}{8\pi} + \frac{\mathbf{A}^2}{8\pi\lambda^2} \right] \mathrm{d}x \,, \tag{35}$$

where $\mathbf{B}(x)$ is the magnetic field inside the structure and $\mathbf{M} = \mathbf{M}_1$ ($\mathbf{M} = \mathbf{M}_2$) is the magnetization inside the F_1 (F_2) layer, with $\mathbf{M}$ equal to zero inside the superconductor. Due to the electromagnetic proximity effect, the magnetization in the F_1 layer induces a magnetic field decreasing on the scale λ in the superconductor, which penetrates into the F_2 layer. As a result, due to the cross term $\propto \mathbf{BM}$, the energies of states with the coincident and oppositely directed collinear magnetizations $\mathbf{M}_1$ and $\mathbf{M}_2$ are different. Interestingly, depending on the thickness of the ferromagnetic layers, the signs of the kernels Q_1 and Q_2 that determine the direction of the magnetic field induced by the ferromagnets can differ and correspond to either the ferromagnetic or the antiferromagnetic ordering of the magnetic moments in the two F layers. Thus, the choice of layer thicknesses allows engineering long-range magnetic interaction in F_1SF_2 systems.

As a final remark, we note that the electromagnetic proximity effect does not allow eliminating stray magnetic fields in SF structures with transparent boundaries using a special choice of the magnetic moment orientation in the F layer. Therefore, taking this effect into account is of key importance in the development of superconducting spintronic devices, because the presence of stray fields is an undesirable effect for many of them.

4.5 Larkin–Ovchinnikov–Fulde–Ferrell instability

The paramagnetic Meissner effect in planar SF structures, due to spin-triplet superconducting correlations, can lead to a loss of stability of the homogeneous superconducting state and the formation of states with the order parameter modulated in the plane of the layer [332, 386]. Such inhomogeneous states are similar to the LOFF states that arise in thin superconducting films placed in a strong longitudinal magnetic field [36, 37].

The conclusion that inhomogeneous LOFF states inevitably occur in SF systems with a paramagnetic response to a weak longitudinal magnetic field is already evident from the dependence of the system free energy F on the vector potential $\mathbf{A}$ characterizing the field. When the thickness of the SF structure is much less than the London length λ, the change in the longitudinal component of the vector potential $\mathbf{A}_\parallel$ in the direction across the layers can be disregarded. Integrating the local London relation (20) for $\mathbf{j}_s(\mathbf{A})$ across the layers gives a relation between the surface current density $\mathbf{I}_s = \int \mathbf{j}_s(x)\,\mathrm{d}x$ (where x is the coordinate across the layers) and $\mathbf{A}_\parallel$, involving the effective inverse length $\Lambda^{-1} = \int \lambda^{-2}(x)\,\mathrm{d}x$:

$$\mathbf{I}_s = -\frac{c}{4\pi}\,\Lambda^{-1}\mathbf{A}_\parallel \,. \tag{36}$$

Expression (36) allows reconstructing the dependence $F(\mathbf{A}_\parallel)$, because the current density can be regarded as the variational derivative of the free energy with respect to the vector potential ($\mathbf{j}_s = -c\,\delta F/\delta\mathbf{A}$). Here, we must take the gauge invariance of the free energy into account and introduce the superconducting order parameter phase φ into consideration. As a result, the free energy F can be represented as

$$F = F_0 + \frac{S}{8\pi}\,\Lambda^{-1}\left(\mathbf{A}_\parallel - \frac{\Phi_0}{2\pi}\,\mathbf{k}\right)^2 , \tag{37}$$

where the vector $\mathbf{k} = \nabla_\parallel\varphi$ is the gradient of the phase in the layer plane, S is the area of the SF structure, and the free energy part F_0 is independent of the vector potential.

It follows from (37) that, in the absence of an external field (for $\mathbf{A}_\parallel = 0$), the stability of a homogeneous superconducting state with $\mathbf{k} = 0$ is determined by the sign of the effective length Λ. For $\Lambda > 0$, the free energy minimum corresponds to a homogeneous state, and for $\Lambda < 0$, the homogeneous state loses stability: states with $\mathbf{k} \neq 0$ become energetically more favorable.

Thus, the sign change of Λ corresponds to the appearance of a LOFF state in the system with the order parameter modulated in the layer plane. At the same time, the problem of the magnitude of the vector $\mathbf{k}$ corresponding to the energy minimum cannot be solved in the framework of the linear response theory and requires taking the terms that are nonlinear in the vector potential $\mathbf{j}_s(\mathbf{A})$ into account. It is also important that, in the LOFF state, the response of the SF system remains diamagnetic, despite Λ^{-1} being formally negative. Indeed, the direction of the superconducting current is determined by the sign of the second derivative of the free energy with respect to the vector potential at the minimum, but when the energy minimum is shifted from the state with $\mathbf{k} = 0$ to the state with a nonzero $\mathbf{k}$, the sign of the second derivative does not change, remaining positive.

The qualitative arguments presented above are corroborated by microscopic calculations. As an example, we consider the simplest system: an SF bilayer in the dirty limit. For the simplicity of calculations, we assume that the

interface between the S and F layers is absolutely transparent to electrons, the superconducting layer thickness d_s is much less than the correlation length $\sqrt{D_s/(2\pi T)}$ (where D_s is the diffusion coefficient in the superconductor), and the exchange field h in the ferromagnet significantly exceeds the critical temperature T_{c0} of the superconducting phase transition for an isolated superconductor film. To describe the transition to the in-plane LOFF state, we assume that the width of the superconducting gap $\Delta(\mathbf{r}_\parallel) = \Delta_0 \exp(i\mathbf{k}\mathbf{r}_\parallel)$ can be phase-modulated in the plane of the layers ($\mathbf{r}_\parallel$ is the 2D radius vector in the plane of the structure). Taking the modulus of $\mathbf{k}$ as a parameter, we can calculate the temperature $T_c(k)$ such that, at temperatures below it, the superconducting state with a given k has a lower free energy than the normal state, and then find the maximum of the function $T_c(k)$, which would correspond to the critical temperature of the phase transition from the normal state to the in-plane LOFF state.

The dependence $T_c(k)$ can be calculated using the linearized Usadel equation for the anomalous Green's function $\hat{f}(k) = f_s + \mathbf{f}_t\boldsymbol{\sigma}$,

$$D\nabla^2\hat{f} - 2\omega_n\hat{f} - i\left(\mathbf{h}\boldsymbol{\sigma}\hat{f} + \hat{f}\mathbf{h}\boldsymbol{\sigma}\right) + 2\hat{\Delta} = 0\,, \tag{38}$$

where $\hat{\Delta} = \Delta(k)i\hat{\sigma}_y$, $\omega_n = \pi T(2n+1)$ are the Matsubara frequencies, and D is the diffusion coefficient (different in the S and F layers). We note that the anomalous Green's function in the bilayer plane is modulated in both layers, while, for the state predicted in [348], modulation is restricted to only the F layer (the inconsistency with the boundary conditions at the interface that arises in that case was discussed in [387]). In the absence of a potential barrier at the interface between the layers, the Kupriyanov–Lukichev boundary conditions reduce to the continuity of the Green's function $\hat{f}$ and of the combination $\sigma\partial_x\hat{f}$ on the SF interface (here, σ is the Drude conductivity of each layer in the normal state). For simplicity, we assume that the Fermi velocities in the S and F layers are equal, which implies the equality of the ratios of the diffusion coefficients and conductivities in the two layers. The sought function $T_c(k)$ is determined by the self-consistency equation

$$\Delta(k)\ln\frac{T_c(k)}{T_{c0}} + \sum_{n=-\infty}^{\infty}\left(\frac{\Delta(k)}{|2n+1|} - \pi T_c(k) f_{12}^{S}\right) = 0\,, \tag{39}$$

where f_{12}^{S} is the counterdiagonal component of the anomalous Green's function in the superconductor. The effective inverse screening length Λ^{-1} is determined by an integral over the thickness of the SF structure,

$$\Lambda^{-1} = \frac{16\pi^3 T_c}{ec\Phi_0}\sum_{n=0}^{\infty}\int\sigma\left(|f_s|^2 - |\mathbf{f}_t|^2\right)\mathrm{d}x\,. \tag{40}$$

To calculate further, we assume the exchange field h in the ferromagnet to be homogeneous and directed along the z-axis. Vector $\mathbf{f}_t$ then has only one component, which is codirectional with the exchange field, and hence the diagonal components of the anomalous Green's function vanish ($f_{11} = f_{22} = 0$). We also assume that the superconductor is in the region $-d_s < x < 0$ and the ferromagnet is in the region $0 < x < d_f$. Then, the solution of the Usadel equation can be obtained from the well-known solution for a homogeneous superconducting state in an SF bilayer (see, e.g., [39]) by the formal change $\omega_n \to \omega_n + Dk^2/2$. The result is

$$f_{12}^{S} = \frac{\Delta_0 \exp(i\mathbf{k}\mathbf{r}_\parallel)}{\omega_n + \tau_s^{-1}(k)}\,, \qquad f_{12}^{F} = f_{12}^{S}\,\frac{\cosh\left[q_k(x-d_f)\right]}{\cosh(q_k d_f)}\,, \tag{41}$$

where $q_k = \sqrt{q^2 + k^2}$, $q = (1+i)/\xi_f$, $\xi_f = \sqrt{D_f/h}$ is the correlation length in the ferromagnet, and

$$\tau_s^{-1}(k) = \frac{D_s k^2}{2} + \frac{D_s}{2d_s}\,\frac{\sigma_f}{\sigma_s}\,q_k\tanh(q_k d_f) \tag{42}$$

is the depairing factor. Substituting the obtained solutions for the anomalous Green's function in (39) and (40), we obtain a relation between the screening parameter Λ^{-1} and the dependence $T_c(k)$,

$$\frac{1}{\Lambda} = \frac{16\pi^2 d_s\sigma_s\Delta_0^2}{ec\Phi_0 D_s T_c(0)}\left[\mathrm{Re}\left\{\nu\Psi_1\left(\frac{1}{2}+\nu\right)\right\} - 1\right]\left.\frac{\partial T_c}{\partial k^2}\right|_{k=0}, \tag{43}$$

where $\nu = \tau_s^{-1}(0)/(2\pi T_c(0))$ and Ψ_1 is the trigamma function. Expression (43) directly confirms the qualitative reasoning given above: the loss of stability of a homogeneous superconducting state, which manifests itself in a sign reversal of the derivative $\partial T_c/\partial k^2$, is accompanied by the sign reversal of the screening parameter Λ^{-1}.

An implicit expression for the function $T_c(k)$ can be obtained from self-consistency equation (39),

$$\ln\frac{T_c(k)}{T_{c0}} = \Psi\left(\frac{1}{2}\right) - \mathrm{Re}\,\Psi\left[\frac{1}{2} + \frac{\tau_s^{-1}(k)}{2\pi T_c(k)}\right], \tag{44}$$

where Ψ is the digamma function. Typical $T_c(k)$ dependences are shown in Fig. 18. At relatively large superconducting layer thicknesses d_s, the contribution of triplet correlations $\mathbf{f}_t$ to the total response of the SF system is much less than the contribution from the singlet component f_s of the anomalous Green's function, and hence $\Lambda^{-1} > 0$ and the dependence $T_c(k)$ is a monotonically decreasing one with a maximum at $k = 0$ (which corresponds to the formation of a homogeneous superconducting state). As the thickness d_s decreases, the

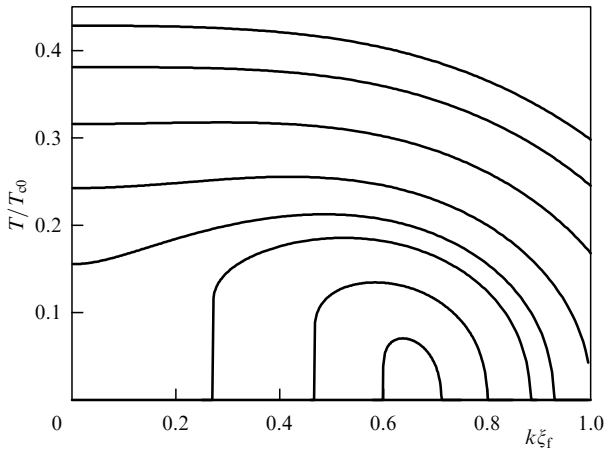

Figure 18. Dependences of critical temperature T_c on the modulus of modulation vector k for various thicknesses d_s of the superconducting layer. System parameters are $\xi_{s0} = \sqrt{D_s/(4\pi T_{c0})} = 0.1\xi_f$ and $d_f = 1.2\xi_f$. Dimensionless quantity $(d_s/\xi_f)(\sigma_s/\sigma_f)$ takes values 0.13, 0.125, 0.12, 0.1165, 0.1148, 0.114, 0.113, and 0.1125. An increase in superconductor thickness d_s corresponds to an increase in the maximum of the $T_c(k)$ dependences. (From [332].)

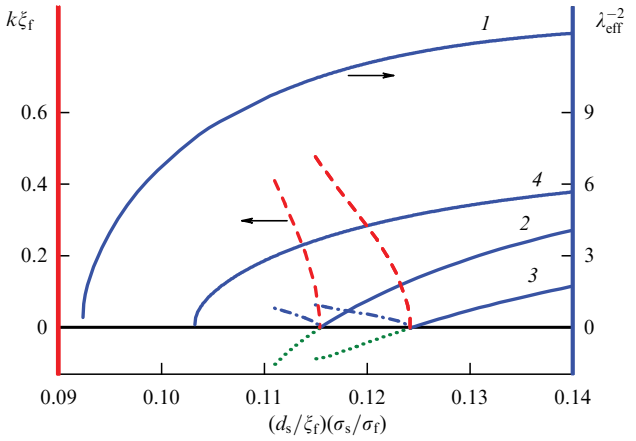

Figure 19. Dependences of the effective inverse London length Λ^{-1} (solid blue curves) and the optimal modulation of the LOFF wave vector k_0 (red curves) on the superconductor layer thickness d_s. Hand-drawn blue dotted lines illustrate the behavior of the screening parameter in the LOFF phase, and green dotted curves correspond to the Λ^{-1} dependences calculated for an unstable homogeneous superconducting state (not realized physically). Parameters are chosen as $\xi_{s0} = \sqrt{D_s/(4\pi T_{c0})} = 0.1\xi_f$, $d_f = 0.75\xi_f$ (*1*), $d_f = 1.0\xi_f$ (*2*), $d_f = 1.2\xi_f$ (*3*), and $d_f = 2.0\xi_f$ (*4*). Notation $\lambda_{eff}^{-2} = \Lambda^{-1}[T_c(0)ec\Phi_0/(2\pi\sigma_s d_s \Delta_0^2)]$ is used. (From [332].)

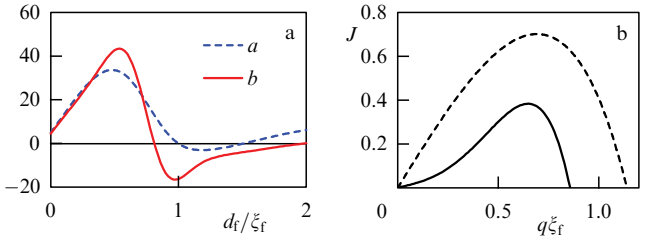

Figure 20. (a) Coefficients $a = \alpha(2\pi T_c)^2\Lambda_c$ and $b = \beta(2\pi T_c)^2\Lambda_c$ in expression (45) as functions of the ferromagnetic layer thickness d_f. (b) Dependences of the superconducting current $J = j_s\Lambda_c T_c/(\xi_f T_{c0})$ on the superconducting velocity q for $T = 0.8T_c(d_f)$, where $T_c(d_f)$ is the dependence of the critical SF-bilayer temperature on the ferromagnet thickness. Solid (dashed) curve corresponds to the F-layer thickness $d_f = 0.91\xi_f$ ($d_f = 0.3\xi_f$). Parameters used in calculations are $\xi_f = 10\xi_s$ and $\sigma_s d_s/(\sigma_f\xi_f) = 0.06$, and the definition $\Lambda_c = ec\Phi_0/(16\pi^3\sigma_s d_s T_c)$ is used. (From [386].)

triplet contribution of correlations to Λ^{-1} becomes comparable to the contribution of f_s, and for $D_f/D_s \gg h/T_{c0}$ at some critical S-layer thickness $d_{sc} \sim (\sigma_f/\sigma_s)\xi_f$, the screening parameter Λ^{-1} can vanish. As d_s decreases further, the maximum of $T_c(k)$ corresponds to a LOFF state with $k = k_0 \neq 0$.

Interestingly, the LOFF states can appear in the range of parameters where the homogeneous superconducting state is suppressed at any temperature. The dependences of the effective London length Λ^{-1} and the optimal modulation vector k_0 in the LOFF state on the superconductor thickness are shown in Fig. 19.

The in-plane LOFF states in SF systems discussed above differ from the LOFF states predicted for thin superconducting films in an external longitudinal magnetic field in a number of important ways. First, the classical LOFF states are disorder-sensitive and can only occur in clean films. Second, in contrast to the classical LOFF phase that occurs at low temperatures, LOFF states in SF systems can form at temperatures close to T_{c0}. This can be most conspicuous in three-layer systems composed of a superconductor, a ferromagnet, and a normal metal. For the LOFF instability to be realized in such a system, the ferromagnet conductivity σ_f can be chosen small compared to σ_s, and the conductivity of the normal metal σ_n, much greater than σ_s. The suppression of the critical temperature due to the proximity effect is mainly determined by the properties of the ferromagnet and is in fact weak. At the same time, the normal metal region, due to its high conductivity, makes a significant contribution to the screening parameter Λ^{-1}. By choosing the ferromagnet thickness such that the triplet component of the anomalous Green's function dominates the singlet component at the FN interface, a significant paramagnetic contribution to Λ^{-1} from the N layer can be ensured, comparable to the diamagnetic contribution from the superconductor. Therefore, there is a region of parameters in which the in-plane LOFF instability in SFN systems arises at temperatures only slightly lower than T_{c0}.

Finally, one of the most important features of the LOFF states in SF systems is the possibility of a phase transition to a modulated state caused by changing the temperature. For classical LOFF states, changes in temperature can only lead to a transition between the normal and modulated states, but for SF systems, there is a wide range of parameters where a transition between the homogeneous superconducting state and the LOFF phase is possible. As a result, in the temperature–exchange-field diagram, the domain of the existence of an inhomogeneous phase can be completely isolated from the stability domain of the normal (nonsuperconducting) phase.

To illustrate the mechanism responsible for the phase transition between the homogeneous and modulated phases as the temperature changes, we consider the case where the temperature T is close to the critical temperature of the superconducting phase transition T_c into the homogeneous phase. In this temperature range, the width of the superconducting gap Δ is small, and hence the effective inverse London length Λ^{-1} can be expanded in a power series in Δ,

$$\Lambda^{-1} = \alpha\Delta^2(T) + \beta\Delta^4(T), \qquad (45)$$

where the coefficients α and β are independent of the temperature, and the superconducting gap $\Delta(T)$ vanishes at $T = T_c$ and increases monotonically as the temperature decreases. The α and β coefficients for the SF bilayer in the dirty limit can be calculated by solving the nonlinear Usadel equation [386]. Typical dependences of these coefficients on the ferromagnetic layer thickness d_f for SF systems with a thin S-layer ($d_s \ll \xi_s$) and a large exchange field in the F-layer ($h \gg T_c$) are shown in Fig. 20a. For sufficiently large values of the conductance ratio σ_f/σ_s, α can become negative in a certain range of d_f, which corresponds to the formation of a LOFF state at the critical temperature. At the same time, at the points where $\alpha = 0$, the coefficient β is always negative. As a result, even for small positive values of α, the second term in (45) completely compensates the term proportional to Δ^2 at some temperature $T_F < T_c$. The vanishing of Λ^{-1} is then accompanied by a phase transition from a homogeneous superconducting phase to a LOFF state (a typical form of the phase diagram of the system is schematically shown in Fig. 21).

Another interesting feature of the low-temperature LOFF phase is the sign reversal of the nonlinear contribution to the

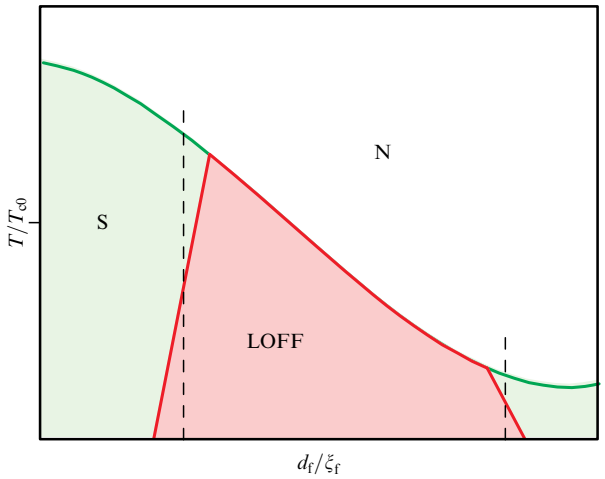

Figure 21. Schematic representation of a typical phase diagram of an SF structure in the parameter range corresponding to the appearance of the LOFF phase. Dashed lines show an example of the ferromagnet thicknesses at which a change in temperature leads to a phase transition to the LOFF state. (From [375].)

relation between the superconducting current $\mathbf{j}_s$ and supervelocity, which is proportional to $\mathbf{q} = \nabla\varphi - (2\pi/\Phi_0)\mathbf{A}$. At a qualitative level, this effect can be illustrated in the framework of the Ginzburg–Landau (GL) theory. Near the phase transition to the LOFF phase, the contribution to the free energy density due to the superconducting order parameter Δ has the form [388]

$$F = (-\alpha_0\tau + \beta_0 q^2 + \delta_0 q^4)\Delta^2 + (\gamma_0 + \eta_0 q^2)\Delta^4\,, \qquad (46)$$

where $\tau = (T_c - T)/T_c$. The superconducting current is proportional to the derivative of the free energy with respect to the supervelocity, $j_s \propto \partial F/\partial q$. For a fixed q, minimizing F with respect to the superconducting gap width Δ gives the optimum value $\Delta^2 = (\alpha_0\tau - \beta_0 q^2)/(2\gamma_0) + O(q^4)$ corresponding to a minimum of F. Substituting the found value of Δ^2 into the expression for the current, we obtain

$$j_s \propto \frac{\beta_0\alpha_0\tau q - \beta_0^2 q^3 + 2\delta_0\alpha_0\tau q^3}{\gamma_0}\,. \qquad (47)$$

Far from the parameter range corresponding to the LOFF phase in the phase diagram, the third term on the right-hand side of (47) is negligible compared to the second term and hence $\partial^2 j_s/\partial q^2 < 0$. But near the LOFF instability threshold, the coefficient β_0 is strongly suppressed, and the last term in (47) with $\delta_0 > 0$ changes the sign of the curvature of the $j_s(q)$ dependence at small q.

The results of microscopic calculations of the $j_s(q)$ dependence in the framework of the nonlinear Usadel theory [386] are shown in Fig. 20b. The predicted change of sign of the curvature of $j_s(q)$ should manifest itself in experiments on measuring the third harmonic of the electromagnetic response of SF structures [363–365] and can be used as an additional tool for detecting LOFF states.

We note that, according to our assumption, the order parameter has the form of a plane wave $\Delta \sim \exp(i\mathbf{qr})$, and this is certainly justified when analyzing the LOFF instability existence problem. At temperatures below the threshold for the emergence of the LOFF phase, the problem of the realization of a curl-free Fulde–Ferrell-type state (also considered in [366, 389]) and its energy competition with states characterized by inhomogeneities of the order parameter modulus requires a separate analysis.

The conditions for the occurrence of LOFF instability turn out to be milder for three-layer SFN systems. There, a normal metal can significantly enhance the contribution of triplet correlations to the screening parameter Λ^{-1}; as a result, the transition temperature to the LOFF phase can reach several kelvins according to estimates in [386].

In general, SF systems open up new prospects for the experimental detection of LOFF states. Although these states were first predicted more than 50 years ago, there are still only a few experiments that provide convincing evidence for the LOFF instability. Quasi-two-dimensional organic superconductors, such as λ-$(BETS)_2GaCl_4$ [390], λ-$(BETS)_2FeCl_4$ [391], κ-$(BEDT-TTF)_2Cu(NCS)_2$ [392–396], and β″-$(ET)_2SF_5CH_2CF_2SO_3$ [397, 398], are used in samples. The layered structure of these compounds contributes to the suppression of the orbital effect for a magnetic field parallel to the layers, and the strong anisotropy of the Fermi surface is conducive to an additional stabilization of the LOFF states [399].

At the same time, SF structures seem to have a number of advantages over the systems listed above. First, the LOFF phase in SF systems can emerge in the dirty limit, which significantly reduces the requirements for the purity of the sample. Second, the LOFF instability in SFN systems can occur at relatively high temperatures. Third, SF systems allow the controlled switching among the normal phase, the homogeneous superconducting states, and the LOFF states by varying the temperature. Experimentally, the occurrence of the LOFF phase can be detected by suppressing the electromagnetic response at the phase transition point and by the sign reversal of the third harmonic of the electromagnetic response in a longitudinal magnetic field.

To conclude this section, we note that the LOFF instability mechanism described here is not specific to planar SF systems. Similar LOFF states have been predicted for ferromagnetic cylinders coated with a superconductor layer [400–403] and for SN bilayers in the case of a nonequilibrium energy distribution of quasiparticles [404, 405].

4.6 Spontaneous currents. Spin–orbit effects

The electrodynamics of hybrid SF systems becomes much richer in the presence of SO coupling at the interface between the materials. The presence in the system of an additional mechanism of spin splitting of electron states makes states with different spin (and hence momentum) projections nonequivalent. The spin splitting mechanism can be either the usual Zeeman interaction of the electron spin with an external magnetic field [307–310] or the exchange interaction of conduction electrons with localized spins in the presence of magnetic ordering in the system [406–408].

In this subsection, we focus on systems with the exchange mechanism of spin splitting arising in SF hybrid systems, which are considered a promising platform for engineering nonconventional superconducting states [77, 243, 245, 264, 304, 321, 409–414]. In such systems, it is natural to expect the presence of a Rashba-type SO coupling [95] associated with symmetry breaking with respect to spatial inversion at the interface between the superconductor and the ferromagnet [252, 253, 264, 304, 321] or with the addition of another thin layer with a strong SO coupling [409].

From an electrodynamic point of view, one of the most interesting questions is whether helicoidal states can generate a spontaneous electric current in the presence of spin splitting. Initially, this question was considered for superconductors without an inversion center placed in an external magnetic field. At first glance, the occurrence of spontaneous currents in such systems seems natural. Indeed, the contribution of the Rashba-type SO coupling to the Hamiltonian is proportional to the mixed product $[\mathbf{n}\times\mathbf{p}]\boldsymbol{\sigma}$, where $\mathbf{n}$ is the unit vector along the direction in which the inversion symmetry is broken. In this case, spin splitting under the action of a magnetic field $\mathbf{H}_0$ induces a difference between energies of the states with $\mathbf{p}\propto\pm[\mathbf{H}_0\times\mathbf{n}]$. As a result, one of the momentum directions becomes energetically more favorable, and the wave function of the Cooper pairs takes the form of a plane wave $\propto\exp(\mathrm{i}\mathbf{pr})$, which suggests the occurrence of a spontaneous current.

But it turns out on closer examination that the presence or absence of a spontaneous current essentially depends on the spin splitting mechanism. In bulk s-wave superconductors without an inversion center, spontaneous current generation is impossible due to the large kinetic energy of the moving condensate. In the case of quasi-two-dimensional superconductors placed in a longitudinal magnetic field, helicoidal states with a preferred momentum direction do arise, but the SO coupling modifies the quantum mechanical expression for the current, such that there is no spontaneous current for these states [306, 310, 415–417]. At the same time, in systems based on superconductors with d- or chiral p-type pairing, as well as at the interfaces between s-wave superconductors and HMs (ferromagnets with full spin polarization of the bands), the occurrence of a spontaneous current is possible due to the formation of states with broken time reversal symmetry [418–428]. We note that, in the systems mentioned above, the current states arise at temperatures much lower than the critical superconducting phase transition temperature.

In spite of above argument, the picture changes completely if the spin splitting is due to the exchange interaction of the electron spins forming a Cooper pair with the exchange field of the ferromagnet (for example, in SF systems with a developed proximity effect). The structure of the helicoidal wave functions of Cooper pairs then coincides with the structure of the wave functions for a superconducting film in a longitudinal magnetic field. However, the ground state is a zero-current one for a film in a magnetic field, but a nonzero spontaneous current is present in SF systems with a strong SO coupling.

The key difference between the two systems under consideration becomes clear if we represent the superconducting current $\mathbf{j}_s$ as the variational derivative of the free energy with respect to the vector potential, $\mathbf{j}_s=-c\,\delta F/\delta\mathbf{A}$. When the spin splitting is due to the magnetic field $\mathbf{B}=\mathrm{rot}\,\mathbf{A}$, the derivative of the magnetic field in the SO term of the Hamiltonian with respect to the vector potential makes a nonzero contribution to the current. This contribution exactly compensates the spontaneous current due to the helical nature of the superconducting state. At the same time, there is no orbital mechanism of the coupling to the superconducting condensate for the exchange field (the exchange field is not related to a vector potential), and hence the compensating contribution to the current does not arise. As a result, the formation of states with a nonzero spontaneous current is possible for a wide class of SF structures: SF bilayers [410, 429], superconducting films with magnetic particles on their surface [430–433], and superconducting rings partially coated with a ferromagnetic insulator [243].

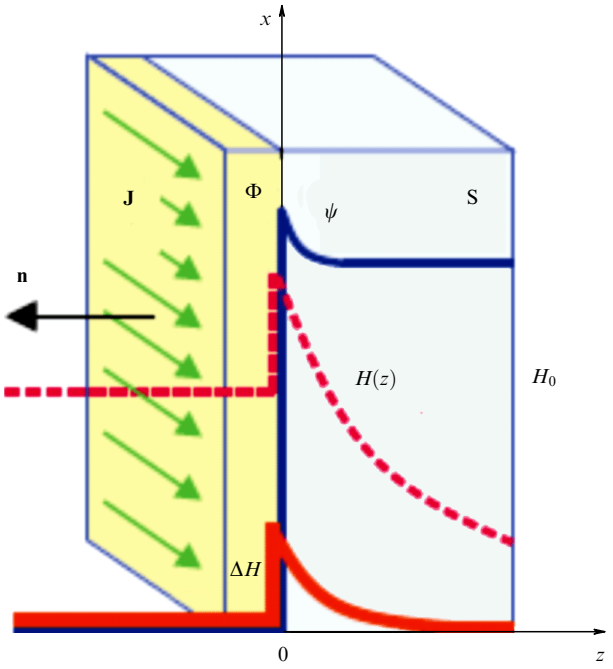

Figure 22. Hybrid SF structure in which the Rashba SO coupling creates spontaneous current $\mathbf{J}=J\mathbf{e}_y$, Eqn (50), in the vicinity of the S/F interface. Corresponding magnetic field profile and superconducting order parameter ψ are shown by solid curves. Dashed curve shows the profile of the magnetic field in the presence of external field H_0. (From [410].)

To describe the mechanism of formation of spontaneous currents in SF structures at temperatures close to the critical superconducting phase transition temperature, it suffices to use the phenomenological Ginzburg–Landau model. The effects of the SO coupling can then be taken into account by including the Lifshitz invariant into the superconductor free energy functional $F=\int f(\mathbf{r})\,\mathrm{d}^3\mathbf{r}$ [301, 302]. As a result, the free energy density can be represented as [308, 309, 434]

$$f(\mathbf{r})=a|\psi|^2+\frac{b}{2}\,|\psi|^4+\frac{1}{4m}|\,\hat{\mathbf{D}}\,\psi|^2+\frac{(\mathrm{rot}\,\mathbf{A})^2}{8\pi}+\left\{\varepsilon(\mathbf{r})[\mathbf{n}\times\mathbf{h}]\,\psi^*\,\hat{\mathbf{D}}\,\psi+\mathrm{c.c.}\right\},\qquad(48)$$

where $\psi=|\psi|\exp(\mathrm{i}\varphi)$ is the superconducting order parameter, $a=-\alpha(T_c-T)$, α and b are standard coefficients of the Ginzburg–Landau functional, $\hat{\mathbf{D}}=-\mathrm{i}\hbar\boldsymbol{\nabla}+(2e/c)\mathbf{A}$ is the gauge-invariant momentum operator ($e>0$), and the parameter $\varepsilon(\mathbf{r})\propto v_R/E_F$ [434] characterizes the SO coupling strength (where v_R is the Rashba velocity and E_F is the Fermi energy).

As an example of a system where superconducting states with a spontaneous current are formed, we consider a two-layer system consisting of a superconductor coated with a ferromagnetic insulator layer (Fig. 22) [410]. The low conductivity requirement for the ferromagnet allows us to assume that superconducting correlations penetrate into the bulk of the ferromagnet only to atomic scales and to ignore the suppression of the superconducting state due to the proximity effect, with the order parameter modulus $|\psi|$ assumed to be independent of the coordinate across the structure. In addition, we assume that the SO coupling is

present only in a narrow layer of atomic thickness $|z| \lesssim l_{SO} \ll \xi = \hbar/\sqrt{4m|a|}$ in the vicinity of the SF interface. For simplicity, we confine ourselves to considering the situation where the exchange field $\mathbf{h}$ in the ferromagnet and the external magnetic field $\mathbf{H}_0$ are directed along the x-axis, such that the spontaneous current due to the SO coupling is localized near the $z = 0$ plane on the atomic scale and is parallel to the y-axis. Then, the term related to the SO coupling in free energy (48) can be represented as a surface term,

$$F_{SO} = 2|\psi|^2 \varepsilon\, l_{SO} S[\mathbf{n} \times \mathbf{h}] \left(\hbar\nabla\varphi + \frac{2e}{c}\,\mathbf{A} \right)\Bigg|_{z=0}, \qquad (49)$$

where S is the area of the SF interface. In (49), we neglected the spin splitting of electron states associated with the magnetic field, assuming it to be small compared to the exchange field ($\mu_B H_0 \ll h$). The surface density of the spontaneous current $\mathbf{J}_{SO}$ flowing along the SF interface is determined by the derivative of (49) with respect to the vector potential,

$$\mathbf{J}_{SO} = -\frac{1}{S}\frac{c\,\partial F_{SO}}{\partial \mathbf{A}} = -\frac{c\,\Phi_{SO}}{2\pi\lambda^2}\,\mathbf{e}_y\,, \qquad (50)$$

where $\Phi_{SO} = q_{SO} l_{SO} \Phi_0/(4\pi)$ is the effective magnetic flux ($\Phi_0 = \pi\hbar c/e$ is the magnetic flux quantum), $q_{SO} = 4m\varepsilon h/\hbar$ is the wave number characterizing the spin splitting magnitude in the presence of SO coupling and of the exchange field ($q_{SO} l_{SO} \sim 1$), $\lambda = [mc^2/(8\pi e^2|\psi|^2)]^{1/2}$ is the London length, and $\mathbf{e}_y$ is the unit vector in the y direction. The above spontaneous surface current leads to the appearance of a magnetic field jump on the $z = 0$ plane. From the Maxwell equations, we find that the field jump is $\Delta H = 2c\Phi_{SO}/\lambda^2$. The excess spontaneous field arising in the superconductor must then be screened by the Meissner currents flowing in the bulk of the S layer.

We emphasize that, in contrast to the spontaneous currents in d- and p-wave superconductors or at interfaces between s-wave superconductors and HMs, which appear in the low-temperature limit [418–428], spontaneous currents and fields in SF systems arise directly at the superconducting phase transition temperature, thus becoming experimentally distinguishable in the background of other magnetic effects. Estimates show that, for type-II superconductors, the spontaneous field is of the order of $\Delta H \sim q_{SO} l_{SO} H_{c1}(T)$ (where $H_{c1}(T) = \Phi_0/(4\pi\lambda^2(T))$ is the lower critical field of the superconductor) and for typical values $l_{SO} \sim 1-10$ nm can even exceed the $H_{c1}(T)$ field. In this case, the spontaneous current can make it advantageous for Abrikosov vortices to enter the sample.

The nature of the effect of the spontaneous surface current on the properties of the superconducting state, the properties of the superconducting phase transition, and the transport properties of the SF system essentially depend on the relation among the superconducting layer thickness L, the superconducting coherence length ξ, and the London depth λ. We consider several cases one after another.

We first discuss the limit of a thick superconductor, $L \gg \max\{\lambda, \xi\}$ [410]. The Meissner currents screening the spontaneous current $\mathbf{J}_{SO}$ are then localized on the λ scale near the SF interface, and the magnetic field profile inside the superconductor has the form $H_x(z) = (H_0 + \Delta H)\exp(-z/\lambda)$. In a region that has a width of the order of ξ near the SF interface, the superconducting order parameter increases by a relative value $\sim (\lambda/\xi)(\Delta H/H_{cm})^2$ (where $H_{cm} = 2\sqrt{2}e\lambda\xi$ is the thermodynamic critical field), but this does not lead to a change in the critical temperature of the superconducting phase transition in the absence of an external magnetic field. At the same time, in type-II superconductors, the spontaneous current significantly affects the temperature dependence of the critical magnetic field H_{c3} that corresponds to the appearance of localized superconductivity at fields exceeding the bulk critical field. This effect is a consequence of the interaction of the spontaneous current with the Meissner current that screens the external field H_0.

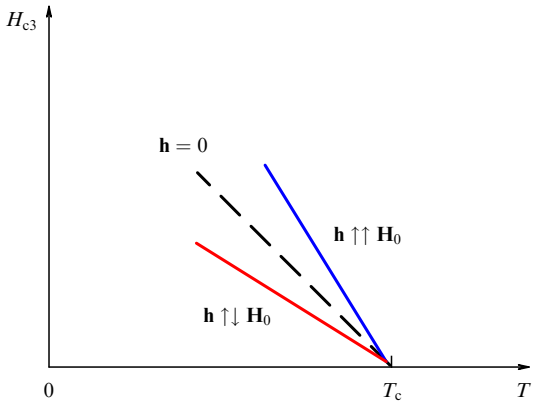

Figure 23. Dependence $H_{c3}(T)$ of the critical field of the emergence of surface superconductivity on the temperature for a thick superconductor coated with a thin ferromagnetic insulator film with a strong SO coupling at the interface (for $\varepsilon > 0$). Red and blue curves correspond to different mutual orientations of external magnetic field $\mathbf{H}_0$ and exchange field $\mathbf{h}$ in the ferromagnetic layer. Black dashed line corresponds to the temperature dependence of the critical field in the absence of a ferromagnet. (From [410].)

Calculations in [410] show that, at temperatures close to T_c, the dependence $H_{c3}(T)$ has the form

$$H_{c3}(T) \approx H^0_{c3}(T)\left(1 + \nu\zeta\,\frac{\Phi_{SO}}{\Phi_0}\right), \qquad (51)$$

where $H^0_{c3}(T) = 1.69(2m\alpha/e)(T_c - T)$ is the temperature dependence of the critical field for surface superconductivity in an isolated S layer, $\zeta \approx 24.9$ is a constant, and the parameter ν takes two values: $\nu = 1$ if the exchange field in the F layer is codirectional with the external magnetic field and $\nu = -1$ if these fields are oppositely directed. Hence, a change in the direction of the external magnetic field should lead to a change in the slope of the $H_{c3}(T)$ dependence (Fig. 23), which can be used as a tool for the experimental detection of spontaneous currents.

The picture described above changes somewhat if the superconductor thickness L is small compared to the superconducting coherence length ξ [429]. In the case of a type-I superconductor, for which the relations $\lambda \ll L \ll \xi$ are satisfied, the local enhancement of superconductivity near the SF interface due to the SO coupling can already lead to an increase in the critical temperature T_c of the SF bilayer compared to the critical temperature T_{c0} of an isolated superconductor. As the temperature decreases, the transition from the normal state to the superconducting state occurs as a first-order phase transition. Assuming that a weak magnetic field ($H_0 \ll \Delta H$) is applied to the SF bilayer, it can be shown

that

$$\frac{T_c^{\pm}}{T_{c0}} = 1 + \frac{1}{8}\left(\frac{\lambda_0}{L}\right)^2 \left(\frac{\Delta H}{H_{cm}}\right)^4 \pm \frac{2|H_0|}{\Delta H}\,, \qquad (52)$$

where λ_0 is the London length at zero temperature and the sign $\pm$ in front of the last term corresponds to the codirected (oppositely directed) external magnetic field $\mathbf{H}_0$ and the exchange field $\mathbf{h}$ in the ferromagnet. The dependence of the critical temperature on the external magnetic field orientation allows using the obtained result to detect spontaneous currents, in particular, to analyze the sign of the SO coupling constant. Indeed, the critical temperature is higher for codirectional $\mathbf{H}_0$ and $\mathbf{h}$ only in the case where $\varepsilon > 0$, while for $\varepsilon < 0$ the relation between T_c^+ and T_c^- is reversed.

Finally, thin SF bilayers with a strong SO coupling should exhibit a peculiar diode effect — a dependence of the critical depairing current on the direction of the current in the layer plane [429]. Such an anisotropy of the critical current does not seem possible at first glance, because the total superconducting current due to the SO coupling and the Meissner effect is equal to zero. But the key point is the spatial inhomogeneity of the distribution of the Meissner current that screens the $\mathbf{J}_{SO}$ current along the thickness of the SF structure. As a result, for a fixed orientation of the exchange field, the local current density (and hence local suppression of the superconducting order parameter) at some point in the superconductor becomes dependent on the angle θ between the external transport current and the spontaneous current $\mathbf{J}_{SO}$ flowing along the SF interface. The maximum current that can flow along the SF structure without destroying superconductivity also acquires a dependence on θ. The described diode effect allows detecting spontaneous currents in transport measurements.

Another way to detect the spontaneous supercurrent induced by the combined action of the Rashba SO coupling and the exchange field at an SF interface can be implemented in systems with a multiply connected geometry [243], for example, in a superconducting circuit partially coated with a ferromagnetic insulator (Fig. 24). The exchange field $\mathbf{h}$ in the SF interface region is formed on a scale $l_{SO} \sim \hbar/\sqrt{2mE_g} \lesssim 2$ Å, where $E_g \sim 1-2$ eV is the typical gap width in the FI band spectrum. Because both the effective exchange field $\mathbf{h}$ and the Rashba SO coupling are present in a range of the order of the interatomic distance l_{SO}, the constant ε in (48) must be averaged over the S-circuit thickness: $\varepsilon \propto (l_{SO}/d)\, v_R/E_F$ [435–437]. Assuming that the circuit is thin and narrow, $d, w \ll \xi_0 \sim \hbar v_F/\Delta_0$, and the temperature T is considerably lower than T_c, we can regard the amplitude of the wave function of the pairs as being homogeneous along the circuit ($|\psi| = \text{const}$). The presence of the SO coupling and the exchange field gives rise to the phase modulation $\psi = |\psi| \exp(iq_1\zeta)$ with the wave vector q_1 in a length-L_h part of the circuit oriented along the vector $\mathbf{n} \times \mathbf{h}$, which is in this case directed along the y-axis (ζ is a coordinate along the circuit and the Rashba vector $\mathbf{n}$ is orthogonal to the circuit plane). The corresponding supercurrent density

$$j = \frac{e\hbar}{m}\,|\psi|^2\left(\frac{\partial\varphi}{\partial\zeta} - q_{SO}\right)$$

in this region is $j_1 = (e\hbar/m)|\psi|^2(q_1 - q_{SO})$. In the remaining length-L_0 part of the circuit, the SO coupling and exchange field are both absent ($q_{SO} = 0$) and the supercurrent density is determined by the usual expression $j_2 = (e\hbar/m)\,|\psi|^2 q_2$, where the wave number q_2 is to be found from the current continuity condition $q_2 = q_1 - q_{SO}$ and the single-valuedness of the wave function phase $q_1 L_h + q_2 L_0 = 2\pi n$. From these conditions, it is easy to determine that the wave number $q_2 = (2\pi n - q_{SO}L_h)/(L_h + L_0)$ is nonzero in general and this means the possibility of spontaneous generation of supercurrent in the circuit. Thus, a superconductor with an exchange field and SO coupling can under certain conditions play the role of a phase battery that produces the phase difference $\Delta\varphi = q_1 L_h$ in part of the circuit [243]. A tunable phase battery based on a combination of SO coupling and exchange interaction in an InAs nanowire was recently implemented in [244].

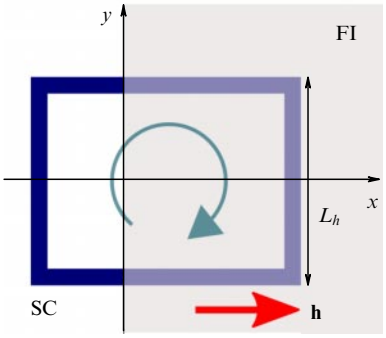

Figure 24. Superconducting circuit (SC) partially covered with a ferromagnetic insulator (FI) with exchange field $\mathbf{h}$. (From [243].)

A characteristic feature of structures with a multiply connected geometry is the Little–Parks (LP) effect [438, 439], which consists in oscillations of the critical superconducting transition temperature $T_c(H)$ with a change in the external magnetic flux $\Phi = HS$ penetrating a closed superconducting circuit of area S. The LP effect, which is a classic and direct illustration of the orbital mechanism of superconductivity suppression, is expressed in transitions, initiated by an external field H, between states with different vorticities L. The nontrivial interaction between the LP effect and helicoidal states with an induced current was studied in [243] using GL functional (48) with the example of a thin and narrow superconducting ring of radius $R \gg \xi_0$ coated with FI in the range $x \geqslant 0$ (see inset in Fig. 25).

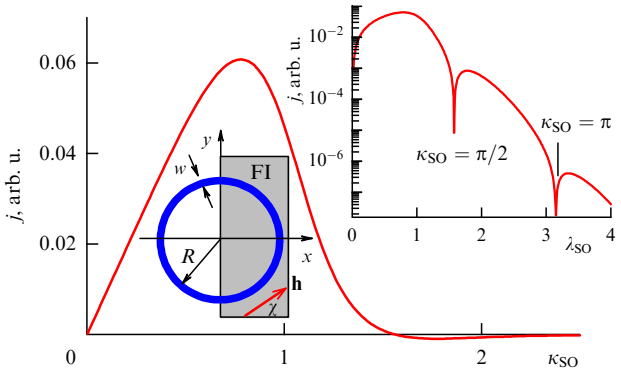

Figure 25. Dependence of the spontaneous current density in a thin superconducting ring, which in the range $x \geqslant 0$ is coated with a ferromagnetic insulator (FI) with exchange field $\mathbf{h}$, on the parameter $\kappa_{SO} = q_{SO}R$ for temperature $T/T_c = 1 - 0.3(\xi_0/R)^2$. (From [260].)

Qualitatively, the influence of spin splitting in the presence of SO coupling on the LP effect can be understood by assuming that the spontaneous current arising in such a ring imitates an additional magnetic flux $\Delta\Phi = \Phi_0(q_{SO}R/\pi)\cos\chi$, which determines the shift in the position of the LP oscillation maxima $T_c(H)$. The direction and magnitude of $\Delta\Phi$ depend on the orientation of the exchange field. The strong SO coupling and exchange field cause a noticeable shift of the LP oscillations, which can be detected experimentally. In the absence of an external magnetic field ($\Phi = 0$), the spontaneous current density j for a fixed ring radius R depends on the subband spin splitting momentum q_{SO} and the average concentration of superconducting electrons $|\psi|^2$, i.e., on the deviation of the temperature T from T_c. The supercurrent amplitude j attains an absolute maximum at $q_{SO} \sim 1/R$, and oscillates and changes sign as q_{SO} varies, as shown in Fig. 25. Damped alternating oscillations are associated with a change in the supercurrent circulation direction in the ring due to the phase difference $\Delta\varphi$ created in the FI coated part of the ring as a result of the combined action of the exchange field and the Rashba SO coupling.

We note that the above spontaneous generation of supercurrent is not specific to SF hybrids with the Rashba SO coupling, but should be relevant for a wide class of interfaces between superconductors and materials with spin polarization and broken spatial inversion symmetry, such as topological insulators and materials with full spin polarization.

5. Proximity effect in strong ferromagnets with full spin polarization of the band

Physical phenomena associated with the influence of the exchange field on the proximity effect and, in particular, with the generation of spin-triplet correlations at the interface between a superconductor and a ferromagnet become especially pronounced when the spin splitting of electron bands in a ferromagnet is of the order of the Fermi energy. In such compounds, called HM ferromagnets or HMs, the DOS at the Fermi level is nonzero for electrons with one of the two possible spin projections (for example, $s_z = \hbar/2$), which corresponds to metallic conductivity, but vanishes for the opposite spin projection $s_z = -\hbar/2$ [74–78]. The proximity effect is then suppressed, because two electrons with opposite spin projections, forming a spin-singlet Cooper pair, cannot simultaneously penetrate into an HM, where one of the spin subbands is located much higher than the Fermi level.

At the same time, the penetration of superconducting correlations into an HM is possible in the presence of an additional ferromagnetic layer or a spin-active interface in the system, which leads to the generation of long-range triplet correlations with the spin projection $s_z = \pm\hbar$. Moreover, if both electron spins are directed along the quantization axis in the HM ($s_z = \hbar$), then the corresponding superconducting correlations penetrate into the HM, and if both spins are directed against the quantization axis ($s_z = -\hbar$), then the penetration of correlations is impossible.

To date, several broad classes of HM ferromagnets are known (see, e.g., reviews [78, 440]). They include Heusler alloys (for example, Co_2MnGe or compounds of the XMnSb type, where X = Ni, Pt, Co, Fe, Cr, etc.), some oxides (for example, CrO_2, Fe_3O_4, and Sr_2FeMoO_6), perovskites (for example, $LaMnO_3$ and $SrMnO_3$), transition metal chalcogenides (for example, CrSe), and manganites (for example, $La_{0.7}Sr_{0.3}MnO_3$). Historically, the existence of HMs was first predicted based on *ab initio* calculations of the electron band structure of NiMnSb [74] and only then confirmed experimentally [441].

From the standpoint of magnetic and transport measurements, characteristic features of HMs are the integer ratio of the magnetic moment of the unit cell to the Bohr magneton and the combination of metallic conductivity and suppressed spin susceptibility (see, e.g., [75]). Magneto-optical measurements [442–444], positron annihilation spectroscopy [445], spin-dependent photoelectron spectroscopy [446], etc. are also used to study HMs. But the most informative technique that allows experimentally detecting the difference between the electron DOSs in two spin subbands and the key transport characteristics of HM ferromagnets is the study of spin-dependent electron tunneling between an HM and a superconductor [447, 448].

The conversion of normal current into supercurrent at the normal metal–superconductor interface is known to be associated with Andreev reflection: an electron with spin projection s_z, penetrating from an N metal into a superconductor, forms a pair with an electron with spin projection $-s_z$, resulting in the formation of a hole with spin projection $-s_z$, which propagates into the bulk of the N metal. Thus, holes that appear under Andreev reflection form an additional conducting channel, as a result of which the conductance of the system is twice the conductance of the system at temperatures exceeding the critical superconducting transition temperature. When an N metal is replaced with a ferromagnet, the exchange field leads to a partial suppression of the Andreev reflection from the FS interface [271]. If the ferromagnet is an HM, then the Andreev reflection is forbidden altogether, because the DOS in the spin subband corresponding to the spin projection of the reflected hole is zero. As a result, in the superconducting state, the conductance of HM/S system is strongly suppressed. In the intermediate case of an incomplete spin polarization of carriers, the ratio of the conductances in the superconducting and normal states provides information on the spin polarization P_n of the ferromagnet [449]:

$$P_n = \frac{N_\uparrow v_{F\uparrow}^n - N_\downarrow v_{F\downarrow}^n}{N_\uparrow v_{F\uparrow}^n + N_\downarrow v_{F\downarrow}^n}, \tag{53}$$

where $N_{\uparrow(\downarrow)}$ is the density of electron states in the subband with the spin directed along (against) the quantization axis, $v_{F\uparrow(\downarrow)}$ are the corresponding spin-dependent Fermi velocities, and the exponent is $n = 1$ for ballistic electron transport and $n = 2$ for diffuse transport. Importantly, just the quantities P_1 or P_2 determine the spin-dependent current in structures involving HMs and play the main role in transport phenomena, in contrast to the spin polarization P_0, which determines the spin response [449].

To study the superconducting proximity effect with HMs, Heusler alloys and CrO_2 are mostly used [76]. The main advantages of the CrO_2 oxide compound are a high spin polarization (close to unity) and the possibility of epitaxially growing homogeneous layers and creating high-quality electrical contacts with superconductors (see, e.g., [450, 451]). In Sections 5.1–5.4, we present the key experimental results related to the proximity effect in S/HM systems and discuss the main theoretical concepts used to describe this effect.

5.1 Main experimental results

One of the first experimental observations of the proximity effect in HMs was the discovery of a long-range superconducting current flowing through an S/HM/S Josephson junction [83, 452]. A CrO_2 layer was used as the HM. The current–voltage characteristics of the contacts indicated the possibility of a nondissipative flow of weak Josephson currents through an HM layer with a thickness up to several hundred nanometers. A significant role of the substrate material was revealed: the critical current of Josephson contacts grown on TiO_2 was two orders of magnitude higher than that of contacts grown on sapphire [83, 185, 452]. The existence of a superconducting current through the HM suggests the conversion of singlet Cooper pairs into triplet correlations at the HM boundary. Such a conversion is assumed to be possible at defects of the CrO_2 layer boundary when it is purified of oxides [83], despite the absence of additional ferromagnetic layers or artificially created spin-active interfaces in the system.

The dependences of the critical current of the junction on the external magnetic field applied along the HM layer demonstrated the presence of characteristic Fraunhofer oscillations with a period approximately corresponding to the ratio of the magnetic flux quantum to the area of the butt end of the HM layer. However, at zero field, a minimum of the critical current was observed in both experiments, in contrast to the maximum observed in traditional Josephson junctions. The authors related this to the presence of a built-in magnetization field in the HM or to the graininess of the HM structure and electron tunneling between grains, but a systematic explanation of the shift in the Fraunhofer pattern is still unavailable.

Later, the possibility of the Josephson current flowing through an HM was also demonstrated for contacts based on HTSCs, where a layer of $La_{0.7}Ca_{0.3}MnO_3$ (LCMO) was used as the HM [453]. The existence of the proximity effect in multilayer HTSC/HM structures is also suggested by resistive measurements, which show a characteristic suppression of the critical temperature of $YBa_2Cu_3O_{7-\delta}$ (YBCO) superconducting layers upon their electrical contact with an HM [454, 455].

Another experimental substantiation of the possibility of the occurrence of triplet superconducting correlations in HMs is the observation of the spin-valve effect in S/F/HM structures [70–73]. We note a significant difference between S/F/HM systems and spin valves based on weak ferromagnets (the exchange field of which is much less than the Fermi energy): in S/F/HM systems, singlet and short-range triplet correlations do not penetrate into the HM layer, and the dependence of the critical temperature T_c on the angle θ between the magnetic moments in the ferromagnetic layers is due only to the presence of long-range triplet correlations with the spin projection $s_z = \pm\hbar$. As a result, both standard and inverse spin valve effects are impossible, and the dependence $T_c(\theta)$ has the symmetry $T_c(\pi - \theta) = T_c(\theta)$ with a minimum at $\theta = \pi/2$ (the triplet spin valve effect). A variation in the critical temperature $T_c(0) - T_c(\pi/2)$ for S/F/HM structures [70] can then significantly exceed the magnitude of the triplet spin valve effect in $S/F_1/F_2$ systems, where typical critical temperature changes are less than 1% [59, 116, 136].

Yet another experimental confirmation of the proximity effect in HMs is the oscillatory behavior of the YBCO/LCMO bilayer conductance as a function of the voltage applied across the structure, with a pronounced peak at zero voltage [456]. Such oscillations are interpreted by the authors as a consequence of the interference of quasiparticle wave functions inside the HM. The application of an external magnetic field to the YBCO/LCMO structure leads to the suppression of the observed conductance oscillations; however, the degree of suppression strongly depends on the orientation of the interfaces between the layers with respect to the crystallographic axes of the materials. For example, for LCMO/YBCO bilayers with the *a*-axis perpendicular to the interface, oscillations already disappear in a field lower than the LCMO saturation field [457], while for structures with a perpendicular *c*-axis, oscillations begin to be smeared only in fields that are larger than the LCMO saturation field [458]. This strange behavior of oscillations is related by the authors of [458] to the effect of magnetic inhomogeneities arising in LCMO/YBCO structures with a perpendicular *c*-axis due to electron reconstruction near the interface [459–461].

Finally, recent experiments [462] have revealed an unusual suppression of Josephson transport in S/F/HM/S/HM/F/S structures under the transition of the central S layer from the normal state to the superconducting one. The unusual behavior of the Josephson current may be caused by the fact that charge transport in such structures is only provided by spin-triplet superconducting correlations, which are destroyed when singlet superconducting pairing occurs in the central layer.

Thus, Josephson systems with HMs open up the possibility of studying not only the generation of triplet correlations at the interfaces with singlet superconductors but also the inverse effect of superconducting pairing on long-range triplet correlations induced due to the proximity effect.

In general, a large amount of experimental data has been accumulated to date, confirming the possibility of penetration of superconducting correlations from singlet superconductors into HM ferromagnets. At the same time, such experimental studies are in the initial phase: many mysteries persist related to the microscopic mechanisms of the generation of triplet correlations at the HM boundaries, the features of the current–voltage characteristics of Josephson S/HM/S junctions, the behavior of the conductance of S/HM bilayers, and other nontrivial effects.

5.2 Theoretical approaches to describing the proximity effect in half-metals

Constructing the theory of the proximity effect with HMs is significantly complicated by the inapplicability of the quasiclassical approximation, which is widely used to describe the penetration of superconducting correlations into ferromagnets with a weak exchange field [39, 93]. Because the splitting of spin subbands in the electron spectrum in an HM is comparable to the Fermi energy, the difference between the phases of the electron- and hole-like quasiparticle wave functions becomes significant, even on atomic scales. This does not in general allow correctly determining the quasiclassical Green's functions inside the HM and necessitates the use of more sophisticated methods, including the Blonder–Tinkham–Klapwijk formalism [463–466] and other modifications of the formalism based on the BdG equations [329, 467–469].

Within these approaches, the possibility of the Josephson current flowing through an HM with spin-active boundaries has been shown. For example, a thin layer of a ferromagnet can be used as such a boundary, with the exchange field being noncollinear to the spin quantization axis in the HM. In a number of ferromagnetic metals, the surface magnetization

can be noncollinear to the bulk magnetization. Spin flip scattering of quasiparticles at a spin-active boundary of an HM can lead to a new type of Andreev reflection in which the electron and the Andreev-reflected hole belong to the same spin subband (in the usual Andreev reflection, the electron and the hole have opposite spin projections) [79, 470–472]. Such an unusual Andreev reflection corresponds to the formation of triplet superconducting correlations that can propagate inside the HM, providing the flow of the Josephson current. A similar conclusion was made previously in [229], where Josephson transport through an HM quantum dot was considered within the phenomenological approach of equivalent electrical circuits.

In some special cases, however, it is still possible to use the technique of quasiclassical Green's functions to describe the proximity effect in HMs. For example, when the exchange field in the HM significantly exceeds the Fermi energy, the filling of the upper spin subband is negligibly small and electrons with only one spin projection are actually present inside the HM. For these electrons, the definition of quasiclassical Green's functions in which only the triplet components with spin projection $s_z = +\hbar$ are nonzero is applicable [79]. But this approach encounters a difficulty when deriving boundary conditions relating the Green's function components inside and outside the HM. In contrast to the Kupriyanov–Lukichev conditions, which are valid on the interfaces between superconductors and weak ferromagnets [473], the conditions on the interface with an HM are much more complicated because of the different number of components of the Green's functions on the opposite sides of the interface.

To solve this problem, various approaches based on the formalism of scattering matrices are typically used. The resulting boundary conditions are widely used to describe the proximity effect with HMs in the framework of both the Eilenberger theory for clean systems [199, 206, 230, 235, 470, 474] and the Usadel formalism for systems in the dirty limit [231, 475–477]. In particular, the derivation of the most general boundary conditions for the Usadel equations was given in [231], with both the difference in the tunneling probability of electrons with opposite spin projections and quantum mechanical phase shifts due to spin-dependent electron scattering at the boundary of an HM taken into account.

An obvious advantage of the approaches based on scattering matrices is their generality. At the same time, despite a number of qualitative predictions [199, 235], most of the results obtained in that framework depend significantly on the microscopic mechanisms of the generation of triplet correlations on the HM boundary and on a large number of phenomenological parameters [471, 478], which cannot be directly extracted from experimental data. Simpler boundary conditions can be obtained in the framework of the so-called adiabatic approximation [232], but the applicability of this approach is limited to the case where the exchange field varies in space on scales much longer than the interatomic distances. This approximation is obviously violated in multilayer structures, where the exchange field undergoes a jump on the atomic scale during the transition from the HM layer to the adjacent layers. We note that similar versions of boundary conditions were also obtained using the Keldysh technique [479, 480].

In a model useful for analyzing the properties of the proximity effect in multilayer superconducting systems containing an HM layer, the layers have an atomic thickness and are separated from each other by a tunnel barrier [127, 234, 481]. For such model systems, it is possible to find exact analytic solutions of the Gor'kov equations beyond the quasiclassical approximation. This allows considering ferromagnetic materials with an arbitrary value of the exchange field and taking the possible relative energy shift for the electron bands in different layers into account. However, an obvious disadvantage of this model is the impossibility of analyzing the interference effects associated with the finite thickness of the ferromagnet.

The above theoretical approaches have allowed not only qualitatively explaining the observed phenomena (Josephson transport through HM layers, anomalous enhancement of the spin-valve effect, etc.) but also predicting a number of new effects, including the formation of φ junctions in S/F/HM/F/S structures [199, 229–235], the appearance of peaks in the density of electron states of S/HM systems due to triplet correlations [279, 329, 482–484], and inversion of the spin-valve effect in S/F/HM structures due to the relative shift of the electron bands in a superconductor and HM [481].

5.3 Josephson transport through a half-metal layer

Josephson junctions containing an HM layer differ significantly in properties from similar structures with conventional ferromagnets. One of the most striking differences is the possibility of forming φ_0 junctions in S/HM/S systems with spin-active HM boundaries [199, 229–235]. The φ_0 junction inside a closed superconducting ring is a source of undamped current [26], which is of considerable interest from the standpoint of the possibility of using such junctions to fabricate so-called quiet qubits.

To illustrate the origin of the φ_0 junction, it is convenient to consider a model system in which the superconducting electrodes are separated by three ferromagnetic layers. Of greatest interest is the situation where the magnetizations in the ferromagnetic layers of such an S/F_1/F_2/F_3/S structure form a triple of noncoplanar vectors, such that the scalar invariant $\mathbf{M}_1(\mathbf{M}_2 \times \mathbf{M}_3)$ is nonzero. In this case, the Josephson transport is determined by the angle χ between the projections of the $\mathbf{M}_1$ and $\mathbf{M}_3$ magnetization vectors onto the plane perpendicular to $\mathbf{M}_2$. This angle enters the current–phase relation additively with the Josephson phase difference φ, but with a different sign for opposite spin projections. As a result, if the exchange field in the F_2 layer is small compared to the Fermi energy, both spin subbands contribute to the Josephson transport, and the Josephson current is proportional to $\sin\varphi$,

$$j_s \sim \sin(\varphi - \chi) + \sin(\varphi + \chi) \sim \sin\varphi\,, \tag{54}$$

and χ only renormalizes the critical current of the junction. If the F_2 layer is an HM, then the current through the contact is determined by only one spin subband, and the current–phase relation takes the form [26, 79, 229]

$$j_s \sim \sin(\varphi - \chi) \tag{55}$$

with a nonzero Josephson phase difference in the ground state.

The advantage of φ_0 junctions based on S/F/HM/F/S structures is the possibility of tuning the Josephson phase difference in the ground state in the range from 0 to 2π using

an external magnetic field to remagnetize one of the ferromagnetic layers. Alternative ways to create φ_0 junctions based on the use of S/F/S structures with SO coupling [223] or with a variable thickness of the ferromagnetic layer [221] have significant limitations. For example, in structures with SO coupling, the spontaneous phase difference in the ground state is limited due to the smallness of the SO coupling constant in typical materials. In the case of S/F/S junctions with a variable thickness of the F layer, the φ_0 junction occurs in a narrow range of parameters, while the spontaneous phase difference is determined by the geometry of the system and cannot be changed in the finished structure.

Another difference between S/F/HM/F/S junctions and traditional $S/F_1/F_2/F_3/S$ contacts is the unusual dependence of the critical current on the mutual orientation of the magnetic moments. This difference is most conspicuous when the magnetizations in the three ferromagnetic layers are mutually orthogonal and the central layer thickness d_2 significantly exceeds the correlation length ξ_f. If the exchange field in the central layer F_2 is small compared to the Fermi energy, the critical current of the junction is exponentially small. At the same time, the Josephson current in S/F/HM/F/S junctions remains finite at $d_2 > \xi_f$.

To illustrate the mechanism of long-range Josephson transport in S/F/HM/F/S structures, we consider the most simplified situation where the temperature is close to the critical one and the system is in the dirty limit. We assume that there are no magnetic impurities, which means that electron scattering is not accompanied by spin flip. In addition, we assume that only one spin subband in the HM layer is filled with electrons, while the other one is well separated from it in energy. These assumptions allow us to determine the quasiclassical Green's functions in the entire system, including the HM layer. In particular, the anomalous Green's function (2), which is a 2×2 matrix in spin space, contains only one nonzero component $f_{\uparrow\uparrow}$ inside the HM, while the other components are equal to zero. Outside the HM, the singlet and triplet components of the Matsubara Green's function satisfy the linearized Usadel equations (3). The magnetization is assumed to be directed along the x-axis in the F_1 layer, along the z-axis in the F_2 layer, and along the y-axis in the F_3 layer. Then, the singlet component of the Green's function f_s, when penetrated from the superconductor into the ferromagnetic layer F_1, becomes the source of the triplet component f_{tx} directed along the exchange field in the F_1 layer.

The scenario of further propagation of superconducting correlations essentially depends on the magnitude of the exchange field in the F_2 layer. If this layer is an ordinary ferromagnet with a weak exchange field, then the f_{tx} component passes through it and enters the F_3 layer. However, the f_{tx} component does not contribute to the Josephson current, because the magnetic moment in the F_3 layer, directed along the y-axis, cannot convert it back into the singlet component f_s. As a result, the critical current of the Josephson junction is exponentially suppressed. If the F_2 layer is an HM, then the f_{ty} component must in addition appear at the F_1/HM interface, although the exchange field has zero projection onto the y-axis in both the F_1 and HM layers. That this component must necessarily be generated is directly related to the total spin polarization of electrons in an HM. Indeed, the conditions $f_{\downarrow\downarrow} = 0$, and $f_{\uparrow\uparrow} \neq 0$ imply that $f_{ty} = \mathrm{i} f_{tx} \neq 0$ inside the HM layer. In the F_3 layer, the f_{ty} component effectively interacts with the exchange field and becomes a source of singlet correlations that contribute to the Josephson current. As a result, the critical current of an S/F/HM/F/HM contact with mutually orthogonal magnetic moments in three ferromagnetic layers is strongly nonzero.

The above features of Josephson transport are of significant interest from the point of view of using S/F/HM/F/S junctions in superconducting spintronic devices as phase batteries that create undamped currents in closed circuits. In S/F/HM/F/S contacts, in contrast to the widely used π-contacts, the current–phase relation can be dynamically tuned by changing the orientation of magnetic moments in the ferromagnetic layers.

5.4 Spin-valve effect in systems with a half-metal layer

In recent years, studies of the spin-valve effect in hybrid devices containing layers of a ferromagnet with a 100% spin polarization (HM) have been actively pursued [70, 485]; only pair correlations with the spin projection $s_z = \hbar$ penetrate into the HM layer, and the rest disappear at its boundary. Interest in such structures is primarily due to the implementation of the triplet spin-valve effect, with the switching between states with collinear and noncollinear configurations of magnetization in F layers attended by an anomalously large change in the critical temperature ($\Delta T_c \sim 1$ K).

The theory of the triplet spin-valve effect in the cases of diffusion and ballistic hybrid structures with an HM layer was developed in [234] and [486], respectively. The discovery that the use of HM ferromagnets significantly suppresses T_c opens the way for the development of magnetization-controlled superconducting switches. Because T_c varies over a wide range, the resistance of such a device is robust as regards possible temperature fluctuations. At low temperatures, triplet superconducting spin valves can perform almost the same set of operations as devices based on the giant magnetoresistance effect, but potentially outperform them in terms of energy efficiency due to the absence of dissipation in the superconducting state.

For systems, one of whose F layers is an HM ferromagnet, a general theory of the proximity effect has not yet been developed. Quantitative results based on the quasiclassical approximation are sensitive to the form of the boundary conditions for the Green's functions at the HM boundaries. For example, in one of the simplest types of phenomenological boundary conditions for the linearized Usadel equation, it is assumed that all components of the anomalous Green's function except $f_{\uparrow\uparrow}$ vanish at the HM boundary, while the indicated component can penetrate into the HM [234]. At the same time, $f_{\uparrow\uparrow}$ and $\sigma(x)\,\partial_x f_{\uparrow\uparrow}$ (where σ is the conductivity of each of the layers in the normal state and x is the coordinate across the layers) are assumed to be continuous at the boundary.

The choice of such boundary conditions leads to two interesting features of the dependence $T_c(\theta)$. First, because singlet and triplet superconducting correlations, both with zero spin projection, do not penetrate into the HM layer, the critical temperatures for the codirectional ($\theta = 0$) and oppositely directed ($\theta = \pi$) magnetic moments coincide, and hence neither the standard nor the inverse spin-valve effect occurs. At the same time, the dependence $T_c(\theta)$ has a minimum at $\theta = \pi/2$, and the difference between the temperatures $T_c(0)$ and $T_c(\pi/2)$ is much greater than the characteristic changes in the critical temperature observed in S/F/F and F/S/F systems (giant spin-valve effect). An

analysis of the dependence of the critical temperature of an S/F/HM system on the F layer thickness showed that, at some parameters, the maximum possible temperature $T_c(0)$ corresponds to the ferromagnet thickness for which $T_c(\pi/2) = 0$. Taking the finite electron transparency of the F/HM boundary into account in the formalism of the Usadel equations leads to the suppression of the spin-valve effect [487], but does not introduce qualitative changes into the behavior of $T_c(\theta)$.

Numerical calculations of the critical temperature of S/F/N/HM structures (where N is a normal metal) in the framework of the BdG formalism not resorting to the quasiclassical approximation also indicate a significant enhancement of the spin-valve effect in the case of full spin polarization of electrons in the outermost ferromagnetic layer [486]. But the critical temperature, in contrast to T_c obtained in quasiclassical approaches, is different for codirectional and oppositely directed collinear magnetic moments in the F and HM layers, which the authors attribute to nonlocal effects.

Finally, the spin-valve effect in F/S/HM and S/F/HM systems must be significantly affected by the properties of the band structure of the ferromagnetic materials used. In the simplest physical model that takes such features into account, the system is taken to be a set of tunnel-connected layers of atomic thickness [127, 234, 481]. Such a simplified model, although it does not allow analyzing the physics of interference effects associated with the finite thickness of the F layer, has an important advantage, because it allows an exact analytic solution of the Gor'kov equations for two-point Green's functions to be constructed.

Calculations of the critical temperature of such model systems have revealed a strong sensitivity of the $T_c(\theta)$ dependence to the position of the conduction band bottom in the F and HM layers relative to the position of the band bottom in the superconductor [481]. For S/F/HM systems, when the bottom of the only filled spin subband in the HM is below the bottom of the conduction band, the standard spin-valve effect ($T_c(0) < T_c(\pi)$) is observed; conversely, when the band bottom in the HM layer is higher than the S-layer band bottom, the inverse spin-valve effect ($T_c(0) > T_c(\pi)$) is observed. The $T_c(\theta)$ dependence has a local minimum characteristic of the triplet spin-valve effect if the relative shift of the bands in the S and HM layers is sufficiently small in absolute value, and is monotonic for large shifts. The indicated sensitivity of the behavior of the critical temperature to the features of the band structure should be taken into account when constructing the theory of the spin-valve effect in structures with a finite layer thickness.

In general, although studies of superconducting spin valves containing an HM layer are in the initial phase, they attract considerable interest due to both the colossal change in the critical temperature of the system because of the noncollinearity of magnetic moments and fundamentally new physical phenomena caused by the full spin polarization of electrons in one of the ferromagnetic layers.

6. Conclusion

To conclude, we summarize some inferences from the rapid recent development of the physics of the interplay between superconductivity and magnetism and discuss some prospects for further advances in the new direction that has taken shape over the past decade, superconducting spintronics.

We first note the success of the experiment in [53], where the quantum mechanical interference effects predicted in early theoretical studies [50–52] was realized for electrons under the action of both the superconducting pairing potential and the exchange field. Experimental confirmation of such interference is certainly a significant step in understanding the foundations of the physics of superconducting and magnetic interactions in condensed matter.

The next important accomplishment in this area is the theoretical prediction and experimental realization of systems with a completely new type of the induced state of Cooper pairs — a triplet state with the total spin projection of the pair equal to $\pm\hbar$ [90, 92]. The resistance of such triplet pairs to the action of the exchange field allowed significantly increasing the scale of penetration of superconducting correlations into ferromagnetic materials, thereby weakening the constraints on observation of interference effects in SF structures.

New interesting possibilities in the development of the physics of the proximity effect and the engineering of the superconducting pairing structure have opened up thanks to studies of structures with strong SO coupling. This area seems to be especially promising for topologically protected quantum computing. The use of SF structures in cryoelectronic devices requires an in-depth understanding of the physics of nonstationary and nonequilibrium processes in these systems, which includes the problem of the joint dynamics of superconducting correlations and the magnetic moment. Considering a number of intriguing theoretical [311, 488–493] and experimental [494–497] results in this field, it can be hoped that progress in the near future will bring about new exciting physical ideas and applied proposals. A review of recent papers on the study of nonequilibrium effects in SF systems can be found in [498].

The successful application of the above effects in instrumentation-related applications certainly raises the question of the most suitable materials for optimizing the parameters of superconducting spintronic devices. Here, without a doubt, an important role is played by work on ferromagnetic materials with a strong spin polarization of carriers (HMs). The use of HMs not only changes the quantitative characteristics of spin valves and other devices but also opens up interesting prospects for fundamentally new manifestations of the proximity effect.

This study was financially supported by the Russian Foundation for Basic Research within research project 20-12-50113. The work of A I B on Sections 3–5 of this review was supported by Russian Science Foundation project 20-12-00053.

Appendix A. Basic equations of the microscopic theory of superconductor–ferromagnet systems

We briefly discuss the basic equations of the microscopic theory of superconductivity used to describe the proximity effect with ferromagnets.

A.1 Bogoliubov–de Gennes equations

It is natural to start reviewing theoretical approaches with the BdG theory, which not only proved to be effective for describing clean (ballistic) systems but also often allows obtaining the most transparent qualitative interpretation of physical effects. The term 'clean systems' is used in this context as a characteristic of structures with a mean free path ℓ much greater than the coherence lengths in a super-

conductor (ξ_s), a ferromagnet (ξ_h), and a normal metal (ξ_n). Within the self-consistent field approximation, hybrid SF systems with an exchange field $\mathbf{h}(\mathbf{r})$ are described by the Hamiltonian

$$\mathcal{H} = \sum_{\alpha\beta} \int \hat{\psi}_\alpha^\dagger(\mathbf{r}) \left[\hat{H}_0(\mathbf{r})\delta_{\alpha\beta} + \mathbf{h}(\mathbf{r})\boldsymbol{\sigma}\right] \hat{\psi}_\beta(\mathbf{r})\, \mathrm{d}\mathbf{r} + \int \left[\Delta^*(\mathbf{r})\hat{\psi}_\uparrow(\mathbf{r})\hat{\psi}_\downarrow(\mathbf{r}) + \Delta(\mathbf{r})\hat{\psi}_\downarrow^\dagger(\mathbf{r})\hat{\psi}_\uparrow^\dagger(\mathbf{r})\right] \mathrm{d}\mathbf{r}\,, \tag{A.1}$$

where $\hat{\psi}_\alpha^\dagger(\hat{\psi}_\alpha)$ is the creation (annihilation) operator for an electron with the coordinate $\mathbf{r}$ and spin projection $\alpha = \uparrow, \downarrow$ on the z-axis,

$$\hat{H}_0(\mathbf{r}) = \frac{1}{2m}\left(-\mathrm{i}\hbar\nabla - \frac{e}{c}\,\mathbf{A}\right)^2 - \mu\,, \tag{A.2}$$

where m is the electron mass, $\mathbf{A}$ is the vector potential of the magnetic field, μ is the chemical potential, $\Delta(\mathbf{r})$ is the superconductivity order parameter, and $\boldsymbol{\sigma} = (\hat{\sigma}_x, \hat{\sigma}_y, \hat{\sigma}_z)$ is the vector of Pauli matrices in spin space. Diagonalizing Hamiltonian (A.1), (A.2), which is bilinear in the $\hat{\psi}_\alpha$ and $\hat{\psi}_\alpha^\dagger$ operators by the canonical Bogoliubov transformation [499], gives the corresponding BdG equations

$$\hat{\tau}_z\left[\frac{1}{2m}\left(-\mathrm{i}\hbar\nabla - \hat{\tau}_z\frac{e}{c}\,\mathbf{A}\right)^2 - \mu\right]\hat{\Psi} + \mathbf{h}(\mathbf{r})\,\boldsymbol{\sigma}\hat{\Psi} + \begin{pmatrix} 0 & \hat{\Delta}(\mathbf{r}) \\ \hat{\Delta}^*(\mathbf{r}) & 0 \end{pmatrix}\hat{\Psi} = \epsilon\hat{\Psi} \tag{A.3}$$

for the electron ($u(\mathbf{r})$) and hole ($v(\mathbf{r})$) components of the wave function $\hat{\Psi} = (u, \mathrm{i}\sigma_y v)$, where $u = (u_\uparrow, u_\downarrow)$ and $v = (v_\uparrow, v_\downarrow)$ are spinors, and $(\hat{\tau}_x, \hat{\tau}_y, \hat{\tau}_z)$ are Pauli matrices in the Nambu (electron–hole) space. Details of the derivation of the BdG equations are given, for example, in books [500–502]. The superconducting order parameter $\hat{\Delta}$ is the scalar function $\Delta(\mathbf{r})$ times the identity matrix in spin space, with $\Delta(\mathbf{r})$ satisfying the self-consistency equation

$$\Delta(\mathbf{r}) = K(\mathbf{r})\sum_p \left\{u_{p\uparrow}(\mathbf{r})v_{p\downarrow}^*(\mathbf{r})\left[1 - n_\mathrm{f}(\varepsilon_p)\right] + u_{p\downarrow}(\mathbf{r})v_{p\uparrow}^*(\mathbf{r})n_\mathrm{F}(\varepsilon_p)\right\}, \tag{A.4}$$

where $K(\mathbf{r})$ is the superconducting pairing potential, n_F is the Fermi distribution function, and the sum over quantum numbers p includes only positive-energy states.

A.2 Quasiclassical methods. Andreev equations

For most typical metals, the Fermi wavelength is small compared to the corresponding coherence length, which allows significantly simplifying the above BdG equations by using the quasiclassical approximation. In this case, the wave functions of electrons and holes are represented as products of rapidly oscillating exponentials $\exp(\mathrm{i}\mathbf{k}_\mathrm{F}\mathbf{r})$ and wave function envelopes $\hat{g}$ that slowly vary in space. This procedure allows writing a system of reduced-order equations for $\hat{g}$ involving derivatives along quasiclassical rays (trajectories). Such equations are called the Andreev equations:

$$-\mathrm{i}\hbar v_\mathrm{F}\hat{\tau}_z\frac{\mathrm{d}}{\mathrm{d}s}\,\hat{g} + \mathbf{h}(\mathbf{R} + s\,\mathbf{n}_\mathrm{F})\,\boldsymbol{\sigma}\hat{g} + \begin{pmatrix} 0 & \hat{\Delta}(\mathbf{R} + s\,\mathbf{n}_\mathrm{F}) \\ \hat{\Delta}^*(\mathbf{R} + s\,\mathbf{n}_\mathrm{F}) & 0 \end{pmatrix}\hat{g} = \epsilon\hat{g}\,. \tag{A.5}$$

Here, we use a system of linear trajectories passing through the point $\mathbf{R}$ with the unit vector $\mathbf{n}_\mathrm{F} = \mathbf{k}_\mathrm{F}/k_\mathrm{F}$ directed along the trajectory, with the coordinate s along the trajectory.

A.3 Quasiclassical methods. Eilenberger's theory

The approaches using the BdG or Andreev equations outlined in Sections A.1 and A.2 without taking scattering on a random impurity potential into account are applicable only to ballistic systems, which significantly limits their range of applicability. Systematically taking disorder into account can be very effectively implemented in the framework of another variant of the microscopic approach describing hybrid SF structures with the formalism of Green's functions. The normal (G) and anomalous (F) Green's functions are then represented as expansions in eigenfunctions of the BdG equations [500]:

$$\mathcal{G}_{\alpha\beta}(\epsilon, \mathbf{r}, \mathbf{r}') = \sum_p \frac{u_{p\alpha}(\mathbf{r})\,u_{p\beta}^*(\mathbf{r}')}{\epsilon - \epsilon_p}\,, \tag{A.6}$$

$$\mathcal{F}_{\alpha\beta}(\epsilon, \mathbf{r}, \mathbf{r}') = \sum_p \frac{v_{p\alpha}(\mathbf{r})\,u_{p\beta}^*(\mathbf{r}')}{\epsilon - \epsilon_p}\,. \tag{A.7}$$

Setting $\epsilon = \mathrm{i}\omega$ in (A.6) and (A.7), where $\omega = \pi T(2n+1)$ is the Matsubara frequency (and n is an integer) gives the Matsubara Green's functions — 2×2 matrices in spin space —

$$\mathcal{G}_\omega(\mathbf{r}, \mathbf{r}') = \begin{pmatrix} \mathcal{G}_{\uparrow\uparrow} & \mathcal{G}_{\uparrow\downarrow} \\ \mathcal{G}_{\downarrow\uparrow} & \mathcal{G}_{\downarrow\downarrow} \end{pmatrix}, \tag{A.8}$$

$$\mathcal{F}_\omega(\mathbf{r}, \mathbf{r}') = \begin{pmatrix} \mathcal{F}_{\uparrow\uparrow} & \mathcal{F}_{\uparrow\downarrow} \\ \mathcal{F}_{\downarrow\uparrow} & \mathcal{F}_{\downarrow\downarrow} \end{pmatrix}, \tag{A.9}$$

that are commonly used in thermodynamically equilibrium problems. Within the quasiclassical approach, it is customary to use the so-called quasiclassical normal ($G_\omega(\mathbf{r}, \mathbf{n}_\mathrm{F})$) and anomalous ($F_\omega(\mathbf{r}, \mathbf{n}_\mathrm{F})$) Green's functions, which are obtained by averaging (A.8) and (A.9) with respect to fast spatial oscillations on the scale $\sim k_\mathrm{F}^{-1}$. These functions are defined on rectilinear trajectories passing through the point $\mathbf{r}$ and specified by the unit vector $\mathbf{n}_\mathrm{F}$. In the presence of an inhomogeneous exchange field $\mathbf{h}(\mathbf{r})$, the Green's functions G_ω and F_ω have an involved spin structure. It is convenient to write the corresponding equations for them in matrix form by introducing the matrix Green's function in the 4×4 Gor'kov–Nambu space,

$$\check{G}_\omega = \begin{pmatrix} G_\omega & F_\omega \\ F_\omega^+ & \bar{G}_\omega \end{pmatrix}, \tag{A.10}$$

where G_ω, F_ω, F_ω^+, and $\bar{G}_\omega$ are 2×2 matrices in spin space. The Green's function $\bar{G}$ is defined by (A.6) with the electron wave functions $u_{p\alpha}(\mathbf{r})$ replaced with hole functions $v_{p\alpha}^*(\mathbf{r})$. The full matrix Green's function satisfies the normalization condition $\check{G}_\omega\check{G}_\omega = -1$.

In the case of singlet pairing, it is convenient to move to the new Green's function $\check{g}_\omega$ by the transformation

$$\check{G}_\omega = \begin{pmatrix} 1 & 0 \\ 0 & -\mathrm{i}\sigma_y \end{pmatrix}\check{g}_\omega\begin{pmatrix} 1 & 0 \\ 0 & \mathrm{i}\sigma_y \end{pmatrix},$$

where we set

$$\check{g}_\omega = \begin{pmatrix} g_\omega & f_\omega \\ -f_\omega^+ & \bar{g}_\omega \end{pmatrix},$$

with $G_\omega = g_\omega$, $F_\omega = f_\omega \mathrm{i}\sigma_y$, $F_\omega^+ = \mathrm{i}\sigma_y f_\omega^+$, and $\bar{G}_\omega = \sigma_y \bar{g}_\omega \sigma_y$. This transformation does not change the normalization conditions, and therefore $\check{g}_\omega \check{g}_\omega = -1$, whence

$$g_\omega g_\omega - f_\omega f_\omega^+ = -1\,, \quad g_\omega f_\omega + f_\omega \bar{g}_\omega = 0\,,$$

$$\bar{g}_\omega \bar{g}_\omega - f_\omega^+ f_\omega = -1\,, \quad f_\omega^+ g_\omega + \bar{g}_\omega f_\omega^+ = 0\,.$$

The Eilenberger equations [503] written for a set of quasiclassical trajectories have the form

$$\mathrm{i}\hbar v_\mathrm{F} \mathbf{n}_\mathrm{F} \nabla \check{g}_\omega + \left[\mathrm{i}\omega \hat{\tau}_z - \hat{\tau}_z \hat{\Delta} - \hat{\tau}_z \mathbf{h}\boldsymbol{\sigma} - \frac{\hbar}{2\tau} \langle \check{g}_\omega \rangle, \check{g}_\omega \right] = 0\,, \tag{A.11}$$

where $\hat{\sigma}_v$ and $\hat{\tau}_v$ $(v = x, y, z)$ are the Pauli matrices in spin space and in the Gor'kov–Nambu space, $[A, B] = AB - BA$, the term with the Green's function averaged over the angles specifying the trajectory orientations

$$\left\langle \check{g}_\omega(\mathbf{r}) \right\rangle = \int \check{g}_\omega(\mathbf{r}, \mathbf{n}_\mathrm{F}) \frac{\mathrm{d}\mathbf{n}_\mathrm{F}}{4\pi} \tag{A.12}$$

is introduced to describe the elastic scattering of quasiparticles by point nonmagnetic impurities with a mean free path time τ, and

$$\check{\Delta} = \begin{pmatrix} 0 & \hat{\Delta} \\ \hat{\Delta}^* & 0 \end{pmatrix},$$

where the matrix $\hat{\Delta}$ is the superconducting gap Δ times the identity matrix in spin space.

A.4 Quasiclassical methods. Usadel's theory

The next step in simplifying the equations of the microscopic superconductivity theory is to derive a closed system of equations for the Green's functions $\langle \check{g}_\omega \rangle$, Eqn (A.12), averaged over the orientation angles of quasiclassical trajectories. Such a step forward in the theoretical description is only suitable in the so-called diffusion (or dirty) limit, when the mean free path $\ell = v_\mathrm{F}\tau$ is small compared to all characteristic scales in the problem, including all possible coherence lengths in various materials that make up the structure under study.

We note that, in view of the standard expression $\xi_\mathrm{f} = \sqrt{\hbar D/h}$ for the coherence length in a dirty ferromagnet (where $D = \ell v_\mathrm{F}/3$ is the diffusion coefficient), the above constraint that the mean free path be small also implies an upper bound on the exchange field magnitude in a ferromagnet. Such a bound in real ferromagnets is by no means always observed, which, obviously, can affect the applicability of the diffusion limit. Usadel's theory is based on the physically obvious assumption that the Green's functions become isotropic as the impurity concentration increases: $\check{g}_\omega \simeq \langle \check{g}_\omega \rangle$. Equations for the Green's functions averaged over the orientation angles $\mathbf{n}_\mathrm{F}$ are called Usadel equations [504]:

$$\hbar D \nabla(\check{g}_\omega \nabla \check{g}_\omega) + \left[\hat{\tau}_z(\mathrm{i}\omega - \check{\Delta} - \mathbf{h}\boldsymbol{\sigma}), \check{g}_\omega \right] = 0\,. \tag{A.13}$$

The solution of these equations in layered structures containing superconducting, normal, and ferromagnetic materials with different parameters requires appropriate boundary conditions. Such conditions for the Usadel equation were formulated in [473]. For two adjacent materials, denoted by subscripts 1 and 2 here, the boundary conditions can be written as

$$\sigma_1 \check{g}_1 \frac{\partial \check{g}_1}{\partial x} = \sigma_2 \check{g}_2 \frac{\partial \check{g}_2}{\partial x}\,, \quad 2\sigma_2 R_\mathrm{b} \check{g}_2 \frac{\partial \check{g}_2}{\partial x} = [\check{g}_1, \check{g}_2]\,, \tag{A.14}$$

where the x-axis, perpendicular to the interface, is directed from material 1 to material 2, σ_i is the specific conductivity of material i in the normal state, and $1/R_\mathrm{b}$ is the conductance of the interface between materials per unit area, characterizing the transparency of the interface for electrons. Similar boundary conditions for the Eilenberger equation were obtained in [505].

Appendix B. Quasiclassical equations along trajectories and current–phase relations for clean superconductor/ferromagnet/superconductor junctions

To calculate the spin-dependent phase shift γ for an arbitrary distribution of the exchange field $\mathbf{h}(\mathbf{r})$ in the F layer, it is convenient to use the methods proposed in [195]. The essence of the method is to choose a unitary transformation $\hat{S}_{u,v} = \alpha_{u,v} + \mathrm{i}\,\boldsymbol{\beta}_{u,v}\hat{\boldsymbol{\sigma}}$, such that Andreev equations (A.5) for the components of the new wave function,

$$\hat{f} = \begin{pmatrix} f_u \\ f_v \end{pmatrix} = \hat{S}\hat{g}\,, \quad \hat{S} = \begin{pmatrix} \hat{S}_u & 0 \\ 0 & \hat{S}_v \end{pmatrix}, \tag{B.1}$$

become independent of the exchange field $\mathbf{h}$, i.e., coincide with the equations describing a ballistic SNS contact. For this, the functions $\alpha_{u,v}(s)$ and $\boldsymbol{\beta}_{u,v}(s)$ at an arbitrary point s of the trajectory must satisfy the differential equations

$$\hbar v_\mathrm{F} \partial_\mathrm{s} \alpha_{u,v} = \mp \mathbf{h}\boldsymbol{\beta}_{u,v}\,, \quad \hbar v_\mathrm{F} \partial_\mathrm{s} \boldsymbol{\beta}_{u,v} = \pm \alpha_{u,v}\mathbf{h} - [\mathbf{h}, \boldsymbol{\beta}_{u,v}] \tag{B.2}$$

with the initial conditions

$$\alpha_{u,v}(0) = 1\,, \quad \boldsymbol{\beta}_{u,v}(0) = 0$$

on the left boundary of the F layer ($s = 0$). The operator transforming the original order parameter $\hat{\Delta}(\mathbf{r})$ is expressed in terms of the functions $\alpha_{u,v}$ and $\boldsymbol{\beta}_{u,v}$; when the spin quantization axis is directed along the vector $\alpha_v\boldsymbol{\beta}_u - \alpha_u\boldsymbol{\beta}_v + [\boldsymbol{\beta}_u, \boldsymbol{\beta}_v]$, it provides an additional phase shift $\hat{\Delta}(\mathbf{r})\exp(\mathrm{i}\gamma)$ created by the exchange field:

$$\exp(\mathrm{i}\gamma) = \alpha_u\alpha_v + (\boldsymbol{\beta}_u\boldsymbol{\beta}_v) \pm \mathrm{i}\left|\alpha_v\boldsymbol{\beta}_u - \alpha_u\boldsymbol{\beta}_v + [\boldsymbol{\beta}_u, \boldsymbol{\beta}_v]\right|. \tag{B.3}$$

Expressing the anomalous Green's function $\hat{f}$ in a ferromagnet in form (2), where the singlet component amplitude is

$$f_\mathrm{s} = \cos\gamma = \alpha_u\alpha_v + \boldsymbol{\beta}_u\boldsymbol{\beta}_v\,,$$

and the vector

$$\mathbf{f}_\mathrm{t} = \mathrm{i}\left(\alpha_u\boldsymbol{\beta}_v - \alpha_v\boldsymbol{\beta}_u + [\boldsymbol{\beta}_u, \boldsymbol{\beta}_v]\right)$$

describes the triplet component, we find that the functions $f_\mathrm{s}(s)$ and $\mathbf{f}_\mathrm{t}(s)$ satisfy the linearized Eilenberger equations [503] at the zero Matsubara frequency,

$$-\mathrm{i}\hbar v_\mathrm{F}\partial_\mathrm{s} f_\mathrm{s} + 2\mathbf{h}\mathbf{f}_\mathrm{t} = 0\,, \quad -\mathrm{i}\hbar v_\mathrm{F}\partial_\mathrm{s}\mathbf{f}_\mathrm{t} + 2f_\mathrm{s}\mathbf{h} = 0\,, \tag{B.4}$$

with the boundary conditions on the left superconducting electrode given by

$$f_\mathrm{s}(s = 0) = 1\,, \quad \mathbf{f}_\mathrm{t}(s = 0) = 0\,. \tag{B.5}$$

Hence, the phase shift γ between the electron and hole parts of the wave function on a quasiclassical trajectory in the SFS junction with an arbitrary distribution of the exchange field $\mathbf{h}(\mathbf{r})$ is determined by the singlet part of the anomalous quasiclassical Green's function $f_s(s = s_R) = \cos\gamma$ evaluated at the boundary of the right superconducting electrode.

The leading contribution to the supercurrent comes from trajectories crossing the short contact and corresponding to the Andreev subgap states, whose spectrum has the form [506, 507]

$$\epsilon = \pm\Delta_0 \cos\left(\frac{\varphi+\gamma}{2}\right), \tag{B.6}$$

and depends both on the Josephson phase difference φ and on the additional phase shift γ. Summing over all trajectories, we obtain a relation between current and phase difference,

$$I = \frac{1}{s_0}\int \mathrm{d}s \int \mathrm{d}\mathbf{n}_F \left(j(\varphi+\gamma)+j(\varphi-\gamma)\right)(\mathbf{n}_F,\mathbf{n}), \tag{B.7}$$

where $s_0^{-1} = k_F/(2\pi)$ ($s_0^{-1} = [k_F/(2\pi)]^2$) for two-dimensional (three-dimensional) junctions, $\int \ldots \mathrm{d}s$ is the integral over the junction cross section, and

$$j(\chi) = \sum_{n\geqslant 1}\frac{j_n}{2}\sin(n\chi) = \frac{e\Delta}{2\hbar}\sin\frac{\chi}{2}\tanh\left(\frac{\Delta_0\cos(\chi/2)}{2T}\right) \tag{B.8}$$

is the current–phase relation of the Josephson junction with the same geometry and zero exchange field. The coefficients j_n in the expansion in terms of Fourier harmonics (B.8) can be written as

$$j_n = \frac{2eT}{\pi\hbar}\sum_{m=0}^{\infty}\int_0^{2\pi}\mathrm{d}\chi\,\frac{\sin\chi\sin(n\chi)}{\mu_m+\cos\chi}, \tag{B.9}$$

where $\mu_m = 2\pi^2T^2(2m+1)^2/\Delta^2+1$. The final relation between the current I and the phase difference φ of a short Josephson SFS junction is

$$I = \sum_n I_n = \sum_n a_n \sin(n\varphi)\,\frac{\left\langle(\mathbf{n},\mathbf{n}_F)\cos(n\gamma)\right\rangle}{\left\langle(\mathbf{n},\mathbf{n}_F)\right\rangle}. \tag{B.10}$$

The angular brackets denote averaging over the quasiclassical trajectories, which are characterized by the angle θ and the position of the trajectory starting point on the superconductor surface. The coefficients

$$a_n = j_nN = j_n\,\frac{1}{s_0}\int \mathrm{d}s\int \mathrm{d}\mathbf{n}_F\,(\mathbf{n}_F,\mathbf{n})$$

in expression (B.10) coincide with the coefficients of the Fourier expansion of $I_{SNS}(\varphi)$ for the Josephson S/N/S junction with the same geometry,

$$a_n = \frac{4eT}{\hbar}\,N(-1)^{n-1}\sum_{m=0}^{\infty}\left(\mu_m-\sqrt{\mu_m^2-1}\right)^n,\ n=1,2,\ldots, \tag{B.11}$$

and the factor N is determined by the number of transverse modes in the junction,

$$N = \frac{1}{s_0}\int \mathrm{d}s\int \mathrm{d}\mathbf{n}_F\,(\mathbf{n}_F,\mathbf{n}) \sim \frac{S}{s_0},$$

where S is the cross-sectional area of the junction. For temperatures $T \approx T_c$, coefficients (B.11) are determined by the simple relations

$$a_1 = \frac{eT_c}{8\hbar}\,N\left(\frac{\Delta}{T_c}\right)^2, \qquad a_2 = -\frac{eT_c}{384\hbar}\,N\left(\frac{\Delta}{T_c}\right)^4, \tag{B.12}$$

where Δ is the temperature-dependent superconducting order parameter in the contact electrodes. In the case of 3D structures, the averaging is done as

$$\frac{\left\langle(\mathbf{n},\mathbf{n}_F)\cos(n\gamma)\right\rangle}{\left\langle(\mathbf{n},\mathbf{n}_F)\right\rangle} = 2\int_0^{\pi/2}\mathrm{d}\theta\,\sin\theta\cos\theta\cos(n\gamma), \tag{B.13}$$

where $\cos\theta = (\mathbf{n},\mathbf{n}_F)$.

References

1. Ginzburg V L *Sov. Phys. JETP* **4** 153 (1957); *Zh. Eksp. Teor. Fiz.* **31** 202 (1956)
2. Blount E I, Varma C M *Phys. Rev. Lett.* **42** 1079 (1979)
3. Ferrel R A, Bhattacharjee J K, Bagchi A *Phys. Rev. Lett.* **43** 154 (1979)
4. Matsumoto H, Umezawa H, Tachiki M *Solid State Commun.* **31** 157 (1979)
5. Matthias B T, Suhl H, Corenzwit E *Phys. Rev. Lett.* **1** 92 (1958)
6. Saint-James D, Sarma D, Thomas E J *Type II Superconductivity* (Oxford: Pergamon Press, 1969)
7. Vonsovskii S V, Svirskii M S *Sov. Phys. JETP* **12** 272 (1961); *Zh. Eksp. Teor. Fiz.* **39** 384 (1960)
8. Vonsovskii S V, Svirskii M S *Izv. Akad. Nauk SSSR Ser. Fiz.* **28** 418 (1964)
9. Abrikosov A A, Gor'kov L P *Sov. Phys. JETP* **12** 1243 (1961); *Zh. Eksp. Teor. Fiz.* **39** 1781 (1961)
10. Anderson P W, Suhl H *Phys. Rev.* **116** 898 (1959)
11. Veshchunov I S et al. *JETP Lett.* **105** 98 (2017); *Pis'ma Zh. Eksp. Teor. Fiz.* **105** 87 (2017)
12. Stolyarov V S et al. *Sci. Adv.* **4** (7) eaat1061 (2018)
13. Aoki D, Flouquet J *J. Phys. Soc. Jpn.* **81** 011003 (2012)
14. Flouquet J, Buzdin A *Phys. World* **15** (1) 41 (2002)
15. Vonsovskii S V, Svirskii M S *Sov. Phys. JETP* **19** 1095 (1961); *Zh. Eksp. Teor. Fiz.* **46** 1619 (1964)
16. Vonsovsky S V, Izyumov Yu A, Kurmaev E Z *Superconductivity of Transition Metals: Their Alloys and Compounds* (Berlin: Springer-Verlag, 1982); Translated from Russian: *Sverkhprovodimost' Perekhodnykh Metallov, Ikh Splavov i Soedinenii* (Moscow: Nauka, 1977)
17. Izyumov Yu A, Katsnel'son M I, Skryabin Yu N *Magnetizm Kollektivizirovannykh Elektronov* (Collectivized Electron Mechanism) (Moscow: Nauka, 1994)
18. Maple M B et al. "Unconventional superconductivity in novel materials", in *The Physics of Superconductors* Vol. 2 (Eds K H Bennemann, J B Ketterson) (Berlin: Springer, 2004) p. 555
19. Carlson E W et al. "Concepts in high temperature superconductivity", in *The Physics of Superconductors* Vol. 2 (Eds K H Bennemann, J B Ketterson) (Berlin: Springer, 2004) p. 275
20. Izyumov Yu A *Sov. Phys. Usp.* **34** 935 (1991); *Usp. Fiz. Nauk* **161** (11) 1 (1991)
21. Izyumov Yu A, Plakida N M, Skryabin Yu N *Sov. Phys. Usp.* **32** 1060 (1989); *Usp. Fiz. Nauk* **159** 621 (1989)
22. Buzdin A I et al. *Sov. Phys. Usp.* **27** 927 (1984); *Usp. Fiz. Nauk* **144** 597 (1984)
23. Buzdin A I, Bulaevskii L N *Sov. Phys. Usp.* **29** 412 (1986); *Usp. Fiz. Nauk* **149** 45 (1986)
24. Fert A *Rev. Mod. Phys.* **80** 1517 (2008); *Usp. Fiz. Nauk* **178** 1336 (2008)
25. Žutić I, Fabian J, Das Sarma S *Rev. Mod. Phys.* **76** 323 (2004)
26. Linder J, Robinson J W A *Nat. Phys.* **11** 307 (2015)
27. Garifullin I A *Phys. Usp.* **49** 652 (2006); *Usp. Fiz. Nauk* **176** 676 (2006)
28. Soloviev I I et al. *Beilstein J. Nanotechnol.* **8** 2689 (2017)

29. Lyuksyutov I F, Pokrovsky V L *Adv. Phys.* **54** 67 (2005)
30. Aladyshkin A Yu et al. *Supercond. Sci. Technol.* **22** 053001 (2009)
31. Buzdin A I, Melnikov A S *Phys. Rev. B* **67** 020503 (2003)
32. Aladyshkin A Yu et al. *Phys. Rev. B* **68** 184508 (2003)
33. Werner R et al. *Phys. Rev. B* **84** 020505 (2011)
34. Iavarone M et al. *Nat. Commun.* **5** 4766 (2014)
35. Ryazanov V V et al. *JETP Lett.* **77** 39 (2003); *Pis'ma Zh. Eksp. Teor. Fiz.* **77** 43 (2003)
36. Larkin A I, Ovchinnikov Yu N *Sov. Phys. JETP* **20** 762 (1965); *Zh. Eksp. Teor. Fiz.* **47** 1136 (1964)
37. Fulde P, Ferrell R A *Phys. Rev.* **135** A550 (1964)
38. Aslamazov L G *Sov. Phys. JETP* **28** 773 (1969); *Zh. Eksp. Teor. Fiz.* **55** 1477 (1968)
39. Buzdin A I *Rev. Mod. Phys.* **77** 935 (2005)
40. Buzdin A I, Kupriyanov M Yu *JETP Lett.* **52** 487 (1990); *Pis'ma Zh. Eksp. Teor. Fiz.* **52** 1089 (1990)
41. Radović Z et al. *Phys. Rev. B* **44** 759 (1991)
42. Khusainov M G, Proshin Yu N *Phys. Rev. B* **56** R14283 (1997)
43. Tagirov L R *Physica C* **307** 145 (1998)
44. Jiang J S et al. *Phys. Rev. Lett.* **74** 314 (1995)
45. Muhge Th et al. *Phys. Rev. Lett.* **77** 1857 (1996)
46. Sidorenko A S et al. *Ann. Physik* **515** 37 (2003)
47. Garifullin I A et al. *Phys. Rev. B* **66** 020505 (2002)
48. Zdravkov V et al. *Phys. Rev. Lett.* **97** 057004 (2006)
49. Zdravkov V I et al. *Phys. Rev. B* **82** 054517 (2010)
50. Bulaevskii L N, Kuzii V V, Sobyanin A A *JETP Lett.* **25** 290 (1977); *Pis'ma Zh. Eksp. Teor. Fiz.* **25** 314 (1977)
51. Buzdin A I, Bulaevskii L N, Panyukov S V *JETP Lett.* **35** 178 (1982); *Pis'ma Zh. Eksp. Teor. Fiz.* **35** 147 (1982)
52. Buzdin A I, Kupriyanov M Yu *JETP Lett.* **53** 321 (1991); *Pis'ma Zh. Eksp. Teor. Fiz.* **53** 308 (1991)
53. Ryazanov V V et al. *Phys. Rev. Lett.* **86** 2427 (2001)
54. Tagirov L R *Phys. Rev. Lett.* **83** 2058 (1999)
55. Buzdin A I, Vedyayev A V, Ryzhanova N V *Europhys. Lett.* **48** 686 (1999)
56. Oh S, Youm D, Beasley M R *Appl. Phys. Lett.* **71** 2376 (1997)
57. Gu J Y et al. *Phys. Rev. Lett.* **89** 267001 (2002)
58. Potenza A, Marrows C H *Phys. Rev. B* **71** 180503 (2005)
59. Leksin P V et al. *Phys. Rev. Lett.* **109** 057005 (2012)
60. Kontos T et al. *Phys. Rev. Lett.* **86** 304 (2001)
61. Kontos T et al. *Phys. Rev. Lett.* **89** 137007 (2002)
62. Kontos T et al. *Phys. Rev. Lett.* **93** 137001 (2004)
63. Sellier H et al. *Phys. Rev. B* **68** 054531 (2003)
64. Robinson J W A et al. *Phys. Rev. Lett.* **89** 177003 (2006)
65. Golubov A A, Kupriyanov M Y, Il'ichev E *Rev. Mod. Phys.* **76** 411 (2004)
66. Ryazanov V V et al. *Phys. Usp.* **47** 732 (2004); *Usp. Fiz. Nauk* **174** 795 (2004)
67. Feofanov K et al. *Nat. Phys.* **6** 593 (2010)
68. Ioffe L B et al. *Nature* **398** 679 (1999)
69. de Gennes P G *Phys. Lett.* **23** 10 (1966)
70. Singh A et al. *Phys. Rev. X* **5** 021019 (2015)
71. Srivastava A et al. *Phys. Rev. Appl.* **8** 044008 (2017)
72. Kamashev A A et al. *Beilstein J. Nanotechnol.* **9** 1764 (2018)
73. Kamashev A A et al. *Beilstein J. Nanotechnol.* **10** 1458 (2019)
74. de Groot R A et al. *Phys. Rev. Lett.* **50** 2024 (1983)
75. Pickett W E, Moodera J *Phys. Today* **54** (5) 39 (2001)
76. Coey J M D, Venkatesan M *J. Appl. Phys.* **91** 8345 (2002)
77. Katsnelson M I et al. *Rev. Mod. Phys.* **80** 315 (2008)
78. Irkhin V Yu, Katsnel'son M I *Phys. Usp.* **37** 659 (1994); *Usp. Fiz. Nauk* **164** 705 (1994)
79. Eschrig M *Rep. Prog. Phys.* **78** 104501 (2015)
80. Giroud M et al. *Phys. Rev. B* **58** R11872 (1998)
81. Petrashov V T et al. *Phys. Rev. Lett.* **83** 3281 (1999)
82. Sosnin I et al. *Phys. Rev. Lett.* **96** 157002 (2006)
83. Keizer R S et al. *Nature* **439** 825 (2006)
84. Wang J et al. *Nat. Phys.* **6** 389 (2010)
85. Khaire T S et al. *Phys. Rev. Lett.* **104** 137002 (2010)
86. Klose C et al. *Phys. Rev. Lett.* **108** 127002 (2012)
87. Banerjee N et al. *Nat. Commun.* **5** 3048 (2014)
88. Robinson J W A, Witt J D S, Blamire M G *Science* **329** 59 (2010)
89. Robinson J W A et al. *Phys. Rev. Lett.* **104** 207001 (2010)
90. Bergeret F S, Volkov A F, Efetov K B *Phys. Rev. Lett.* **86** 4096 (2001)
91. Bergeret F S, Volkov A F, Efetov K B *Phys. Rev. B* **64** 134506 (2001)
92. Kadigrobov A, Shekhter R I, Jonson M *Europhys. Lett.* **54** 394 (2001)
93. Bergeret F S, Volkov A F, Efetov K B *Rev. Mod. Phys.* **77** 1321 (2005)
94. Linder J, Balatsky A V *Rev. Mod. Phys.* **91** 045005 (2019)
95. Rashba E I *Sov. Phys. Solid State* **2** 1109 (1960); *Fiz. Tverd. Tela* **2** 1224 (1960)
96. Kitaev A Yu *Phys. Usp.* **44** (10S) 131 (2001); *Usp. Fiz. Nauk* **171** (Suppl. 10) 131 (2001)
97. Alicea J *Rep. Prog. Phys.* **75** 076501 (2012)
98. Zutic I, Fabian J, Das Sarma S. *Rev. Mod. Phys.* **76** 323 (2004)
99. Dieny B et al. *Phys. Rev. B* **43** 1297 (1991)
100. Moraru I C et al. *Phys. Rev. Lett.* **96** 037004 (2006)
101. Moraru I C et al. *Phys. Rev. B* **74** 220507 (2006)
102. Miao G-X, Ramos A V, Moodera J S *Phys. Rev. Lett.* **101** 137001 (2008)
103. Peña V et al. *Phys. Rev. Lett.* **94** 057002 (2005)
104. Rusanov A Y, Habraken S, Aarts J *Phys. Rev. B* **73** 060505 (2006)
105. Steiner R, Ziemann P *Phys. Rev. B* **74** 094504 (2006)
106. Singh A et al. *Appl. Phys. Lett.* **91** 152504 (2007)
107. Singh A, Surgers C, v Lohneysen H *Phys. Rev. B* **75** 024513 (2007)
108. Leksin P V et al. *JETP Lett.* **90** 59 (2009); *Pis'ma Zh. Eksp. Teor. Fiz.* **90** 64 (2009)
109. Zhu J et al. *Phys. Rev. Lett.* **103** 027004 (2009)
110. Flokstra M, van der Knaap J M, Aarts J *Phys. Rev. B* **82** 184523 (2010)
111. Leksin P V et al. *Appl. Phys. Lett.* **97** 102505 (2010)
112. Leksin P V et al. *Phys. Rev. B* **93** 100502 (2016)
113. Leksin P V et al. *Phys. Rev. Lett.* **106** 067005 (2011)
114. Leksin P V et al. *Phys. Rev. B* **85** 024502 (2012)
115. Fominov Ya V et al. *JETP Lett.* **91** 308 (2010); *Pis'ma Zh. Eksp. Teor. Fiz.* **91** 329 (2010)
116. Zdravkov V I et al. *Phys. Rev. B* **87** 144507 (2013)
117. Wu C-T, Valls O T, Halterman K *Phys. Rev. B* **86** 014523 (2012)
118. Baladie I, Buzdin A *Phys. Rev. B* **67** 014523 (2003)
119. You C-Y et al. *Phys. Rev. B* **70** 014505 (2004)
120. Fominov Ya V, Golubov A A, Kupriyanov M Yu *JETP Lett.* **77** 510 (2003); *Pis'ma Zh. Eksp. Teor. Fiz.* **77** 609 (2003)
121. Bozovic M, Radovic Z *Europhys. Lett.* **70** 513 (2005)
122. Halterman K, Valls O T *Phys. Rev. B* **72** 060514 (2005)
123. Linder J, Zareyan M, Sudbo A *Phys. Rev. B* **79** 064514 (2009)
124. Lofwander T, Champel T, Eschrig M *Phys. Rev. B* **75** 014512 (2007)
125. Cadden-Zimansky P et al. *Phys. Rev. B* **77** 184501 (2008)
126. Buzdin A, Daumens M *Europhys. Lett.* **64** 510 (2003)
127. Tollis S, Daumens M, Buzdin A *Phys. Rev. B* **71** 024510 (2005)
128. Montiel X et al. *Europhys. Lett.* **86** 67002 (2009)
129. Kinsey R J, Burnell G, Blamire M G *IEEE Trans. Appl. Supercond.* **11** 904 (2001)
130. Westerholt K et al. *Phys. Rev. Lett.* **95** 097003 (2005)
131. Kim D H, Hwang T *J. Phys. C* **455** 58 (2007)
132. Luo Y, Samwer K *Europhys. Lett.* **91** 37003 (2010)
133. Zhu J et al. *Phys. Rev. Lett.* **105** 207002 (2010)
134. Aarts J, Rusanov A Yu *C.R. Phys.* **7** 99 (2006)
135. Banerjee N et al. *Nat. Commun.* **5** 3048 (2014)
136. Jara A J et al. *Phys. Rev. B* **89** 184502 (2014)
137. Flokstra M G et al. *Phys. Rev. B* **91** 060501 (2015)
138. Wang X L et al. *Phys. Rev. B* **89** 140508 (2014)
139. Mironov S V, Buzdin A *Phys. Rev. B* **89** 144505 (2014)
140. Gu Y et al. *Phys. Rev. Lett.* **115** 067201 (2015)
141. Garifullin I A *JETP Lett.* **106** 57 (2017); *Pis'ma Zh. Eksp. Teor. Fiz.* **106** 58 (2017)
142. Zdravkov V I et al. *Appl. Phys. Lett.* **103** 062603 (2013)
143. Demler E A, Arnold G B, Beasley M R *Phys. Rev. B* **55** 15174 (1997)
144. Oboznov V A et al. *Phys. Rev. Lett.* **96** 197003 (2006)
145. Veretennikov A V et al. *Physica B* **284** 495 (2000)
146. Buzdin A *Phys. Rev. B* **71** 180501 (2005)
147. Houzet M, Vinokur V, Pistolesi V F *Phys. Rev. B* **72** 220506 (2005)
148. Frolov S M et al. *Phys. Rev. B* **74** 020503 (2006)
149. Goldobin E et al. *Phys. Rev. B* **76** 224523 (2007)

150. Golubov A A, Kupriyanov M Yu, Fominov Ya V *JETP Lett*. **75** 190 (2002); *Pis'ma Zh. Eksp. Teor. Fiz*. **75** 223 (2002)
151. Golubov A A, Kupriyanov M Yu, Fominov Ya V *JETP Lett*. **75** 588 (2002); *Pis'ma Zh. Eksp. Teor. Fiz*. **75** 709 (2002)
152. Bakurskiy S V et al. *Phys. Rev. B* **95** 094522 (2017)
153. Ryazanov V V et al. *Phys. Rev. B* **65** 020501 (2001)
154. Guichard W et al. *Phys. Rev. Lett*. **90** 167001 (2003)
155. Frolov S M et al. *Phys. Rev. B* **70** 144505 (2004)
156. Levin K, Mills D L *Phys. Rev. B* **9** 2354 (1974)
157. Houghton R W, Sarachik M P, Kouvel J S *Phys. Rev. Lett*. **25** 238 (1970)
158. Bauer A et al. *Phys. Rev. Lett*. **92** 217001 (2004)
159. Frolov S M et al. *Nat. Phys*. **4** 32 (2008)
160. Ortlepp T et al. *Science* **312** 1495 (2006)
161. Feofanov A K et al. *Nat. Phys*. **6** 593 2010
162. Blum Y et al. *Phys. Rev. Lett*. **89** 187004 (2002)
163. Bell C et al. *Phys. Rev. B* **71** 180501 (2005)
164. Shelukhin V et al. *Phys. Rev. B* **73** 174506 (2006)
165. Karminskaya T Yu, Kupriyanov M Yu *JETP Lett*. **85** 286 (2007); *Pis'ma Zh. Eksp. Teor. Fiz*. **85** 343 (2007)
166. Karminskaya T Yu, Kupriyanov M Yu *JETP Lett*. **86** 61 (2007); *Pis'ma Zh. Eksp. Teor. Fiz*. **86** 65 (2007)
167. Karminskaya T Yu et al. *Phys. Rev. B* **79** 214509 (2009)
168. Karminskaya T Yu et al. *Phys. Rev. B* **81** 214518 (2010)
169. Golikova T. E. et al. *Phys. Rev. B* **86** 064416 (2012)
170. Heim D M et al. *New J. Phys*. **17** 113022 (2015)
171. Buzdin A *JETP Lett*. **78** 583 (2003); *Pis'ma Zh. Eksp. Teor. Fiz*. **78** 1073 (2003)
172. Faure M et al. *Phys. Rev. B* **73** 064505 (2006)
173. Buzdin A *Phys. Rev. B* **62** 11377 (2000)
174. SanGiorgio P et al. *Phys. Rev. Lett*. **100** 237002 (2008)
175. Boden K M, Pratt W P, Birge N O *Phys. Rev. B* **84** 020510 (2011)
176. Tanaka Y, Kashiwaya S *Physica C* **274** 357 (1997)
177. Barash Yu S, Bobkova I V *Phys. Rev. B* **65** 144502 (2002)
178. Barash Yu S, Bobkova I V, Kopp T *Phys. Rev. B* **66** 140503 (2002)
179. Strambini E et al. *Phys. Rev. Mater*. **1** 054402 (2017)
180. Senapati K et al. *Phys. Rev. B* **83** 014403 (2011)
181. Senapati K, Blamire M G, Barber Z H *Nat. Mater*. **10** 849 (2011)
182. Cascales J P et al. *Appl. Phys. Lett*. **114** 022601 (2019)
183. Alidoust M et al. *Phys. Rev. B* **81** 014512 (2010)
184. Volkov A F, Efetov K B *Phys. Rev. B* **81** 144522 (2010)
185. Anwar M S et al. *Appl. Phys. Lett*. **100** 052602 (2012)
186. Klose C et al. *Phys. Rev. Lett*. **108** 127002 (2012)
187. Houzet M, Buzdin A I *Phys. Rev. B* **76** 060504 (2007)
188. Khaire T S et al. *Phys. Rev. Lett*. **104** 137002 (2010)
189. Halasz G B et al. *Phys. Rev. B* **79** 224505 (2009)
190. Sosnin I et al. *Phys. Rev. Lett*. **96** 157002 (2006)
191. Witt J D S, Robinson J W A, Blamire M G *Phys. Rev. B* **85** 184526 (2012)
192. Chiodi F et al. *Europhys. Lett*. **101** 37002 (2013)
193. Di Bernardo A et al. *Nat. Commun*. **6** 8053 (2015)
194. Fominov Ya V, Volkov A F, Efetov K B *Phys. Rev. B* **75** 104509 (2007)
195. Buzdin A I, Melnikov A S, Pugach N G *Phys. Rev. B* **83** 144515 (2011)
196. Robinson J W A et al. *Sci. Rep*. **2** 106 (2012)
197. Silaev M A *Phys. Rev. B* **79** 184505 (2009)
198. Kalenkov M S, Zaikin A D, Petrashov V T *Phys. Rev. Lett*. **107** 087003 (2011)
199. Eschrig M, Löfwander T *Nat. Phys*. **4** 138 (2008)
200. Diesch S et al. *Nat. Commun*. **9** 5248 (2018)
201. Linder J, Sudbo A *Phys. Rev. B* **76** 134509 (2007)
202. Gingrich E C et al. *Phys. Rev. B* **86** 224506 (2012)
203. Blanter Ya M, Hekking F W J *Phys. Rev. B* **69** 024525 (2004)
204. Pajovic Z et al. *Phys. Rev. B* **74** 184509 (2006)
205. Crouzy B, Tollis S, Ivanov D A *Phys. Rev. B* **75** 054503 (2007)
206. Eschrig M et al. *Phys. Rev. Lett*. **90** 137003 (2003)
207. Grein R et al. *Phys. Rev. Lett*. **102** 227005 (2009)
208. Samokhvalov A V, Buzdin A I, Shekhter R I *Sci. Rep*. **4** 05671 (2014)
209. Khaire T S, Pratt W P (Jr.), Birge N O *Phys. Rev. B* **79** 094523 (2009)
210. Weides M *Appl. Phys. Lett*. **93** 052502 (2008)
211. Bol'ginov V V et al. *JETP Lett*. **95** 366 (2012); *Pis'ma Zh. Eksp. Teor. Fiz*. **95** 408 (2012)
212. Bakurskiy S V et al. *Appl. Phys. Lett*. **102** 192603 (2013)
213. Bakurskiy S V et al. *Phys. Rev. B* **88** 144519 (2013)
214. Vernik I V et al. *IEEE Trans. Appl. Supercond*. **23** 1701208 (2013)
215. Ruppelt N et al. *Appl. Phys. Lett*. **106** 022602 (2015)
216. Golovchanskiy I A et al. *Phys. Rev. B* **94** 214514 (2016)
217. Bakurskiy S V et al. *Appl. Phys. Lett*. **108** 042602 (2016)
218. Klenov N et al. *Beilstein J. Nanotechnol*. **10** 833 (2019)
219. Khasawneh M A, Pratt W P, Birge N O *Phys. Rev. B* **80** 020506 (2009)
220. Zaitsev A *JETP Lett*. **90** 475 (2009); *Pis'ma Zh. Eksp. Teor. Fiz*. **90** 521 (2009)
221. Buzdin A, Koshelev A E *Phys. Rev. B* **67** 220504 (2003)
222. Goldibin E et al. *Phys. Rev. B* **76** 224523 (2007)
223. Buzdin A *Phys. Rev. Lett*. **101** 107005 (2008)
224. Samokhvalov A V *J. Exp. Theor. Phys*. **104** 451 (2007); *Zh. Eksp. Teor. Fiz*. **131** 500 (2007)
225. Meng Hao, Samokhvalov A V, Buzdin A I *Phys. Rev. B* **99** 024503 (2019)
226. Margaris I, Paltoglou V, Flytzanis N *J. Phys. Condens. Matter* **22** 445701 (2010)
227. Pal S, Benjamin C *Europhys. Lett*. **126** 57002 (2019)
228. Rabinovich D S, Bobkova I V, Bobkov A M *Phys. Rev. Res*. **1** 033095 (2019)
229. Braude V, Nazarov Y V *Phys. Rev. Lett*. **98** 077003 (2007)
230. Eschrig M et al. *J. Low Temp. Phys*. **147** 457 (2007)
231. Eschrig M et al. *New J. Phys*. **17** 083037 (2015)
232. Bobkova I V, Bobkov A M, Silaev M A *Phys. Rev. B* **96** 094506 (2017).
233. Moor A, Volkov A F, Efetov K B *Phys. Rev. B* **92** 180506 (2015)
234. Mironov S, Buzdin A *Phys. Rev. B* **92** 184506 (2015)
235. Grein R et al. *Phys. Rev. Lett*. **102** 227005 (2009)
236. Terzioglu E, Beasley M R *IEEE Trans. Appl. Supercond*. **8** 48 (1998)
237. Yamashita T et al. *Phys. Rev. Lett*. **95** 097001 (2005)
238. Ustinov A V, Kaplunenko V K *J. Appl. Phys*. **94** 5405 (2003)
239. Tsuei C C, Kirtley J R *Physica C* **367** 1 (2002)
240. Ortlepp T et al. *Science* **312** 1495 (2006)
241. Ioffe L B et al. *Nature* **398** 679 (1999)
242. Feofanov K et al. *Nat. Phys*. **6** 593 (2010)
243. Robinson J W A, Samokhvalov A V, Buzdin A I *Phys. Rev. B* **99** 180501 (2019)
244. Strambini E et al. *Nat. Nanotechnol*. **15** 656 (2020)
245. Silaev M A, Tokatly I V, Bergeret F S *Phys. Rev. B* **95** 184508 (2017)
246. Shukrinov Yu M *Phys. Usp*. **65** 317 (2022); *Usp. Fiz. Nauk* **192** 345 (2022)
247. Goldobin E et al. *Phys. Rev. Lett*. **107** 227001 (2011)
248. Sickinger H et al. *Phys. Rev. Lett*. **109** 107002 (2012)
249. Mayer W et al. *Nat. Commun*. **11** 212 (2020)
250. Szombati D B et al. *Nat. Phys*. **12** 568 (2016)
251. Assouline A et al. *Nat. Commun*. **10** 126 (2019)
252. Gor'kov L P, Rashba E I *Phys. Rev. Lett*. **87** 037004 (2001)
253. Edelstein V M *Phys. Rev. B* **67** 020505 (2003)
254. Dolcini F, Houzet M, Meyer J S *Phys. Rev. B* **92** 035428 (2015)
255. Yokoyama T, Eto M, Nazarov Yu V *Phys. Rev. B* **89** 195407 (2014)
256. Ying Z-J et al., in *2017 16th Intern. Superconductive Electronics Conf. (ISEC)* (Piscataway, NJ: IEEE, 2017) https://doi.org/10.1109/ISEC.2017.8314198; arXiv:1803.07900
257. Spånslätt C *Phys. Rev. B* **98** 054508 (2018)
258. Kutlin A G, Mel'nikov A S *Phys. Rev. B* **101** 045418 (2020)
259. Kopasov A A, Kutlin A G, Mel'nikov A S *Phys. Rev. B* **103** 144520 (2021)
260. Samokhvalov A V et al. *JETP Lett*. **113** 34 (2021); *Pis'ma Zh. Eksp. Teor. Fiz*. **113** 38 (2021)
261. Ando F et al. *Nature* **584** 373 (2020)
262. Proshin Yu N, Avdeev M V *Phys. Rev. B* **97** 100502 (2018)
263. Mel'nikov A S et al. *Phys. Rev. Lett*. **109** 237006 (2012)
264. Bergeret F S, Tokatly I V *Phys. Rev. Lett*. **110** 117003 (2013)
265. Samokhvalov A V, Mel'nikov A S, Buzdin A I *Phys. Usp*. **59** 571 (2016); *Usp. Fiz. Nauk* **186** 640 (2016)
266. Trifunovic L *Phys. Rev. Lett*. **107** 047001 (2011)
267. Trifunovic L, Popović Z, Radović Z *Phys. Rev. B* **84** 064511 (2011)

268. Andreev A F *Sov. Phys. JETP* **19** 1228 (1964); *Zh. Eksp. Teor. Fiz.* **46** 1823 (1964)
269. Blonder G E, Tinkham M, Klapwijk T M *Phys. Rev. B* **25** 4515 (1982)
270. Pannetier B, Courtois H *J. Low Temp. Phys.* **118** 599 (2000)
271. de Jong M J M, Beenakker C W J *Phys. Rev. Lett.* **74** 1657 (1995)
272. Mel'nikov A S, Buzdin A I *Phys. Rev. Lett.* **117** 077001 (2016)
273. Bulaevskii L N, Rusinov A I, Kulic M *J. Low Temp. Phys.* **39** 255 (1980)
274. Ivanov D A, Fominov Ya V *Phys. Rev. B* **73** 214524 (2006)
275. Champel T, Eschrig M *Phys. Rev. B* **71** 220506 (2005)
276. Eschrig M, Lofwander T *Nat. Phys.* **4** 138 (2008)
277. Usman I T M et al. *Phys. Rev. B* **83** 144518 (2011)
278. Chtchelkatchev N M, Burmistrov I S *Phys. Rev. B* **68** 140501 (2003)
279. Knežević M, Trifunovic L, Radović Z *Phys. Rev. B* **85** 094517 (2012)
280. Pajovic Z et al. *Phys. Rev. B* **74** 184509 (2006)
281. Mel'nikov A S et al. *Phys. Rev. Lett.* **109** 237006 (2012)
282. Konschelle F, Cayssol J, Buzdin A I *Phys. Rev. B* **78** 134505 (2008)
283. Bulaevskii L N, Buzdin A I, Panyukov S V *Solid State Commun.* **44** 539 (1982)
284. Cottet A *Phys. Rev. Lett.* **107** 177001 (2011)
285. Annunziata G et al. *Phys. Rev. B* **83** 060508 (2011)
286. Yokoyama T, Tanaka Y, Golubov A A *Phys. Rev. B* **75** 134510 (2007)
287. Yokoyama T, Tserkovnyak Y *Phys. Rev. B* **80** 104416 (2009)
288. Trifunovic L, Radovic Z *Phys. Rev. B* **82** 020505 (2010)
289. Alidoust M, Linder J *Phys. Rev. B* **82** 224504 (2010)
290. Duckheim M, Brouwer P W *Phys. Rev. B* **83** 054513 (2011)
291. Volkov A F, Fominov Ya V, Efetov K B *Phys. Rev. B* **72** 184504 (2005)
292. Champel T, Eschrig M, Löfwander T *Phys. Rev. Lett.* **100** 077003 (2008)
293. Khaire T S et al. *Phys. Rev. Lett.* **104** 137002 (2010)
294. Robinson J W A, Witt J D S, Blamire M G *Science* **329** 59 (2010)
295. Volkov A F, Bergeret F S, Efetov K B *Phys. Rev. Lett.* **90** 117006 (2003)
296. Volkov A F et al. *Phys. Rev. B* **78** 024519 (2008)
297. Blanter Ya M, Hekking F W J *Phys. Rev. B* **69** 024525 (2004)
298. Pajović Z et al. *Phys. Rev. B* **74** 184509 (2006)
299. Crouzy B, Tollis S, Ivanov D A *Phys. Rev. B* **76** 134502 (2007)
300. Hubert A, Schäfer R *Magnetic Domains: the Analysis of Magnetic Microstructures* (Berlin: Springer, 2000)
301. Mineev V P, Sigrist M, in *Non-Centrosymmetric Superconductors* (Lecture Notes in Physics, Vol. 847, Eds E Bauer, M Sigrist) (Berlin: Springer, 2012) p. 129
302. Smidman M et al. *Rep. Prog. Phys.* **80** 036501 (2017)
303. Edelstein V M *JETP Lett.* **77** 182 (2003); *Pis'ma Zh. Eksp. Teor. Fiz.* **77** 212 (2003)
304. Annunziata G, Manske D, Linder J *Phys. Rev. B* **86** 174514 (2012)
305. Edelstein V M *Sov. Phys. JETP* **68** 1244 (1989); *Zh. Eksp. Teor. Fiz.* **95** 2151 (1989)
306. Mineev V P, Samokhin K V *J. Exp. Theor. Phys.* **78** 401 (1994); *Zh. Eksp. Teor. Fiz.* **105** 747 (1994)
307. Barzykin V, Gor'kov L P *Phys. Rev. Lett.* **89** 227002 (2002)
308. Samokhin K V *Phys. Rev. B* **70** 104521 (2004)
309. Kaur R P, Agterberg D F, Sigrist M *Phys. Rev. Lett.* **94** 137002 (2005)
310. Dimitrova O, Feigel'man M V *Phys. Rev. B* **76** 014522 (2007)
311. Konschelle F, Buzdin A *Phys. Rev. Lett.* **102** 017001 (2009)
312. Krive I V et al. *Low Temp. Phys.* **30** 398 (2004)
313. Szombati D B et al. *Nat. Phys.* **12** 568 (2016)
314. Konschelle F, Bergeret F S, Tokatly I V *Phys. Rev. Lett.* **116** 237002 (2016)
315. Konschelle F, Tokatly I V, Bergeret F S *Phys. Rev. B* **94** 014515 (2016)
316. Bergeret F S, Tokatly I V *Europhys. Lett.* **110** 57005 (2015)
317. Reynoso A A et al. *Phys. Rev. Lett.* **101** 107001 (2008)
318. Silaev M A, Bobkova I V, Bobkov A M *Phys. Rev. B* **102** 100507 (2020)
319. Kadigrobov A et al. *Europhys. Lett.* **67** 948 (2004)
320. Proshin Yu N, Avdeev M V *J. Magn. Magn. Mater.* **459** 359 (2018)
321. Bergeret F S, Tokatly I V *Phys. Rev. B* **89** 134517 (2014)
322. Konschelle F, Tokatly I V, Bergeret F S *Phys. Rev. B* **92** 125443 (2015).
323. Tokatly I V *Phys. Rev. B* **96** 060502 (2017)
324. Burkov A A, Nunez A S, MacDonald A H *Phys. Rev. B* **70** 155308 (2004)
325. Shen K, Raimondi R, Vignale G *Phys. Rev. B* **90** 245302 (2014)
326. Raimondi R et al. *Ann. Phys.* **524** 153 (2012)
327. Al'tshuler B L, Spivak B Z *Sov. Phys. JETP* **65** 343 (1987); *Zh. Eksp. Teor. Fiz.* **92** 609 (1987)
328. Zyuzin A Yu, Spivak B, Hruska M *Europhys. Lett.* **62** 97 (2003)
329. Asano Y et al. *Phys. Rev. B* **76** 224525 (2007)
330. Ioselevich P A, Ostrovsky P M, Fominov Ya V *Phys. Rev. B* **98** 144521 (2018)
331. Houzet M, Meyer J S *Phys. Rev. B* **80** 012505 (2009)
332. Mironov S, Mel'nikov A, Buzdin A *Phys. Rev. Lett.* **109** 237002 (2012)
333. Asano Y et al. *Phys. Rev. Lett.* **107** 087001 (2011)
334. Yokoyama T, Tanaka Y, Nagaosa N *Phys. Rev. Lett.* **106** 246601 (2011)
335. Di Bernardo A et al. *Phys. Rev. X* **5** 041021 (2015)
336. Flokstra M G et al. *Nat. Phys.* **12** 57 (2016)
337. Flokstra M G et al. *Phys. Rev. Lett.* **120** 247001 (2018)
338. Stahn J et al. *Phys. Rev. B* **71** 140509 (2005)
339. Khaydukov Yu N et al. *JETP Lett.* **98** 107 (2013); *Pis'ma Zh. Eksp. Teor. Fiz.* **98** 116 (2013)
340. Nagy B et al. *Europhys. Lett.* **116** 17005 (2016)
341. Ovsyannikov G A et al. *J. Exp. Theor. Phys.* **122** 738 (2016); *Zh. Eksp. Teor. Fiz.* **149** 852 (2016)
342. Lemberger T R et al. *J. Appl. Phys.* **103** 07C701 (2008)
343. Hinton M J et al. *Phys. Rev. B* **94** 014518 (2016)
344. Claassen J H, Reeves M E, Soulen R J *Rev. Sci. Instrum.* **62** 996 (1991)
345. Turneaure S J, Ulm E R, Lemberger T R *J. Appl. Phys.* **79** 4221 (1996)
346. Turneaure S J, Pesetski A, Lemberger T R *J. Appl. Phys.* **83** 4334 (1998)
347. Kamlapure A et al. *Appl. Phys. Lett.* **96** 072509 (2010)
348. Izyumov Yu A, Proshin Yu N, Khusainov M G *Phys. Usp.* **45** 109 (2002); *Usp. Fiz. Nauk* **172** 113 (2002)
349. Buzdin A I, Bujicic B, Kupriyanov M Yu *Sov. Phys. JETP* **74** 124 (1992); *Zh. Eksp. Teor. Fiz.* **101** 231 (1992)
350. Buzdin A I, Kupriyanov M Yu, Vujičić B *Physica C* **185–189** 2025 (1991)
351. Tollis S *Phys. Rev. B* **69** 104532 (2004)
352. Sellier H et al. *Phys. Rev. Lett.* **92** 257005 (2004)
353. Barsic P H, Valls O T, Halterman K *Phys. Rev. B* **73** 144514 (2006)
354. Barsic P H, Valls O T, Halterman K *Phys. Rev. B* **75** 104502 (2007)
355. Zaikin A D *Solid State Commun.* **41** 533 (1982)
356. Visani P, Mota A C, Pollini A *Phys. Rev. Lett.* **65** 1514 (1990)
357. Muller-Allinger F B, Mota A C *Phys. Rev. Lett.* **84** 3161 (2000)
358. Pompeo N et al. *Phys. Rev. B* **90** 064510 (2014)
359. Loria R et al. *Phys. Rev. B* **92** 184106 (2015)
360. Trunin M R *JETP Lett.* **72** 583 (2000); *Pis'ma Zh. Eksp. Teor. Fiz.* **72** 845 (2000)
361. Trunin M R *Phys. Usp.* **48** 979 (2005); *Usp. Fiz. Nauk* **175** 1017 (2005)
362. Samokhvalov A V, Buzdin A I *Phys. Rev. B* **92** 054511 (2015)
363. Vdovichev S N et al. *JETP Lett.* **104** 329 (2016); *Pis'ma Zh. Eksp. Teor. Fiz.* **104** 336 (2016)
364. Pestov E E et al. *IEEE Trans. Appl. Supercond.* **11** 131 (2001)
365. Baryshev S V et al. *Phys. Rev. B* **76** 054520 (2007)
366. Marychev P M, Vodolazov D Yu *Phys. Rev. B* **98** 214510 (2018)
367. Aladyshkin A Yu *Supercond. Sci. Technol.* **22** 053001 (2009)
368. Krivoruchko V N, Koshina E A *Phys. Rev. B* **66** 014521 (2002)
369. Bergeret F S, Volkov A F, Efetov K B *Phys. Rev. B* **69** 174504 (2004)
370. Bergeret F S, Yeyati A L, Matín-Rodero A *Phys. Rev. B* **72** 064524 (2005)
371. Löfwander T et al. *Phys. Rev. Lett.* **95** 187003 (2005)
372. Faure M, Buzdin A, Gusakova D *Physica C* **454** 61 (2007)
373. Mironov S, Mel'nikov A S, Buzdin A *Appl. Phys. Lett.* **113** 022601 (2018)
374. Devizorova Zh et al. *Phys. Rev. B* **99** 104519 (2019)

375. Mironov S V et al. *JETP Lett*. **113** 92 (2021); *Pis'ma Zh. Eksp. Teor. Fiz*. **113** 102 (2021)
376. Bergeret F S, García N *Phys. Rev. B* **70** 052507 (2004)
377. Kharitonov M Yu, Volkov A F, Efetov K B *Phys. Rev. B* **73** 054511 (2006)
378. Volkov A F, Bergeret F S, Efetov K B *Phys. Rev. B* **99** 144506 (2019)
379. Salikhov R I et al. *Phys. Rev. Lett*. **102** 087003 (2009)
380. Xia J et al. *Phys. Rev. Lett*. **102** 087004 (2009)
381. Nagy B et al. *Europhys. Lett*. **116** 17005 (2016)
382. Khaydukov Yu N et al. *Phys. Rev. B* **99** 140503 (2019)
383. Stewart R et al. *Phys. Rev. B* **100** 020505 (2019)
384. Flokstra M G et al. *Appl. Phys. Lett*. **115** 072602 (2019)
385. Hoppler J et al. *Nat. Mater*. **8** 315 (2009)
386. Mironov S V et al. *Phys. Rev. Lett*. **121** 077002 (2018)
387. Fominov Ya V, Kupriyanov M Yu, Feigel'man M V *Phys. Usp*. **46** 105 (2003); *Usp. Fiz. Nauk* **173** 113 (2003)
388. Buzdin A I, Kachkachi H *Phys. Lett. A* **225** 341 (1997)
389. Plastovets V D, Vodolazov D Yu *Phys. Rev. B* **101** 184513 (2020)
390. Coniglio W A et al. *Phys. Rev. B* **83** 224507 (2011)
391. Uji S et al. *Phys. Rev. B* **85** 174530 (2012)
392. Lortz R et al. *Phys. Rev. Lett*. **99** 187002 (2007)
393. Bergk B et al. *Phys. Rev. B* **83** 064506 (2011)
394. Wright J A et al. *Phys. Rev. Lett*. **107** 087002 (2011)
395. Mayaffre H et al. *Nat. Phys*. **10** 928 (2014)
396. Agosta C C et al. *Phys. Rev. B* **85** 214514 (2012)
397. Beyer R et al. *Phys. Rev. Lett*. **109** 027003 (2012)
398. Koutroulakis G et al. *Phys. Rev. Lett*. **116** 067003 (2016)
399. Matsuda Y, Shimahara H *J. Phys. Soc. Jpn*. **76** 051005 (2007)
400. Samokhvalov A V, Mel'nikov A S, Buzdin A I *Phys. Rev. B* **76** 184519 (2007)
401. Samokhvalov A V et al. *Phys. Rev. B* **79** 174502 (2009)
402. Samokhvalov A V *J. Exp. Theor. Phys*. **125** 298 (2017); *Zh. Eksp. Teor. Fiz*. **152** 350 (2017)
403. Samokhvalov A V, Robinson J W A, Buzdin A I *Phys. Rev. B* **100** 014509 (2019)
404. Moor A, Volkov A F, Efetov K B *Phys. Rev. B* **80** 054516 (2009)
405. Bobkova I V, Bobkov A M *Phys. Rev. B* **88** 174502 (2013)
406. Lutchyn R M, Sau J D, Das Sarma S *Phys. Rev. Lett*. **105** 077001 (2010)
407. Oreg Y, Refael G, von Oppen F *Phys. Rev. Lett*. **105** 177002 (2010)
408. Alicea J *Phys. Rev. B* **81** 125318 (2010)
409. Jacobsen S H, Kulagina I, Linder J *Sci. Rep*. **6** 23926 (2016)
410. Mironov S, Buzdin A *Phys. Rev. Lett*. **118** 077001 (2017)
411. Rabinovich D S et al. *Phys. Rev. B* **99** 180501 (2019)
412. de Groot R A et al. *Phys. Rev. Lett*. **50** 2024 (1983)
413. Lewis S P, Allen P B, Sasaki T *Phys. Rev. B* **55** 10253 (1997)
414. Kobayashi K-I et al. *Nature* **395** 677 (1998)
415. Agterberg D F, in *Non-Centrosymmetric Superconductors* (Lecture Notes in Physics, Vol. 847, Eds E Bauer, M Sigrist) (Berlin: Springer, 2012) p. 155
416. Samokhin K V *Phys. Rev. B* **89** 094503 (2014)
417. Edelstein V M *Phys. Rev. Lett*. **75** 2004 (1995)
418. Fogelstrom M, Rainer D, Sauls J A *Phys. Rev. Lett*. **79** 281 (1997)
419. Vorontsov A B *Phys. Rev. Lett*. **102** 177001 (2009)
420. Hakansson M, Lofwander T, Fogelstrom M *Nat. Phys*. **11** 755 (2015)
421. Barash Yu S, Kalenkov M S, Kurkijarvi J *Phys. Rev. B* **62** 6665 (2000)
422. Higashitani S *J. Phys. Soc. Jpn*. **66** 2556 (1997)
423. Honerkamp C, Wakabayashi K, Sigrist M *Europhys. Lett*. **50** 368 (2000)
424. Fauchere A L, Belzig W, Blatter G *Phys. Rev. Lett*. **82** 3336 (1999)
425. Bobkova I V, Barash Yu S *JETP Lett*. **80** 494 (2004); *Pis'ma Zh. Eksp. Teor. Fiz*. **80** 563 (2004)
426. Matsumoto M, Sigrist M *J. Phys. Soc. Jpn*. **68** 994 (1999)
427. Stone M, Roy R *Phys. Rev. B* **69** 184511 (2004)
428. Kwon H-J, Yakovenko V M, Sengupta K *Synth. Met*. **133–134** 27 (2003)
429. Devizorova Zh et al. *Phys. Rev. B* **103** 064504 (2021)
430. Pershoguba S S et al. *Phys. Rev. Lett*. **115** 116602 (2015)
431. Mal'shukov A G *Phys. Rev. B* **93** 054511 (2016); *Phys. Rev. B* **95** 064517 (2017)
432. Olde Olthof L A B et al. *Phys. Rev. B* **100** 220505 (2019)
433. Baumard J et al. *Phys. Rev. B* **99** 014511 (2019)
434. Edelstein V M *J. Phys. Condens. Matter* **8** 339 (1996)
435. Pal A, Blamire M G *Phys. Rev. B* **92** 180510 (2015)
436. Pal A et al. *Nat. Commun*. **5** 3340 (2014)
437. Zhu Y et al. *Nat. Mater*. **16** 195 (2017)
438. Little W A, Parks R D *Phys. Rev. Lett*. **9** 9 (1962)
439. Little W A, Parks R D *Phys. Rev*. **133** A97 (1964)
440. Galanakis I, Dederichs P H (Eds) *Half-Metallic Alloys*: *Fundamentals and Applications* (Berlin: Springer, 2005)
441. Castelliz L *Monatshefte Chemie* **82** 1059 (1951)
442. Buschow K H J, van Engen P G, Jongebreur R *J. Magn. Magn. Mater*. **38** 1 (1983)
443. Ebert H *Rep. Prog. Phys*. **59** 1665 (1996)
444. van Engen P G et al. *Appl. Phys. Lett*. **42** 202 (1983)
445. Hanssen K E H M et al. *Phys. Rev. B* **42** 1533 (1990)
446. Park J H et al. *Nature* **392** 794 (1998)
447. Soulen R J (Jr.) et al. *Science* **282** 85 (1998)
448. Ji Y et al. *Phys. Rev. Lett*. **86** 5585 (2001)
449. Mazin I I *Phys. Rev. Lett*. **83** 1427 (1999)
450. Li X W, Gupta A, Xiao G *Appl. Phys. Lett*. **75** 713 (1999)
451. DeSisto W J et al. *Appl. Phys. Lett*. **76** 3789 (2000)
452. Anwar M S et al. *Phys. Rev. B* **82** 100501 (2010)
453. Egilmez M et al. *Europhys. Lett*. **106** 37003 (2014)
454. Sefrioui Z et al. *Phys. Rev. B* **67** 214511 (2003)
455. Peña V et al. *Phys. Rev. B* **69** 224502 (2004)
456. Visani C et al. *Nat. Phys*. **8** 539 (2012)
457. Kalcheim Y et al. *Phys. Rev. B* **89** 180506 (2014)
458. Visani C et al. *Phys. Rev. B* **92** 014519 (2015)
459. Salafranca J et al. *Phys. Rev. Lett*. **112** 196802 (2014)
460. Salafranca J, Okamoto S *Phys. Rev. Lett*. **105** 256804 (2010)
461. Chakhalian J et al. *Nat. Phys*. **2** 244 (2006)
462. Komori S et al. *Sci. Adv*. **7** eabe0128 (2021)
463. Linder J, Cuoco M, Sudbo A *Phys. Rev. B* **81** 174526 (2010)
464. Enoksen H, Linder J, Sudbo A *Phys. Rev. B* **85** 014512 (2012)
465. Zheng Z M, Xing D Y *J. Phys. Condens. Matter* **21** 385703 (2009)
466. Feng C D et al. *Phys. Rev. B* **81** 224510 (2010)
467. Asano Y, Tanaka Y, Golubov A A *Phys. Rev. Lett*. **98** 107002 (2007)
468. Sawa Y, Tanaka Y, Asano Y *J. Phys. Chem. Solids* **69** 3247 (2008)
469. Beri B et al. *Phys. Rev. B* **79** 024517 (2009)
470. Grein R et al. *Phys. Rev. B* **81** 094508 (2010)
471. Kupferschmidt J N, Brouwer P W *Phys. Rev. B* **83** 014512 (2011)
472. Wilken F B, Brouwer P W *Phys. Rev. B* **85** 134531 (2012)
473. Kuprianov M Y, Lukichev V F *Sov. Phys. JETP* **67** 1163 (1988); *Zh. Eksp. Teor. Fiz*. **94** (6) 139 (1988)
474. Tokuyasu T, Sauls J A, Rainer D *Phys. Rev. B* **38** 8823 (1988)
475. Cottet A et al. *Phys. Rev. B* **80** 184511 (2009)
476. Bergeret F S, Verso A, Volkov A F *Phys. Rev. B* **86** 060506 (2012)
477. Bergeret F S, Verso A, Volkov A F *Phys. Rev. B* **86** 214516 (2012)
478. Takahashi S et al. *Phys. Rev. Lett*. **99** 057003 (2007)
479. Bergeret F S, Verso A, Volkov A F *Phys. Rev. B* **86** 214516 (2012)
480. Zaitsev A V *JETP Lett*. **108** 205 (2018); *Pis'ma Zh. Eksp. Teor. Fiz*. **108** 206 (2018)
481. Devizorova Zh, Mironov S *Phys. Rev. B* **95** 144514 (2017)
482. Baladie I, Buzdin A *Phys. Rev. B* **64** 224514 (2001)
483. Bergeret F S, Volkov A F, Efetov K B *Phys. Rev. B* **65** 134505 (2002)
484. Alidoust M, Halterman K, Valls O T *Phys. Rev. B* **92** 014508 (2015)
485. Voltan S, Singh A, Aarts J *Phys. Rev. B* **94** 054503 (2016)
486. Halterman K, Alidoust M *Phys. Rev. B* **94** 064503 (2016)
487. Ouassou J A et al. *Sci. Rep*. **7** 1932 (2017)
488. Richard C, Houzet M, Meyer J S *Phys. Rev. Lett*. **109** 057002 (2012)
489. Trif M, Tserkovnyak Y *Phys. Rev. Lett*. **111** 087602 (2013)
490. Shukrinov Yu M, Rahmonov I R, Sengupta K *Phys. Rev. B* **99** 224513 (2019)
491. Silaev M A *Phys. Rev. B* **102** 180502 (2020)
492. Silaev M A *Phys. Rev. B* **102** 144521 (2020)
493. Rabinovich D S et al. *Phys. Rev. Lett*. **123** 207001 (2019)
494. Golovchanskiy I A et al. *Adv. Sci*. **6** 1900435 (2019)
495. Jeon K-R et al. *Phys. Rev. Appl*. **11** 014061 (2019)
496. Golovchanskiy I A et al. *Phys. Rev. Appl*. **14** 024086 (2020)
497. Golovchanskiy I A et al. *Sci. Adv*. **7** eabe8638 (2021)
498. Bergeret F S et al. *Rev. Mod. Phys*. **90** 041001 (2018)
499. Bogoliubov N N *Sov. Phys. Dokl*. **3** 292 (1958); *Dokl. Akad. Nauk SSSR* **119** 244 (1958)

500. Svidzinskii A V *Prostranstvenno-neodnorodnye Zadachi Teorii Sverkhprovodimosti* (Spatially Inhomogeneous Problems of the Theory of Superconductivity) (Moscow: Nauka, 1982)
501. Kopnin N B *Theory of Nonequilibrium Superconductivity* (New York: Oxford Univ. Press, 2001)
502. de Gennes P *Superconductivity of Metals and Alloys* (New York: W.A. Benjamin, 1966); Translated into Russian: *Sverkhprovodimost' Metallov i Splavov* (Moscow: Mir, 1968)
503. Eilenberger G *Z. Phys.* **214** 195 (1968)
504. Usadel K D *Phys. Rev. Lett.* **25** 507 (1970)
505. Zaitsev A V *Sov. Phys. JETP* **59** 1015 (1984); *Zh. Eksp. Teor. Fiz.* **86** 1742 (1984)
506. Beenakker C W J, van Houten H *Phys. Rev. Lett.* **66** 3056 (1991)
507. Beenakker C W J *Phys. Rev. Lett.* **67** 3836 (1991)